



THE HONG KONG
POLYTECHNIC UNIVERSITY

香港理工大學

Pao Yue-kong Library

包玉剛圖書館

Copyright Undertaking

This thesis is protected by copyright, with all rights reserved.

By reading and using the thesis, the reader understands and agrees to the following terms:

1. The reader will abide by the rules and legal ordinances governing copyright regarding the use of the thesis.
2. The reader will use the thesis for the purpose of research or private study only and not for distribution or further reproduction or any other purpose.
3. The reader agrees to indemnify and hold the University harmless from and against any loss, damage, cost, liability or expenses arising from copyright infringement or unauthorized usage.

IMPORTANT

If you have reasons to believe that any materials in this thesis are deemed not suitable to be distributed in this form, or a copyright owner having difficulty with the material being included in our database, please contact lbsys@polyu.edu.hk providing details. The Library will look into your claim and consider taking remedial action upon receipt of the written requests.

The Hong Kong Polytechnic University
Department of Health Technology and Informatics

**ULTRASOUND EVALUATION OF
SALIVARY AND THYROID GLANDS IN
PATIENTS TREATED WITH
EXTERNAL BEAM RADIOTHERAPY FOR
NASOPHARYNGEAL CARCINOMA**

CHENG CHI HIM

A thesis submitted in partial fulfillment of
the requirements for the degree of Master of Philosophy

July 2011

Certificate of Originality

I hereby declare that this thesis is my own work and that, to the best of my knowledge and belief, it reproduces no material previously published or written, nor material that has been accepted for the award of any other degree or diploma, except where due acknowledgement has been made in the text.

_____ (Signed)

CHENG CHI HIM (Name of Student)

Dedicated
to my beloved grandmother,
Ms. Kwok Sau Chun.

Abstract

Radiation-induced xerostomia and hypothyroidism from damaged salivary and thyroid glands respectively are the common complications in head and neck cancer patients treated with external beam radiotherapy (RT). Ultrasound is a common imaging tool in the assessment of salivary and thyroid glands, which should be useful in investigating their post-RT morphological changes aiding differential diagnosis of the glands. In the present study, the sonographic appearances of salivary and thyroid glands in nasopharyngeal carcinoma (NPC) patients treated with different RT techniques were investigated and compared.

In the investigation of parotid glands, 43 NPC patients treated with conventional RT, 38 NPC patients treated with intensity-modulated radiotherapy (IMRT) and 58 healthy subjects were involved. Parotid glands were sonographically assessed for their size, echogenicity and internal architectures. The mean transverse dimension of parotid glands in patients treated with conventional RT and those treated with IMRT were significantly smaller than that in healthy subjects ($p < 0.05$). Parotid glands of the IMRT group tended to be hyperechoic, homogenous, without hypoechoic areas and with marginally-seen intra-parotid ducts, which are similar to the findings in healthy subjects. Parotid glands in the conventional RT group tended to be hypoechoic, heterogeneous, with hypoechoic areas and had obviously-seen intra-parotid ducts.

For the submandibular glands, a total of 81 NPC patients treated with external beam radiotherapy and 66 healthy subjects were recruited and had a submandibular gland ultrasound examination. Bilateral submandibular glands were sonographically assessed for their size, echogenicity, border sharpness and internal architectures. The mean transverse dimension of submandibular glands in patients treated with RT was significantly smaller than that of the healthy subjects ($p < 0.05$). Submandibular glands in patients treated with RT tended to be heterogeneous with hypoechoic areas and ill-defined borders, whereas submandibular glands in healthy subjects usually appeared homogeneous without hypoechoic areas and had well-defined borders. However, there were no significant differences in echogenicity and conspicuity of intra-glandular ducts of submandibular glands between patients and healthy subjects ($p > 0.05$), in which the glands in both study groups tended to be hyperechoic and with marginally seen intra-glandular ducts.

In the investigation of thyroid glands, 103 NPC patients who had finished radiotherapy of cervical lymph nodes using anterior cervical field, 30 NPC patients who had finished radiotherapy of cervical lymph nodes using IMRT and 61 healthy subjects were involved. Thyroid glands were sonographically assessed for their size, echogenicity, vascularity and internal architectures. Thyroid function test was also performed on each subject/patient. Compared to the patients with abnormal thyroid function, thyroid glands of the patients with normal thyroid function tended to be homogenous, and greater in thyroid volume and echogenicity index ($p < 0.05$).

However, there were no significant differences in vascularity index, incidence and number of nodules, and echogenicity of thyroid glands between the two patient groups ($p > 0.05$). On the other hand, compared with the healthy subjects, the thyroid glands of patients treated with IMRT and those treated with anterior cervical field showed significantly lower thyroid volume, lower incidence and number of nodules, and higher vascularity index ($p < 0.05$). However, there were no significant differences in the thyroid echogenicity and echogeneity ($p > 0.05$).

Ultrasound is a useful imaging tool in the evaluation of radiation-induced changes of salivary and thyroid glands in NPC patients with previous radiotherapy. For more accurate detection and to prevent misdiagnosis, the sonographic appearances of post-RT salivary and thyroid glands should be noted in ultrasound examination of patients with previous radiotherapy for NPC or other head and neck neoplasms.

Presentations and Publications Originating from the Present Study

Conference Presentation and Proceeding

1. **Cheng SCH**, Ying M, Wu VWC, Kowng DLW. Sonographic appearance of parotid glands after treatment with intensity-modulated radiotherapy or conventional radiotherapy for nasopharyngeal carcinoma. *Ultrasound Med Biol* 2009; 35: S213. (Abstract)

Publications

1. **Cheng SC**, Ying MT, Kwong DL, Wu VW. Sonographic appearance of parotid glands in patients treated with intensity-modulated radiotherapy or conventional radiotherapy for nasopharyngeal carcinoma. *Ultrasound Med Biol* 2011; 37: 220-230.
2. **Cheng SC**, Wu VW, Kwong DL, Ying MT. Assessment of post-radiotherapy salivary glands. *Br J Radiol* 2011; 84: 393-402
3. Ying MTC, **Cheng SCH**, Wu VWC, Kwong DLW. Post-radiotherapy morphological changes of parotid gland are dose- and radiotherapy technique-dependent. *Br J Radiol* 2011; 84: 1157
4. **Cheng SC**, Ying MT, Kwong DL, Wu VW. Sonographic appearance of submandibular glands in patients treated with external beam radiotherapy for nasopharyngeal carcinoma. *J Clin Ultrasound*. (*Submitted*)

5. **Cheng SC**, Wu VW, Kwong DL, Lu CY, Cheng AC, Kot BC, Ying MT. Sonographic appearance of thyroid glands in patients treated with intensity-modulated radiotherapy or conventional radiotherapy for nasopharyngeal carcinoma. *Thyroid. (Submitted)*

Acknowledgements

I have to thank Dr. Michael Ying, my chief supervisor, for his enormous support, guidance and patience to me during different difficulties and problems throughout this project, in particular for his invaluable advice on the study design, ultrasound scanning technique and statistical analysis.

I have to thank Dr. Vincent Wu, my co-supervisor, for his advice and support to my work. He paid great effort on supporting my radiotherapy knowledge and he played a crucial role in collaborating with different radiotherapy centres for my study.

I have to thank Prof. Dora Kwong, my clinical advisor, for her invaluable advice and comments for my study and manuscripts, and for all of her kind arrangement in data collection in Queen Mary Hospital.

I have to thank Dr. Ashley Cheng and Dr. Lui Cheuk Yu for their kind support and data collection arrangement in Princess Margaret Hospital

I would like to thank my friends and colleagues from the Department of Clinical Oncology in Queen Mary Hospital and those from the Department of Oncology in Princess Margaret Hospital for all of their efforts in subject recruitment, radiation dose evaluation and all the aspects in data collection arrangement.

I would like to thank all the teachers, supporting staff and friends from the Department of Health Technology and Informatics at the Hong Kong Polytechnic University, especially to those from Radiography and Medical Laboratory Sciences programmes, for their technical support in performing head and neck ultrasound scanning and thyroid function test.

I would like to thank my family and relatives for their indefinite support, patience, care and love.

Last but not least, I would like to extend my gratitude to all of my friends, especially to Dr. Brian Kot, Ms. Isabella Cheuk, Dr. Douglas Ng, Dr. John Yuen, Ms. Vivian Li, Ms. Esther Lee, Mr. Rico Hung, Ms. Holly Chen, Ms. Lilian Hui, Mr. Jeff Chu, Ms. Mong Lau, Ms. Yeung Chung Yan, Dr. Chow Ka Ho, Ms. Lau Ching Ching, Mr. Philip Wan, Mr. Derek Lo, Mr. Donald Ng and Mr. Newton Law, for their advice, unfailing support and encouragement.

Table of Contents

Certificate of Originality	i
Dedication	ii
Abstract	iii
Presentations and Publications Originating from the Present Study	vi
Acknowledgements	viii
Table of Contents	x
List of Figures	xiii
List of Tables	xvi
Chapter One Introduction	1
Chapter Two Literature Review	
2.1 Epidemiology of nasopharyngeal carcinoma.....	4
2.1.1 Etiology of NPC.....	4
2.1.2 Pathology of NPC.....	6
2.1.3 Investigation of NPC.....	7
2.2 Radiotherapy for NPC.....	8
2.2.1 Two-dimensional conventional radiotherapy.....	8
2.2.2 Intensity-modulated radiotherapy.....	10
2.3 Radiation-induced complications in salivary and thyroid glands.....	12
2.3.1 Overview of complications in salivary glands.....	12
2.3.2 Overview of complications in thyroid glands.....	40
2.4 Basis of this study.....	54

Chapter Three Study One: Sonographic appearance of parotid glands in patients treated with intensity-modulated radiotherapy or conventional radiotherapy for nasopharyngeal carcinoma

3.1 Introduction.....56

3.2 Materials and methodologies.....59

 3.2.1 Subjects.....59

 3.2.2 Equipment.....61

 3.2.3 Parotid gland ultrasound examination.....61

 3.2.4 Evaluation of parotid dose.....65

 3.2.5 Xerostomia questionnaire.....65

 3.2.6 Statistical analysis.....66

3.3 Results.....67

3.4 Discussion.....79

Chapter Four Study Two: Sonographic appearance of submandibular glands in patients treated with external beam radiotherapy for nasopharyngeal carcinoma

4.1 Introduction.....88

4.2 Materials and methodologies.....91

 4.2.1 Subjects.....91

 4.2.2 Equipment.....93

 4.2.3 Submandibular gland ultrasound examination.....93

 4.2.4 Statistical analysis.....97

4.3 Results.....98

4.4 Discussion.....105

Chapter Five Study Three: Sonographic appearance of thyroid glands in patients treated with intensity-modulated radiotherapy or conventional radiotherapy for nasopharyngeal carcinoma

5.1 Introduction.....111

5.2 Materials and methodologies.....115

 5.2.1 Subjects.....115

 5.2.2 Thyroid ultrasound examination.....117

 5.2.3 Thyroid function test.....124

 5.2.4 Evaluation of thyroid gland dose.....124

 5.2.5 Statistical analysis.....125

5.3 Results.....127

 5.3.1 Part I: Comparison between patients with normal thyroid function and those with abnormal thyroid function.....127

 5.3.2 Part II: Comparison between healthy subjects and patients treated with different radiotherapy techniques.....135

5.4 Discussion.....144

Chapter Six Summary of thesis.....155

References.....162

Appendix I.....176

Appendix II.....180

List of Figures

Figure 2.1: Schematic diagram shows the relative position of parotid gland within the lateral opposing facio-cervical field in conventional RT.....	9
Figure 2.2: Schematic diagram shows the relative position of parotid gland within the lateral opposing field in conventional RT.....	9
Figure 2.3: Computed tomography image shows the parotid glands out of the high dose region in IMRT.....	11
Figure 2.4: Schematic diagram shows the relative position of parotid gland and submandibular gland in the head and neck region.....	14
Figure 2.5: Fig. 2.2A shows an axial CT scan of skull in a NPC patient before radiotherapy. Fig. 2.2B shows an axial CT scan of a skull in the same patient after radiotherapy.....	32
Figure 2.6: Sonogram shows a transverse scan of a normal parotid gland, which is hyperechoic compared with the adjacent masseter muscle.....	35
Figure 2.7: Sonogram shows a longitudinal scan of a normal parotid gland with homogenous echotexture.....	36
Figure 2.8: Sonogram shows a transverse scan of a normal submandibular gland with homogenous echotexture.....	37
Figure 2.9: Sonogram shows a longitudinal scan of a parotid gland in a patient treated with conventional RT.....	39
Figure 2.10: Schematic diagram shows the relative position of thyroid gland in the cervical region using software Virtual Human Atlas 1.0.....	41
Figure 2.11: Sonogram shows a transverse scan of a normal thyroid gland with homogenous echotexture.....	47
Figure 3.1: Longitudinal grey scale extended field-of-view sonogram shows the measurement of the longitudinal dimension of a parotid gland in a patient treated with intensity-modulated radiotherapy.....	62
Figure 3.2: Transverse grey scale sonogram shows the measurement of the transverse dimension of a parotid gland in a healthy subject.....	62
Figure 3.3: Transverse grey scale sonogram shows the measurement of the echo-intensity of a normal parotid gland and the adjacent masseter muscle by outlining their boundaries using the software QLab™.....	64

Figure 3.4: Transverse grey scale sonograms show the parotid glands and the adjacent masseter muscles of a healthy subject, a patient treated with intensity-modulated radiotherapy and a patient treated with conventional radiotherapy.....	71
Figure 3.5: Longitudinal grey scale sonograms show the parotid glands of a healthy subject, a patient treated with intensity-modulated radiotherapy and a patient treated with conventional radiotherapy.	74
Figure 3.6: Longitudinal grey scale sonograms show the parotid glands in a healthy subject, a patient treated with intensity-modulated radiotherapy and a patient treated with conventional radiotherapy.....	76
Figure 3.7: Longitudinal grey scale sonograms show the parotid glands and the intra-parotid ducts in a healthy subject, a patient treated with intensity-modulated radiotherapy and a patient treated with conventional radiotherapy.....	78
Figure 4.1: Computed tomography image shows the submandibular glands within high dose region in the anterior cervical field.....	89
Figure 4.2: Transverse grey scale sonogram shows the measurement of the transverse dimension of a normal submandibular gland.....	94
Figure 4.3: Transverse grey scale sonogram shows the measurement of the echo-intensity of a normal submandibular gland and the adjacent mylohyoid muscle by outlining their boundaries using software QLab™	95
Figure 4.4: Transverse grey scale sonogram shows a normal submandibular gland.....	102
Figure 4.5: Transverse grey scale sonogram shows an irradiated submandibular gland.....	102
Figure 4.6: Transverse grey scale sonogram shows an irradiated submandibular gland.....	103
Figure 4.7: Transverse grey scale sonogram shows a small irradiated submandibular gland with marginally seen intra-glandular ducts.....	104
Figure 5.1: Computed tomography image shows the thyroid gland within the high dose region in the anterior cervical field.....	112
Figure 5.2: Transverse grey scale sonogram shows the measurement of the lateromedial dimension and anteroposterior dimension of the thyroid lobe in a patient with the neck treated with intensity-modulated radiotherapy.....	118
Figure 5.3: Longitudinal grey scale sonogram shows the measurement of the longitudinal dimension of the thyroid lobe in a patient with the neck treated with intensity-modulated radiotherapy.....	119

Figure 5.4: Transverse grey scale sonogram shows the measurement of the echointensity of a normal thyroid gland and the adjacent sternomastoid muscle by outlining their boundaries using the software QLab™120

Figure 5.5: Transverse Power Doppler sonogram shows the vascularity measurement of the thyroid lobe in a patient with his neck treated with intensity-modulated radiotherapy.....122

Figure 5.6: Sonograms demonstrated the extraction of colour pixel in the region of interest for the measurement of vascularity index of thyroid gland.....123

Figure 5.7: Transverse grey scale sonograms show the thyroid lobes (arrowheads) of a post-RT patient with normal thyroid function and of a post-RT patient with abnormal thyroid function.....132

Figure 5.8: ROC curve of the thyroid volume of the post-RT NPC patients.....134

Figure 5.9: ROC curve of the thyroid echogenicity index of the post-RT NPC patients.....134

Figure 5.10: Transverse power Doppler sonograms show the measurement of the thyroid vascularity in a patient with the neck treated with anterior cervical field, a patient with the neck treated with intensity-modulated radiotherapy and a healthy subject.....138

Figure 5.11: Transverse grey scale sonograms show the thyroid lobes in a patient with the neck treated with anterior cervical field, in a patient with the neck treated with intensity-modulated radiotherapy and in a healthy subject.....141

Figure 5.12: Transverse grey scale sonograms show the thyroid lobes in a patient with the neck treated with anterior cervical field, in a patient with the neck treated with intensity-modulated radiotherapy and in a healthy subject.....143

List of Tables

Table 3.1: Comparison of the mean transverse and longitudinal dimensions and the mean echogenicity index of the parotid glands in healthy subjects, and patients treated with conventional RT and those treated with IMRT.....	69
Table 3.2: Comparison of echogenicity, echogeneity, incidence of hypoechoic areas and conspicuity of intra-parotid ducts of parotid glands in healthy subjects, and patients treated with conventional RT and those treated with IMRT.....	72
Table 4.1: Comparison of the mean transverse dimension and the mean echogenicity index of submandibular glands between healthy subjects and post-RT NPC patients; between left and right sides (normal and irradiated); and between irradiated by 66 Gy and 60 Gy.....	99
Table 4.2: Comparison of echogenicity, echogeneity, incidence of hypoechoic areas, conspicuity of intra-glandular ducts and border sharpness of submandibular glands in healthy subjects and post-RT NPC patients.....	101
Table 5.1: Comparison of the mean thyroid volume, mean echogenicity index, mean vascularity index, mean number of thyroid nodules, mean TSH level and mean fT4 level of the thyroid glands in the post-RT NPC patients with normal thyroid function and those with abnormal thyroid function.....	129
Table 5.2: Comparison of echogenicity, echogeneity, incidence of nodules of thyroid glands in the post-RT NPC patients with normal thyroid function and those with abnormal thyroid function.....	131
Table 5.3: Comparison of the mean thyroid volume, mean echogenicity index, mean vascularity index, mean number of thyroid nodules, mean TSH level and mean fT4 level of the thyroid glands in healthy subjects, and NPC patients with their necks treated with IMRT and those with anterior cervical field.....	136
Table 5.4: Comparison of echogenicity, echogeneity, incidence of nodules of thyroid glands in healthy subjects, and patients with their neck treated with IMRT and those treated with anterior cervical field.....	140
Table 6.1: Summary of the sonographic appearance of parotid glands and submandibular glands in healthy subjects and NPC patients after radiotherapy.....	160
Table 6.2: Summary of the sonographic appearance of thyroid glands in healthy subjects and NPC patients after radiotherapy; and in the post-radiotherapy NPC patients with normal and abnormal thyroid functions.....	161

Chapter One

Introduction

Radiation-induced xerostomia and hypothyroidism from the damaged salivary and thyroid glands respectively are the common post-radiotherapy (post-RT) complications for nasopharyngeal carcinoma (NPC) and other head and neck cancers because salivary and thyroid glands are usually included in the radiation fields. Xerostomia and hypothyroidism adversely affect patients' health and quality of life. Early and accurate detection of radiation-induced changes in the glands allows early management of these complications. High-resolution ultrasound is commonly used in detecting morphological abnormalities in salivary and thyroid glands. However, the information about the use of ultrasound in evaluating post-RT salivary and thyroid glands is scarce. It is hypothesized that ultrasound is useful in the assessment of post-RT morphological changes of salivary and thyroid glands.

Radiation-induced xerostomia is the most common post-RT complication for head and neck cancer, especially in the conventional radiotherapy (RT). Xerostomia could lead to oral discomfort and oral infection, affecting patient's daily life. Parotid glands are prone to be irradiated with high dose in conventional RT due to their close proximity to the high dose zone of radiation. Nevertheless, with the recent introduction of the advanced technique of intensity-modulated radiotherapy (IMRT) in treating NPC, the radiation dose to parotid glands and the risk of xerostomia in the

patients have been significantly reduced (Lu and Yao 2008; Kubicek and Machtay 2008).

Ultrasound is useful in assessing superficial soft tissue structures including parotid glands. However, there is scant information in the literature about ultrasound evaluation of post-RT changes in the parotid glands. Available data is only limited to a single RT technique, and the sample size of the study was small (Ying et al. 2007). There is also lack of literature comparing the sonographic appearances of parotid glands in head and neck cancer patients treated with different RT techniques. This is one of the main objectives of this study and the details are presented in Chapter 3.

Apart from parotid glands, submandibular glands are also commonly irradiated during RT for head and neck cancers. Although saliva secretion in eating status is predominantly contributed by parotid glands, submandibular glands secrete more than 60% of saliva in the non-eating status, and hence the impairment of its function could adversely affect patient's quality of life after RT especially when the patients are not eating. Wada et al. (2009) reported that reduced function of the irradiated submandibular glands was the most influential reason for the severity of radiation-induced xerostomia. Hence, understanding the post-RT changes of submandibular gland could help understanding the cause of xerostomia and improving the assessment of this post-RT complication, which in turn, may help investigating methods to relieve the symptom and improve patients' quality of life. Ultrasound is useful in assessing submandibular glands but the information on post-RT evaluation

is scarce. The sonographic appearances of the submandibular glands in NPC patients treated with radiotherapy were therefore investigated in the present study and are presented in Chapter 4.

There is a high incidence rate of associated cervical lymph node metastases (around 60-96%) in NPC patients (Glastonbury 2007), and a separate anterior cervical field is routinely employed to treat the cervical lymph nodes of the patients. Since the anterior cervical field involved irradiation of thyroid glands, post-RT thyroid disorders including hypothyroidism are common in the patients (Alterio et al. 2007, Ulger et al. 2007, Bonato et al. 2008). Hypothyroidism presents with slow body movements, tiredness, depression, inability to tolerate cold etc. which could seriously impair patient's health and quality of life. Hence, an early detection of radiation-induced hypothyroidism or other associated thyroid disorders is necessary for early disease management in order to sustain patient's health status. Ultrasound has been widely used for assessing thyroid glands, but has not been commonly used in the evaluation of radiation-induced changes of thyroid glands. The sonographic appearances of thyroid glands in NPC patients with the cervical lymph nodes treated with different RT techniques, and the sonographic appearances of thyroid glands in post-RT patients with different thyroid function status were investigated in the present study. This information is presented in Chapter 5.

Chapter Two

Literature Review

2.1 Epidemiology of nasopharyngeal carcinoma

Nasopharyngeal carcinoma (NPC) is a common head and neck malignancy in Southern China and Southeast Asia with a fairly high incidence rate (15-50 per 100,000) (Chan et al. 2002). In Hong Kong, it is the fourth most common cancer in males and the 10th most common cancer in females, and it accounts for more than 5% of the total number of new cancer cases annually (Ching et al. 2003). The peak age of incidence of NPC is around 50-58 years old, and males are more vulnerable to NPC than females (Hong Kong Cancer Registry, 2009).

2.1.1 Etiology of NPC

Previous studies found that NPC is closely associated with three major factors including environmental factor, genetic factor and Epstein-Barr virus (EBV) infection (Chan et al. 2002, Chong and Ong 2008).

Since NPC is endemic in Southern China with fewer cases found in other regions like Europe and North America, NPC may be thus closely associated with environmental factor. A number of studies found that there is an association between

increased incidence of NPC and the consumption of preserved and pickle food in the Southern Chinese diet like Cantonese-style salted fish and preserved vegetables (Chan et al. 2002, Glastonbury 2007). Such association is particularly significant when those foods, which are widely accepted with the presence of carcinogenic nitrosamines, are firstly taken in the childhood stage (Vokes et al. 1997, Yu et al. 1998). Carcinogenic nitrosamines is associated with allelic loss on the short arms of chromosomes 3 and 9, inactivating certain tumor suppressor genes especially p14, p15 and p16, which results in the development of tumour in the nasopharynx (Chan et al. 2002).

Genetic factor also plays a crucial role in the development of NPC. It had been found that people with family history of NPC would have an increased risk of NPC, and the higher risk of NPC could occur in the existence of both genotypes of HLA A2 and HLA B_{sin2} on the same chromosome (Glastonbury 2007). Thus, it is believed that genetic factor is associated with the development of NPC.

In addition to environmental and genetic factors, NPC is also closely related to EBV infection. EBV could lead to the development of severe dysplasia (Chan et al, 2002). EBV infection had already been proven to be an early event of NPC development, which is evidenced by the existence of EBV DNA in both benign nasopharyngeal lesions and tumour cells of NPC (Glastonbury 2007). It was also found that increased amount of immunoglobulin IgG and IgA antibodies against EBV viral

antigen complexes are usually observed in the blood test of NPC patients (Glastonbury 2007, Heussinger et al. 2004).

2.1.2 Pathology of NPC

Generally NPC can be divided into three types based on its histo-pathology: Types I, II and III (Chan et al. 2002, Van De Graaff 2002). Fossa of Rosenmuller is the most common site of the origin of NPC (Saeed et al. 2001, Glastonbury 2007, Chong and Ong 2008). Type I NPC is squamous cell carcinoma, and is the least common form of NPC (Chan et al. 2002). It is more common in the non-endemic regions such as western countries, and its prognosis is the worst among the three types of NPC (Glastonbury 2007). Type I NPC is associated with cigarette smoking and alcohol consumption, and it can be subdivided into well, moderately and poorly differentiated forms in which the moderately and poorly differentiated Type I NPC are more common (Glastonbury 2007). Type II NPC is non-keratinizing carcinoma whilst Type III NPC is undifferentiated carcinoma (Chan et al. 2002). These two types of NPC are generally considered as the same disease because they are also non-keratinizing carcinoma, but Type III is more common than Type II (Glastonbury 2007). Compared with Type I NPC, Types II and III NPC are more common in both endemic and non-endemic regions, and have higher radiation sensitivity and better patient prognosis (Glastonbury 2007).

There is a high incidence of cervical lymph node metastases in NPC patients (60-90%) (Glastonbury 2007). Retropharyngeal nodes are the sentinel nodes of NPC, which are usually followed by upper jugular (level II) and spinal accessory (level V) nodal groups (Glastonbury 2007).

2.1.3 Investigation of NPC

Once NPC is suspected, a series of investigations is necessary to confirm or rule out the disease. There are several methods commonly used for the initial investigation of NPC including endoscopy, computed tomography (CT) and magnetic resonance imaging (MRI). In the endoscopy examination, biopsy of the suspected lesion can be obtained by endoscopic guided biopsy (EGB). However, such procedure is invasive and associated with a risk of haemorrhage (King et al. 2006). Moreover, the primary tumour of NPC tends to have submucosal spread to deeper nasopharyngeal or parapharyngeal structures, where EGB may miss the tumour because only a small fraction of nasopharynx can be sampled (King et al. 2006). In Hong Kong, although biopsy is a mandatory procedure providing histological information about NPC, CT and MRI are also commonly and complementarily used to investigate the extent of the disease as they delineate the morphology of nasopharynx, and help to visualize the peripheral structures where tumour may spread to such as skull base. CT and MRI generate cross-sectional images for localization and delineation of the tumour, which aid staging, prognosis estimation as well as treatment planning of the disease.

2.2 Radiotherapy for NPC

Radiotherapy is the treatment of choice for NPC because the primary tumour is relatively sensitive to radiation (Pow et al. 2006). Surgery is difficult in nasopharynx due to its deep seated anatomical location and is inaccessible by surgery (Pow et al. 2006). Early stage of NPC is usually treated by radical radiotherapy alone, while chemo- radiotherapy is recommended for more advanced stages (Lu and Yao 2008). With the use of appropriate treatment, the long term survival rate of the patients can be up to 90% for stage I disease (Liu et al. 2004).

2.2.1 Two-dimensional conventional radiotherapy

Two-dimensional conventional radiotherapy (conventional RT) has been used for the treatment of NPC before the introduction of 3-D conformal radiotherapy and intensity modulated radiotherapy (IMRT). In the conventional RT, two lateral opposing facio-cervical fields followed by 3 facial fields (1 anterior + 2 lateral opposing) are commonly used to deliver a tumour dose of 66 Gy (Figure 2.1 and 2.2). The subclinical regions including the oropharynx, sphenoid and parapharyngeal region (for those with parapharyngeal space involvement) are covered by the radiation fields (King et al. 2007). Proper shielding is applied at a predetermined distance from bony landmarks in order to protect the normal vital structures (Lu and Yao 2008).

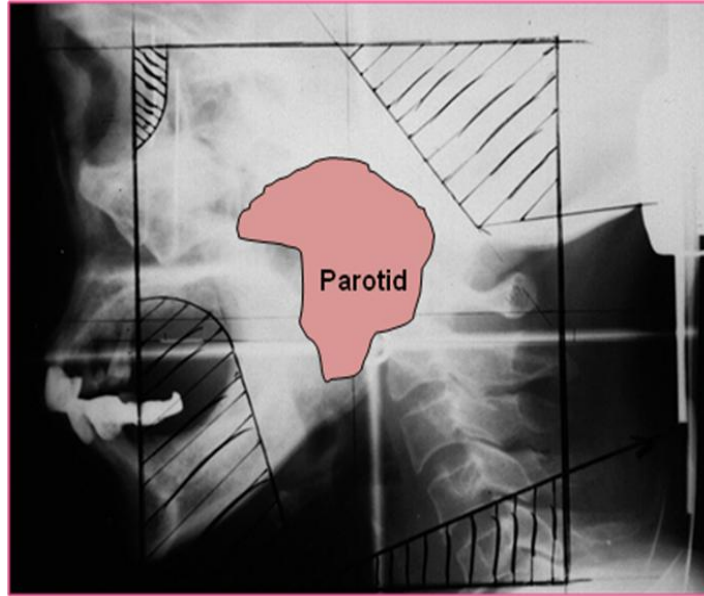


Figure 2.1: Schematic diagram shows that parotid gland is within the lateral opposing facio-cervical field (non-shaded region within the square) in conventional RT.

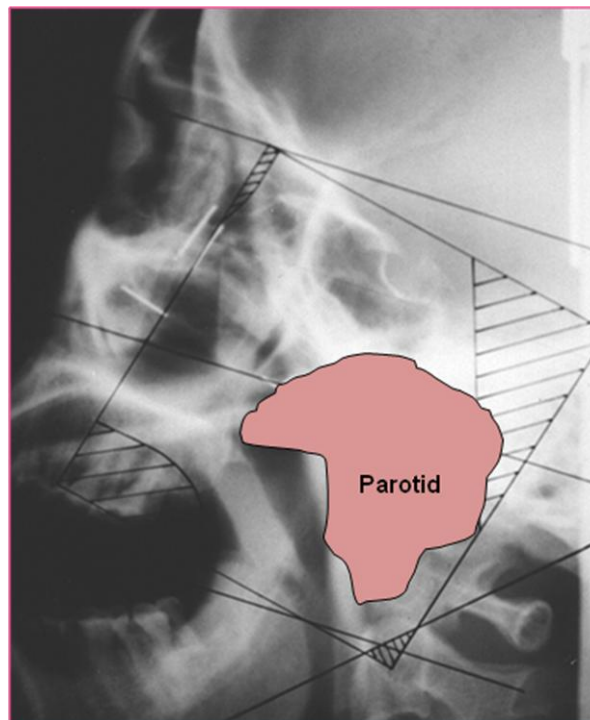


Figure 2.2: Schematic diagram shows that parotid gland is within the lateral opposing field (non-shaded region within the square) in conventional RT.

Neck lymphatics are usually irradiated by a separate radiation beam down to the supra sternal notch with a median block to spare the spinal cord and larynx (Ulger et al. 2007, Loevner et al. 2008). If the tumour extends to the parapharyngeal space, an additional posterior oblique cervical field will be applied to boost the dose to this area for another 10 Gy. However, conventional RT has been reported that it brings about various radiation toxicities. Conventional RT has limitations in shaping the dose distribution and thus it cannot effectively spare the organs at risk such as parotid glands, submandibular glands, pituitary gland, optic nerve, spinal cord, brain stem, inner ear and eustachian tube, which are incidentally covered by the radiation fields (King et al. 2007, Lu and Yao 2008). High radiation dose to these normal structures may damage their function and accordingly impair patients' quality of life (QOL) (King et al. 2007, Lu and Yao 2008).

2.2.2 Intensity-modulated radiotherapy

With the availability of more advanced radiotherapy techniques such as IMRT, better dose conformity to the target can be achieved and at the same time the normal structures can be better spared from radiation (Figure 2.3). With the use of advanced treatment planning system and multileaf collimator installed in the linear accelerator, IMRT can deliver multiple non-uniform radiation beam intensities from different directions. The desired radiation dose is obtained after the beams are superimposed at the target, which allows the radiation to better conform to the tumour target and

simultaneously reduces the radiation dose to the surrounding normal structures (Gregoire et al. 2007, King et al. 2007, Lu and Yao 2008). IMRT generates a steep dose gradient between the target and the adjacent normal tissues, which facilitates the delivery of higher radiation dose to the target than conventional RT, and limits the dose to the peripheral normal structures such as brain stem, parotid glands and temporomandibular joints (Eisbruch 2002, Lu and Yao 2008). Previous studies proved that IMRT not only improved the local tumour control, but also reduced treatment morbidity and hence improved patients' QOL (Eisbruch 2002, Gregoire et al. 2007, Lu and Yao 2008).

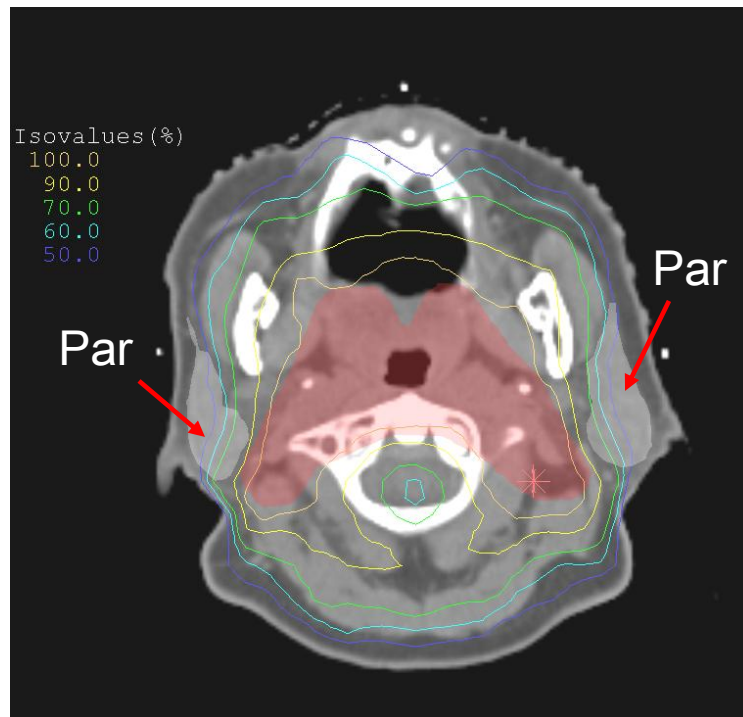


Figure 2.3: Computed tomography image shows that parotid glands (Par) are out of the high dose region in IMRT.

2.3 Radiation-induced complications in salivary and thyroid glands

Salivary glands are usually included in the radiation field during radiotherapy for NPC. At the same time, a large portion of the thyroid gland is also included in the anterior cervical field when treating the neck lymphatics. High radiation dose of radiotherapy could damage salivary and thyroid glands, leading to radiation-induced xerostomia and thyroid disorders respectively, which impairs patients' QOL. Xerostomia may lead to oral discomfort and oral infection, affecting patients' daily life and social activities; whilst thyroid disorders may affect thyroid hormonal level, triggering a number of associated complications like chronic fatigue, weight gain and cardio-vascular disease. Hence, early and accurate detection of radiation-induced complications in both salivary and thyroid glands allows early complication management for improving the QOL of the NPC survivors.

2.3.1 Overview of complications in salivary glands

2.3.1.1 Anatomy of salivary glands

There are three pairs of major salivary glands in human body namely parotid glands, submandibular glands and sublingual glands. Moreover, numerous minor salivary glands are also found in the oral cavity.

Parotid Gland:

Parotid gland is the largest salivary gland, which is located in the retromandibular fossa (Figure 2.4). It is anterior to external auditory meatus, inferior to zygomatic arch, posterior and superior to angle of mandible and anteriorly overlaps with masseter muscle (Shah 2002). It is composed of serous acinar cells, which produce serous saliva, mainly water in content. The imaginary plane formed by facial nerve divides the parotid gland into superficial and deep lobes (Shah 2002, Gritzmann et al. 2003). The main salivary duct of parotid gland is Stensen's duct which passes through buccinator muscle and enters the oral cavity through buccal mucosa at the upper second molar tooth level (Shah 2002). Parotid gland mainly secretes saliva in stimulated conditions like chewing, and it secretes up to 60% of total saliva during mastication (Eisbruch et al. 2003a).

Submandibular Gland:

Submandibular gland is the second largest salivary gland, which is located under the floor of the oral cavity (Figure 2.4), anterior and inferior to parotid gland, posterior and inferior to mylohyoid muscle and superior to digastrics muscle (Shah 2002, Gritzmann et al. 2003). Submandibular gland is composed of both serous and mucous acinar cells, which produce thicker and more viscous saliva. The main salivary duct of the submandibular gland is Wharton's duct which passes through sublingual space and enters the oral cavity near the lingual frenula (Shah 2002). Submandibular gland mainly secretes saliva in non-stimulated conditions and

contributes up to 90% of total salivary output at the resting state. It secretes 20-40% of total saliva in stimulated condition (Coppes et al. 2002, Eisbruch et al. 2003a).

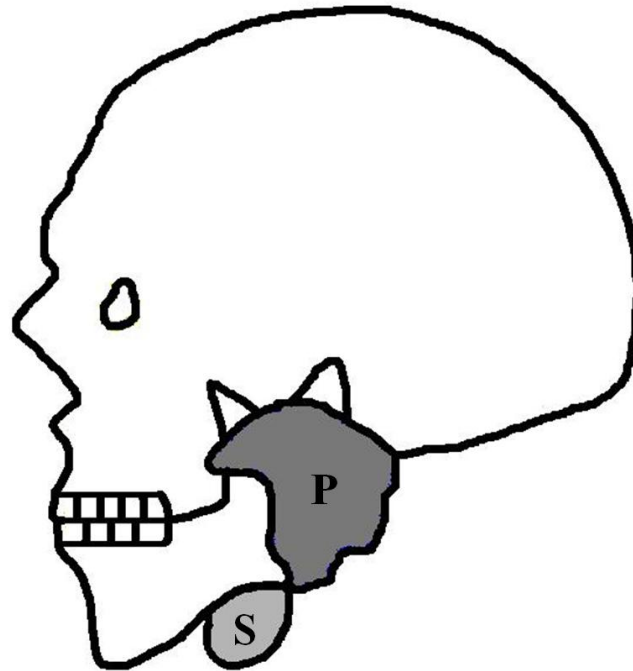


Figure 2.4: Schematic diagram shows the relative position of parotid gland (P) and submandibular gland (S) in the head and neck region. Parotid gland is located in the retromandibular fossa whilst submandibular gland is located under the mandible and in the floor of the oral cavity.

Sublingual Gland:

Sublingual gland is the smallest major salivary gland, which is located in the floor of the oral cavity, lateral to geniohyoid muscle, superior to mylohyoid muscle and medial to mandible (Shah 2002, Gritzmann et al. 2003). Similar to submandibular gland, sublingual gland is also composed of both serous and mucous acinar cells, which produce 2-5% of the total saliva upon stimulation (Eisbruch et al. 2003a). The

intraglandular ducts of sublingual glands may either drain into the Wharton's duct or empty into the floor of oral cavity directly (Shah 2002).

2.3.1.2 Radiation-induced Xerostomia

Major salivary glands are situated at the lateral facial and submandibular regions where they are commonly included into or close to the target volume in radiotherapy of head and neck cancers. Parotid glands are commonly irradiated with high radiation dose in conventional RT for some head and neck cancers like NPC, as they are usually in close proximity or within the radiation field. High radiation dose may damage salivary glands leading to xerostomia. Xerostomia is a symptom of oral dryness due to reduced salivary secretion from the impaired salivary glands. Saliva is produced by acinar cells and drained to the excretory duct through ductal cells, and finally secreted into the oral cavity (Astreinidou et al. 2007). Saliva is mainly composed of water (99.5%) and other components (0.5%) including amylase, inorganic salts, mucin and bicarbonate (Marmiroli et al. 2005). It is important in the normal daily life since saliva is responsible for moistening and softening food during ingestion, protecting oral mucosa and teeth, and breaking down starch by its amylase. Xerostomia may seriously impair the health-related QOL and even social activities of long term survivors after head and neck RT (Coppes et al. 2002, Eisbruch et al. 2003b, Nishimura et al. 2005). It is because xerostomia may lead to alterations in speech and taste, malnutrition and difficulty in mastication and deglutition (Eisbruch et al. 2003a&b, Chambers et al. 2004). Oral mucosal dryness can also change the

oral pH level and predispose to mucosal ulcerations, fissures, dental caries and oral infection (Vissink et al. 1990, Criswell and Sinha 2001, Eisbruch et al. 2003a).

Clinically, fractionated doses of 50 to 70 Gy are prescribed over 5 to 7 weeks (i.e. 2 Gy per day for 5 successive days per week) for common head and neck cancers (Shiboski et al. 2007). However, Eisbruch et al. (1999) reported that a mean dose of 26 Gy or above to the parotid gland showed significant decrease or immeasurable salivary flow upon stimulation. One must note that the radiation-induced xerostomia is an irreversible complication for the parotid gland received radiation with a mean dose of 26 Gy or above (Eisbruch et al. 1999). The study suggested that a mean dose of 26 Gy was a threshold dose for stimulated parotid glands. Other studies showed different thresholds of radiation dose for parotid gland ranging from 20 Gy to 40 Gy (Gregoire et al. 2007). Some studies however suggested that irreversible xerostomia could occur with a mean dose of over 60 Gy (Leek and Albertsson 2002, Shiboski et al. 2007). The discrepancy in different threshold mean doses might be due to different methodologies used in these studies, such as different radiotherapy techniques, treatment protocols and methods in assessing salivary function.

Although reduced risk of xerostomia with the use of intensity modulated radiotherapy (IMRT) has been reported, IMRT may not always achieve the suggested mean threshold dose for parotid glands because extensive tumours situated close to the parotid glands in advanced diseases inevitably deliver high dose to the glands (Saarilahti et al. 2006, Gregoire et al. 2007, Munter et al. 2007, Lu and Yao

2008). Kwong et al. (2004a) reported that the mean dose of the parotid glands could be as high as 32.0 Gy to 46.1 Gy for early stage NPC patients treated with IMRT. Besides, Eneroth et al. (1972) found that radiation dose as low as 2 to 3 doses of 2 Gy could cause radiation-induced xerostomia. It has also been found that a significant decrease in salivary secretion could appear in the first week of radiotherapy (Franzen et al. 1992). Hence, head and neck cancer patients treated with radiotherapy could develop different degrees of xerostomia. In order to accurately assess post-RT changes of salivary glands or xerostomia, different assessment methods have been reported in the literature. Improvement in the assessment of xerostomia or salivary gland function may allow more accurate evaluation of the dose conformity to the target and the normal structure sparing capability of advancing radiotherapy technologies in the head and neck. Accurate assessment of salivary gland morphological and functional changes after radiotherapy may also help better understanding of the mechanism of post-RT xerostomia which in turn aids the investigation of methods to relief the conditions of xerostomia and improve the QOL of the patients. It is also important to identify the post-RT changes of the salivary glands and differentiate them from other salivary gland diseases to ensure accurate diagnosis and appropriate disease management of this group of patients.

Currently there are various methods for the assessment of post-RT salivary glands and radiation-induced xerostomia, which include questionnaire, histological

evaluation, sialometry, magnetic resonance imaging, scintigraphy, computed tomography and ultrasonography .

2.3.1.3 Xerostomia Questionnaire

Xerostomia questionnaire has been used in assessing the QOL of patients with radiation-induced xerostomia. Some questionnaires have been validated to evaluate the QOL of post-RT xerostomic patients by assessing the easiness or difficulty of different oral activities in their daily life (Zimmerman et al. 1997, Eisbruch et al. 2001).

In order to quantify the QOL of patients with xerostomia, a visual analog scale or an 11-point ordinal Likert scale is usually used to evaluate the oral dryness or oral discomfort of the patients (Zimmerman et al. 1997, Eisbruch et al. 2001, Chambers et al. 2004). The summation of the score of each item (xerostomia score) in the questionnaire is used to indicate the severity of xerostomia of the patient (Eisbruch et al. 2001).

Eisbruch et al. (1999) showed that the xerostomia score obtained from the patients after head and neck RT was significantly higher than the score obtained from the same group of patients before RT. This demonstrated that xerostomia questionnaire could detect oral discomfort due to reduced salivary secretion after radiotherapy. In the follow-up examinations, significant decrease in xerostomia scores was found in

patients indicating improvement in oral dryness and discomfort. Besides, Eisbruch and colleagues (2003b) reported a lower xerostomia score (less oral dryness) in patients receiving radiotherapy with parotid glands sparing than those treated with conventional radiotherapy.

There are limitations of using questionnaires in the assessment of xerostomia. The assessment method is subjective, and does not provide quantitative analysis of the function of the salivary glands. There was a weak correlation between xerostomia score and the salivary flow (Franzen et al. 1992, Liem et al. 1996, Eisbruch et al. 2001). The weak correlation may be due to the large variation in the normal salivary flow rate and the discrepancy between mucosa hydration status and salivary output (Eisbruch et al. 2001). Moreover, oral sensory change or alteration in the perception of oral dryness in the mucosal tissue may occur after radiotherapy (Fox et al. 1987).

2.3.1.4 Histological Evaluation

Histological evaluation can assess post-RT changes of salivary glands because functional change is closely related to histological change (Radfar and Sirois 2003). In the animal studies, it was found that normal parotid glands were characterized by homogenous pure serous acinar cells with densely packed translucent granules and branching intercalated ducts (Henriksson et al. 1994, Eisbruch et al. 2003a, Radfar and Sirois 2003). The densely packed acini and the intercalated ducts were surrounded by myoepithelial cells (Henriksson et al. 1994). Acini were well

differentiated from the interlobular excretory ducts and the striated ducts (Henriksson et al. 1994). On the other hand, a normal submandibular gland consisted of both mucous and serous acinar cells and they were slightly vacuolated (Radfar and Sirois 2003).

Radfar and Sirois (2003) investigated the histological changes in salivary glands of Hanford minipigs (a small-sized pig which is a common animal model used to examine post-RT salivary gland damage) following a fractionated irradiation scheme of 70 Gy, which was commonly prescribed in human head and neck cancer radiotherapy. They found that both irradiated parotid and submandibular glands were characterized by parenchymal loss, acinar atrophy and interstitial fibrosis, duct proliferation, dilated intercalated and striated duct. Loss of secretory granules in acinar cells, and infiltration of inflammatory cells like lymphocytes and plasma cells were also found. However, acinar destruction and degranulation were more obvious in submandibular glands, suggesting that histological change in submandibular glands was more prominent than that in parotid glands. Price et al. (1995) performed a similar study on monkeys with 50-55 Gy of irradiation, and they found similar histological changes in post-RT parotid and submandibular glands. In addition, they also found that the size of parotid and submandibular glands was reduced after irradiation (Price et al. 1995). However, due to size reduction of the salivary glands, Price et al. (1995) argued that there should be an increase in number of ducts per unit volume in each gland rather than duct proliferation as reported by Radfar and Sirois (2003). Moreover, Henriksson et al. (1994) found mast cells and hyaluronic acid

infiltration in irradiated salivary glands of rats, and they believed that the presence of mast cells and hyaluronic acid might be the key elements in activating fibrosis in the glands after radiotherapy.

Grehn et al. (1997) performed an animal study and reported that the loss of acini in parotid glands was dose dependent. With a radiation dose of 30 Gy, there was a slight decrease in acinar cells from 75.2% in the non-irradiated glands to 69.8% in the irradiated glands. However, with 40 Gy, a more significant decrease in acinar cells from 77.3% in non-irradiated glands to 31.9% in irradiated glands was found. Compared to 30 Gy, a radiation dose of 40 Gy induced over 50% reduction in parotid acinar density.

Histology can provide information about the histological variation of post-RT salivary glands. However, the accuracy of histological findings could be influenced by aging. Aging causes loss of acinar cells in which around 30% of acinar tissue would be lost between 20 and 90 years of age (Tylenda et al. 1988). Scott (1987) reported that uniform and densely packed parenchymal tissue of submandibular glands in the young people would be replaced by loosely fibro-adipose tissue with advancing age.

Although the value of histological examination in assessing post-radiation salivary glands has been reported in animal studies, histological evaluation of salivary glands has not yet been established in clinical practice for humans. It is because xerostomia

is not a life threatening condition, and the conduction of the risk-bearing gland biopsy may not be justified for routine clinical practice. Biopsy is an invasive procedure and it may cause complications such as infection, poor wound healing and fistula formation (Becker et al. 1997). Hence, safer or non-invasive assessment methods such as salivary flow measurement or medical imaging are commonly employed in assessing xerostomia clinically. Nevertheless, histological studies based on animal model have provided an invaluable insight in predicting the radiation response or post-RT changes of salivary glands in human population.

2.3.1.5 Sialometry

Sialometry (salivary output measurement) has been widely used in assessing salivary gland function. It directly measures the function of salivary glands, and can be classified into the whole mouth salivary output measurement and selective salivary gland output measurement. Both methods involve the collection of saliva over a period of time (usually for at least 5 minutes), and hence the saliva volume and the salivary flow rate (usually expressed as mL/minute) can be determined (Eisbruch et al. 2003a). In sialometry, both un-stimulated and stimulated salivary outputs are measured in order to assess salivary gland function at rest and upon stimulation such as eating (Eisbruch et al. 2003a).

Whole mouth salivary output measurement can be simply achieved by drainage, spitting or weighting the cotton wool balls soaked with saliva in the mouth (Eisbruch

et al. 2003a). The procedure is fast, easily performed and inexpensive, however it cannot evaluate the function of the individual salivary gland. Parotid saliva collection can be done by catheterization of the Stensen's duct or using a suction cup such as Lashley cup and Carlson-Crittenden cup attached to the buccal mucosa surrounding to the duct orifice (Eisbruch et al. 1999, 2001&2003a, Astreinidou et al. 2007). On the other hand, submandibular saliva can be collected by gentle suction at the Wharton's duct orifice of the submandibular gland using micropipette (Fox et al. 1987, Tylenda et al. 1988). Nevertheless, submandibular secretion is actually the combination of saliva from the submandibular gland and sublingual gland as the sublingual saliva also drains into Wharton's duct (Kohn et al. 1992, Eisbruch et al. 2001, Shah 2002). Therefore, evaluation of submandibular secretion and function by this method should be performed with caution.

Previous studies have used sialometry in the investigation of post-RT changes of salivary glands. Eisbruch et al. (1999) found that parotid glands receiving a mean dose higher than 24 Gy and 26 Gy showed no measurable salivary flow and did not recover 12 months after the completion of RT. Hence, 24 Gy and 26 Gy were the respective threshold dose of un-stimulated and stimulated salivary flow. In addition, Eisbruch et al. (2001) studied 84 head and neck cancer patients who received conformal RT and IMRT throughout a 2-year post-RT follow-up, and both stimulated and un-stimulated parotid salivary flows were investigated. They demonstrated that in bilateral neck irradiation group, the salivary flow rate of contralateral parotid glands receiving a mean dose of 21.9 Gy decreased in the early

post-RT period but increased persistently afterward and nearly returned to the pre-radiotherapy (pre-RT) level after 12 months. The contralateral parotid glands in unilateral neck irradiation group receiving relatively lower doses (mean dose of 4.1 Gy) showed continuous salivary flow improvement during the second year after radiotherapy and even higher than the pre-RT level, indicating a compensatory mechanism (Eisbruch et al. 2001, Astreinidou et al. 2007). However, in both bilateral and unilateral neck irradiation groups, no salivary flow could be detected in the ipsilateral parotid glands which received mean dose higher than 30 Gy (Eisbruch et al. 2001). Submandibular glands in unilateral neck irradiation group demonstrated retention of about 50% of the pre-RT salivary flow in the first 3 months after RT, but the flow rate increased persistently to the pre-RT level after one year (Eisbruch et al. 2001). Besides, Eisbruch et al. (2001) only measured the total output of both submandibular glands but the contralateral glands received much lower mean dose compared to the ipsilateral glands (14.7 Gy vs. 51.4 Gy). Therefore, they believed that the salivary output was mainly contributed by the contralateral glands. In the bilateral neck irradiation group, the salivary flow rates of submandibular glands remained very low in most patients, in which ipsilateral and contralateral glands received mean doses of 66.9 Gy and 57.6 Gy respectively (Eisbruch et al. 2001).

Pow et al. (2006) used sialometry to study the sparing of salivary gland in IMRT for NPC. They found that both stimulated parotid and whole mouth salivary flow were higher in IMRT compared with conventional RT at 2, 6 and 12 months after

radiotherapy. Also, the recovery of salivary flow was only noted in patients receiving IMRT but not in the conventional RT group.

Although sialometry can directly measure the salivary gland function, there are limitations in the evaluation of post-RT salivary functional change. The low reproducibility of sialometry may lead to inconsistent results of the assessment (Eisbruch et al. 2003a). Besides, aging may also be a factor leading to the decrease in salivary flow rate, which affects the accuracy of post-RT salivary gland assessment (Baum 1981, Tylanda et al. 1988, Kohn et al. 1992).

2.3.1.6 Magnetic Resonance Imaging

MRI is a useful imaging modality for follow-up of head and neck cancer patients treated with high-dose radiotherapy (Becker et al. 1997). MRI has excellent spatial resolution, and it is superior to CT in delineating soft tissue structures. Moreover, it does not involve ionizing radiation; and allows visualization of the deeply situated tissues such as the deep lobe of parotid gland (Lee et al. 2008b).

Nomayr et al. (2001) evaluated the appearances of radiation-induced changes in normal cervical structures including salivary glands using MRI. They found that volume reduction in parotid glands occurred after radiotherapy of 60-70Gy; and hyperintense signal was detected in 22% of post-RT parotid glands, and 31% of post-RT submandibular glands in T2-weighted (T2W) images. In follow-up

examinations, the signal intensity of the glands decreased in T2W images but the gland volume persistently reduced (Nomayr et al. 2001). Volume reduction and increased signal intensity in salivary glands after radiotherapy were also documented in other studies using MRI for post-RT evaluation (Marmioli et al. 2005, Wada et al. 2009). Increased signal intensity in T2W images suggested the presence of oedema in the glands due to the damage of blood and lymph vessels and hence resulted in reduced lymph transport with accumulation of interstitial fluid (Calcaterra et al. 1972, Nomayr et al. 2001).

Nomayr et al. (2001) found that there was volume reduction of parotid glands in all patients with primary head and neck tumours after radiotherapy, and such volume reduction might be due to the loss of acinar cells. It is believed that reduced gland parenchyma is mainly due to serous acinar cell loss. Larger extent of parenchyma loss would occur in parotid glands compared to submandibular glands upon irradiation since parotid glands constituted more serous acini (Nomayr et al. 2001). Parotid glands are therefore believed to be more radiosensitive than submandibular glands. However, the difference in the radiosensitivity of parotid and submandibular glands is still controversial because some studies reported the radiosensitivity in parotid and submandibular glands should be similar as they were equally vulnerable to RT (Coppes et al. 2002, Saarilahti et al. 2006, Munter et al. 2007).

Apart from conventional MRI, a more advanced MRI technique named magnetic resonance sialography (MR sialography) is becoming popular in the clinical

assessment of radiation-induced changes in salivary glands. MR sialography uses heavily T2W sequence to show salivary ducts, and saliva appears as hyperintense signal whilst the surrounding salivary gland tissues appear hypointense (Marmioli et al. 2005, Astreinidou et al. 2006). Unlike conventional X-ray sialography, MR sialography does not involve any ionizing radiation and cannulation of the salivary ducts, and does not require introduction of contrast medium, avoiding uncomfortable feeling during the procedure, radiation risk and possible allergy to patients. Astreinidou et al. (2006) showed that MR sialography could provide high quality three-dimensional images of both parotid and submandibular ductal architectures with high reproducibility. They suggested that MR sialography could be used in follow-up examinations to detect the location of potential radiation-induced changes in salivary ducts in post-RT patients. Astreinidou et al. (2007) also found that there was no significant change in the visibility of the salivary ducts in post-RT compared to pre-RT stage in a low dose level of below 20 Gy. However, reduced visibility of the ducts occurred in the salivary glands that received more than 20 Gy, and increased visibility happened in 6 months post-RT when compared to 6 weeks post-RT, indicating that there was a recovery mechanism of the gland (Astreinidou et al. 2007). Wada and colleagues (2009) also noted the poor visualization of the intra-glandular ducts (main ducts and branches) in stimulated post-RT parotid and submandibular glands, indicating radiation-induced injury of the glands. It has been reported that the poor visualization of small intra-parotid ducts on MRI after RT may be due to the increased signal intensity in post-RT salivary gland tissues or damage of the ducts (Astreinidou et al. 2007).

Although MRI is capable to show post-RT morphological changes in salivary glands and salivary ducts, it has a number of limitations which have restricted its wide clinical application. MR sialography is not effective to detect or visualize small branches of the salivary ducts (Shah 2002). Compared with other imaging modalities, MRI is relatively expensive and more susceptible to motion artifacts due to its long image acquisition time (Lee et al. 2008b). Also, MRI is not suitable for claustrophobic patients or patients with metallic implants such as pace-makers, bullets, non-MRI compatible surgical clips and other ferromagnetic implants (Shah 2002).

2.3.1.7 Scintigraphy

Salivary gland scintigraphy has been used in the assessment of salivary gland function including the post-RT salivary gland functional change. It makes use of the absorption and excretion properties of radio-isotopes such as ^{99m}Tc-Technetium pertechnetate (Tc-99m) at the salivary glands for functional assessment (Kohn et al. 1992, Marmiroli et al. 2005). It has been found that Tc-99m is readily trapped and secreted in the ductal epithelium of salivary glands and excreted in the saliva, which allows salivary gland scintigraphy to perform and provides quantitative information on the glandular function (Liem et al. 1996, Anjos et al. 2006). Apart from its minimum invasiveness, the low radiation dose and good patient tolerance, no interference with the normal physiology of the salivary glands, and readily available of Tc-99m makes scintigraphy valuable to salivary functional studies (Kohn et al.

1992, Anjos et al. 2006). In scintigraphy, different parameters were used to assess the salivary gland function such as time-activity curve analysis, visual interpretation, salivary target to background ratio and salivary excretion fraction (SEF) (Hermann et al. 1999). However, there was a lack of standardization of using some parameters to interpret the salivary scintigrams. Among different assessment parameters, SEF was commonly used to assess radiation-induced xerostomia or other salivary gland diseases (Kohn et al. 1992, Liem et al. 1996, Van Acker et al. 2001, Tenhunen et al. 2008).

Liem et al. (1996) found that post-RT salivary glands tended to show impaired saliva excretion with large amount of radiopharmaceutical (i.e. Tc-99m) retained in the salivary glands, and there was no decline in time-activity curves even the glands were stimulated. As damaged salivary glands failed to excrete saliva into the oral cavity, the radiopharmaceutical thus could not be removed by the saliva from the gland, and was accumulated within the gland. They also found that there was a dose-response relationship of both parotid and submandibular glands, which demonstrated that higher radiation dose to the glands caused greater reduction in SEF of the salivary glands. A rapid decrease in SEF could occur in salivary glands received radiation dose of 30-70 Gy as early as one month after RT, but SEF could remain unchanged in the glands received radiation less than 24 Gy. Persistent decrease in SEF in 6 and 12 months after radiotherapy was seen in both parotid and submandibular glands received more than 30 Gy of radiation (Liem et al. 1996). Kohn et al. (1992) also demonstrated a positive correlation between the salivary flow

rate and the scintiscan rating (the summary score of different salivary gland scintigram parameters including initial uptake of the tracer, appearance of unstimulated radionuclide in the oral cavity, radiopharmaceutical concentration in the glands and response to stimulation) of salivary gland scintigraphy in xerostomia patients.

Although salivary gland scintigraphy could reflect the functional change of salivary glands after radiotherapy, its spatial resolution was low and was not suitable for the evaluation of morphological change of the glands (Kohn et al. 1992). Moreover, scintigraphy may not be sensitive enough in detecting slight changes in salivary gland excretion (Cooper et al. 1999). Besides, Hermann et al. (1999) found that SEF could only distinguish Sjogren's syndrome or radiation damage from normal salivary glands but not from each other, which reflected the poor specificity of scintigraphy in identifying radiation-induced injury in salivary glands. The complexity of the procedures including a range of patient's preparation and cooperation such as fasting and post-imaging radiation management, and the involvement of ionizing radiation restrict the use of scintigraphy in routine clinical assessment of salivary gland function.

2.3.1.8 Computed Tomography

CT has been widely used in head and neck cancer imaging. However, there is scant information regarding the application of CT in post-RT salivary gland evaluation.

CT has been proven to be an effective imaging method in the assessment of salivary glands with nearly 100% sensitivity in detecting salivary gland lesions (Nomayr et al. 2001, Lee et al. 2008b). A normal parotid gland is a fatty glandular tissue encapsulated by a dense capsule, which is shown as a radiolucent structure in CT compared to the surrounding muscles (Bryan et al. 1982, Bronstein et al. 1987). In CT, parotid ducts are hardly seen. However, the introduction of iodinated contrast medium, via intravenous injection, increases the sensitivity in the detection of parotid ducts (Bryan et al. 1982, Larsson et al. 1987). CT can also demonstrate the entire physical volume of the parotid glands.

In CT, the superficial portion of a normal submandibular gland is usually shown as a globular soft tissue structure superior and lateral to the hyoid bone on CT images (Bryan et al. 1982). It is more radio-opaque than parotid gland but with a similar opacity to the adjacent muscle (Bryan et al. 1982, Bronstein et al. 1987). The deep portion of the submandibular gland and the intra-glandular ducts are also well visualized on CT scans (Bryan et al. 1982).

Bronstein et al. (1987) reported an increased image density in post-RT salivary glands on contrast-enhanced CT scan (Figure 2.5). They found that the increased image density was associated with high dose of irradiation of the glands (> 45 Gy). Both parotid and submandibular glands showed similar degree of increased image density after RT, and the increased image density might be due to the contrast

medium stored in the expanded extracellular space resulted by the loss of acinar cells after radiotherapy (Bronstein et al. 1987).

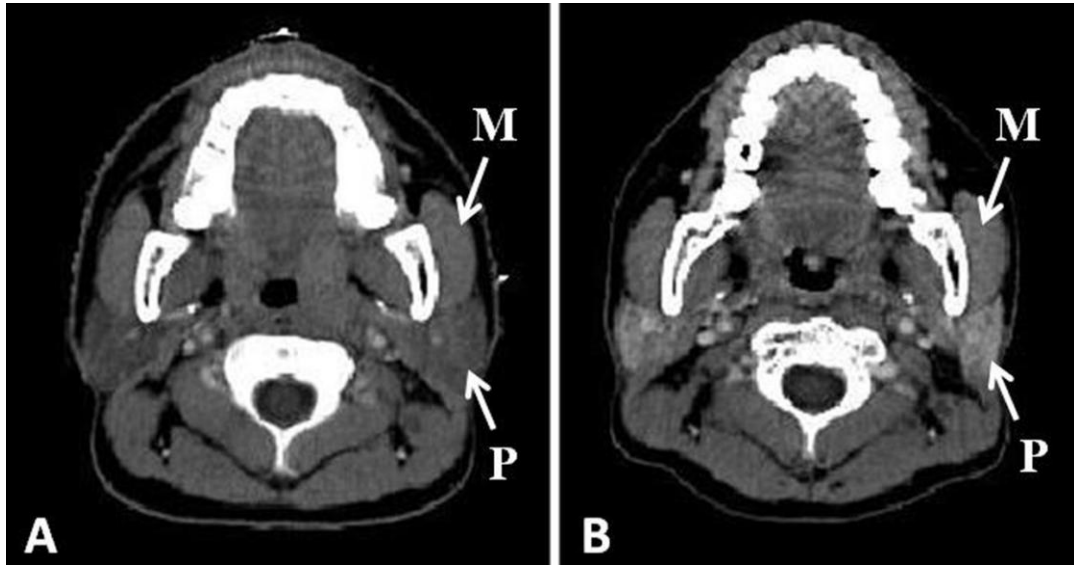


Figure 2.5: Fig. 2.5A shows an axial CT scan of skull in a NPC patient before radiotherapy. The image density of the parotid gland (P) is about the same as the adjacent masseter muscle (M). Fig. 2.5B shows an axial CT scan of a skull in the same patient after radiotherapy. There is an increased image density of the parotid gland (P) when compared to the pre-radiotherapy scan. The image density of the parotid gland is greater than that of the adjacent masseter muscle (M).

Since CT generates cross-sectional images of the region of interest, localization and volume determination of organs and lesion are possible. Previous studies found that there was a decrease in parotid gland volume with a rate of 0.6-0.7% volume loss per day during radiotherapy for head and neck cancers, and the median parotid volume loss at the end of treatment was 21.3% (Lee et al. 2008a) and 28.1% (Barker et al. 2004). Apart from volume reduction, medial shift of parotid gland with median values of 5.26 mm (Lee et al. 2008a) and 3.1 mm (Barker et al. 2004) after

radiotherapy was also noted. The reduced volume and positional change of salivary glands are important for physicians to determine the post-RT changes in salivary glands and treatment planning since the change in volume or position may lead to a higher dose received by the glands than expected in the initial treatment planning, especially in IMRT (Lee et al. 2008a). Hence, re-planning within the treatment course may be necessary to ensure the optimal treatment outcomes.

There are some limitations in using CT to assess post-RT salivary gland changes. Increased image density of salivary glands occurred in radiation dose higher than 45 Gy but salivary gland dysfunction or radiation-induced xerostomia can happen with a radiation dose below 45 Gy (Franzen et al. 1992, Tartaglino et al. 1994, Gregoire et al. 2007). Also, increased image density was noted in salivary gland tumour and hence, image density variations of the glands might not be an accurate indicator to show post-radiation changes (Bronstein et al. 1987). Moreover, decrease in CT number of salivary gland due to aging and increase in adipose tissue (Heo et al. 2001); and spray artifact from dental filling would also limit the use of CT on salivary gland diagnosis (McGahan et al. 1984). CT involves ionizing radiation and iodinated contrast medium is usually required for the examination, which increase the risk of radiation and risk of allergic reaction towards the contrast agents. The use of contrast medium in CT is also contraindicated to patients with poor renal function.

2.3.1.9 Ultrasonography

Ultrasonography is widely used in cancer imaging and screening as it is safe, non-invasive, inexpensive, highly available and carries no radiation hazard (Kotecha et al. 2008). High-resolution ultrasonography is useful in delineating superficial soft tissue structures including those in head and neck regions like thyroid gland, lymph nodes and salivary glands. Although ultrasonography is commonly used in the assessment of salivary gland diseases like neoplasms, Sjogren's syndrome, sialadenitis and sialolithiasis, there is scant information in the literatures about the ultrasound evaluation of radiation-induced xerostomia or post-RT changes in the salivary glands (Ying et al. 2007).

Ultrasonography allows visualization of the whole submandibular gland, sublingual gland and the superficial lobe of the parotid gland. However, the deep lobe of parotid gland cannot be assessed by ultrasound because it is obscured by the acoustic shadow of the mandibular ramus (Gritzmann 1989, Gritzmann et al. 2003, Bialek et al. 2006). In ultrasonography, a normal parotid gland appears as a homogenous speckle pattern structure (Bialek et al. 2006, Chikui et al. 2006). Parotid gland is markedly or slightly hyperechoic compared to the adjacent muscle (Figure 2.6), and the echogenicity is determined by the amount of fatty glandular tissue deposited in the gland (Howlett 2003, Bialek et al. 2006). Normal parotid lymph nodes are usually observed at the pre-auricle level or at the tail of the gland, which

demonstrated as hypoechoic oval structures with or without hyperechoic central hilus (Howlett 2003, Ying et al. 1996). Normal intra-glandular ducts are rarely visualized but they may appear as slight echogenic linear structures (Figure 2.7) (Gritzmann et al. 2003, Howlett 2003).

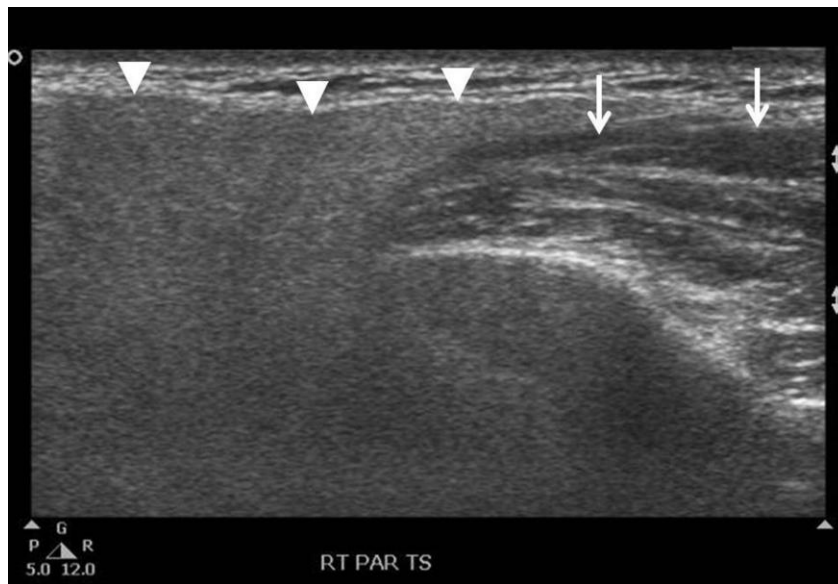


Figure 2.6: Sonogram shows a transverse scan of a normal parotid gland (arrowheads), which is hyperechoic compared with the adjacent masseter muscle (arrows).



Figure 2.7: Sonogram shows a longitudinal scan of a normal parotid gland with homogenous echotexture. The intra-glandular ducts (arrows) are marginally seen.

A normal submandibular gland is ultrasonographically shown as a triangular structure in the transverse scan plane (Gritzmann et al. 2003). Similar to the parotid gland, the normal submandibular gland appears as a homogenous structure and is markedly or slightly hyperechoic when compared to the adjacent muscle (Figure 2.8) (Gritzmann 1989, Bialek et al. 2006). The normal non-dilated intra-glandular ducts of the submandibular gland are rarely seen ultrasonographically (Gritzmann et al. 2003).



Figure 2.8: Sonogram shows a transverse scan of a normal submandibular gland (arrowheads) with homogenous echotexture. The gland is hyperechoic compared to the adjacent mylohyoid muscle (black arrows) and the intra-glandular ducts (white arrows) are marginally seen.

To the best of our knowledge, there is only one study which had documented the post-RT changes of salivary gland ultrasonographically. Ying et al. (2007) used high-resolution ultrasound to compare the sonographic appearances of normal and post-RT parotid glands. They found that grey-scale ultrasound could be used to assess the size, echogenicity and internal architecture of the parotid glands. The post-RT parotid glands appeared as a heterogeneous structure, and were hypo- or isoechoic relative to adjacent muscles, with multiple hyperechoic lines or spots and hypoechoic areas (Figure 2.9). Higher conspicuity of intra-parotid ducts was noted in post-RT parotid glands compared to the normal group. The heterogeneous appearance of the post-RT glands might be due to the patches of inflammatory

infiltrate appearing as multiple hypoechoic areas; whilst the presence of the hyperechoic lines or spots might reflect fibrosis (Ying et al. 2007). Fibrosis was characterized with hyperechoic lines of irregular course and thickness but not parallel to each other, in contrary to the intra-parotid ducts which were demonstrated as hyperechoic lines with regular course and thickness and parallel to each other (Ying et al. 2007). Higher conspicuity of intra-parotid ducts in the post-RT parotid glands might be due to fibrosis or proliferation of the ducts, which provided higher reflective interfaces for ultrasound beam and thus, increased ductal echogenicity (Ying et al. 2007). In Doppler ultrasound, the authors found that the mean peak systolic velocity (PSV), resistive index (RI) and pulsatility index (PI) of normal parotid glands were significantly higher than that of post-RT parotid glands (Ying et al. 2007). The relatively lower vascular resistance and PSV in post-RT parotid glands might be due to the lower compression pressure on the vessels by the reduced number of surrounding acinar cells and granules (Ying et al. 2007). Although this study documented the sonographic appearances of the post-RT parotid glands, the sample size of the study was small (n=10). Moreover, the study focused on the assessment of the parotid glands in NPC patients treated with conventional radiotherapy.



Figure 2.9: Sonogram shows a longitudinal scan of a parotid gland in a patient treated with conventional RT. There are multiple hypoechoic areas (arrows) within the gland, and the intra-glandular ducts (arrowheads) are obviously seen.

There are few limitations of using ultrasonography in assessing the post-RT changes in the salivary glands. The reported sonographic appearances of the parotid gland in the Sjogren's syndrome were similar to those observed in the post-RT parotid changes, including heterogeneous echotexture, multiple hypoechoic areas and multiple hyperechoic lines or spots (Miedany et al. 2004, Niemela et al. 2004, Shimizu et al. 2006). Such similarity in sonographic appearances could make confusion in differentiating post-RT changes with Sjogren's syndrome, leading to inaccurate diagnosis. Besides, ultrasound could not evaluate the deep lobe of the parotid gland as it is obscured by the acoustic shadow of the ramus of mandible (Gritzmann et al. 2003, Bialek et al. 2006). Therefore, the size of the parotid gland

cannot be fully evaluated. Operator dependency is also a limitation of ultrasonography (Kotecha et al. 2008).

2.3.2 Overview of complications in thyroid glands

2.3.2.1 Anatomy and physiology of thyroid glands

Thyroid gland is located in the anterior aspect of the neck just below the larynx, and is the largest endocrine gland in the human body (Figure 2.10). It is composed of the left and right lobes on the lateral sides of trachea, connecting by the isthmus. Thyroid gland has abundant vascular supply (80-120 mL/min) through the paired superior thyroidal arteries derived from the respective external carotid arteries, and the paired inferior thyroidal arteries originated from the subclavian arteries (Van De Graaff 2002, Loevner et al. 2008). The paired superior and middle thyroidal veins empty into the internal jugular veins whilst the inferior thyroidal veins drain into the brachiocephalic veins (Van De Graaff 2002).

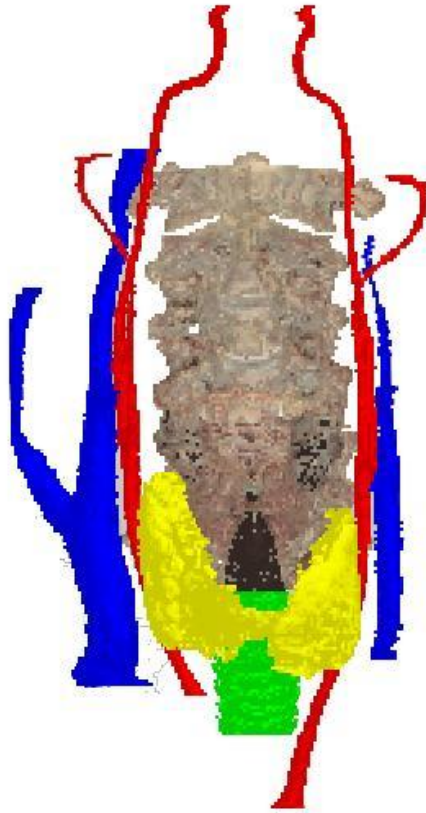


Figure 2.10: Schematic diagram shows the relative position of thyroid gland (yellow) in the cervical region using software Virtual Human Atlas 1.0. Thyroid gland is located in the anterior aspect of the neck (cervical spine: brownish grey) and on the lateral sides of trachea (green). Carotid arteries (red) and jugular veins (blue) run laterally and posteriorly to the thyroid gland.

On the histological level, thyroid gland is composed of numerous thyroid follicles lined with a layer of follicular cells (Van De Graaff 2002). The fluid material within each thyroid follicle is called colloid where the large protein molecules, thyroglobulin, are stored inside (Bernal and Refetoff 1977, Loevner et al. 2008). The follicular cells synthesize two major thyroid hormones called thyroxine (T₄) and triiodothyronine (T₃), which help regulating the level of metabolic activity (Bernal and Refetoff 1977, Van De Graaff 2002). T₃ and T₄ could accelerate oxygen consumption and heat production, as well as increases energy generation through

accelerating metabolism of carbohydrates, proteins and fats (Bernal and Refetoff 1977, Van De Graaff 2002). They also associate with sexual maturity and regulate the growth rate of the young people (Van De Graaff 2002). T4 is the main secretory product of the thyroid gland whilst around 80% of T3 is synthesized by conversion of T4 in the liver and muscle (Bernal and Refetoff 1977, Loevner et al. 2008). The major portion (>99%) of synthesized T3 and T4 are bound with thyroglobulin in circulation; and only 0.3% of T3 and 0.03% of T4 are the active form of thyroid hormones, which are not binding to thyroglobulin (Bernal and Refetoff 1977, Loevner et al. 2008).

The release of thyroid hormones is regulated by the hypothalamic-pituitary-thyroid axis. When there are insufficient thyroid hormones in the circulation, the hypothalamus would secrete more thyroid releasing hormone (TRH) to trigger the pituitary gland to release more thyroid stimulating hormone (TSH). The TSH would then stimulate the thyroid gland to secrete more thyroid hormones into the circulation. The increased circulating level of thyroid hormones would inhibit the release of TRH from the hypothalamus through negative feedback in order to maintain an optimum level of thyroid hormones in the circulation (Van De Graaff 2002).

2.3.2.2 Radiation-induced thyroid disorders

In radiotherapy for NPC, anterior cervical field to the neck is usually employed for the patients due to the high incidence of associated cervical lymph node metastases in NPC. Since the anterior cervical field to the neck involved irradiation of the thyroid glands which are radiosensitive, post-RT thyroid disorders are common in post-RT NPC survivors (Ulger et al. 2007). Hypothyroidism is the most common manifestation of post-RT head and neck cancer patients (Alterio et al. 2007, Ulger et al. 2007, Bonato et al. 2008). Overt hypothyroidism is defined as increased level of TSH and decreased free T4 level, whilst subclinical hypothyroidism is characterized with increased level of TSH and normal free T4 level (Jereczek-Fossa et al. 2004). Hypothyroidism can be subdivided into primary hypothyroidism and central hypothyroidism in which the former is due to the direct injury of thyroid gland from radiation (Nishihara et al. 2006), whilst the latter is caused by the damaged hypothalamic-pituitary gland complex leading to impaired release of thyroid stimulating hormones (TSH) (Paulino 2002). Primary hypothyroidism is more common than central hypothyroidism in post-RT head and neck cancer patients, in which 20-30% of patients might ultimately develop primary hypothyroidism (Ricardi et al. 2001, Paulino 2002, Jereczek-Fossa et al. 2004, Nishihara et al. 2006, Alterio et al. 2007, Ozawa et al. 2007, Ulger et al. 2007, Bonato et al. 2008) and only few percents of patients might develop central hypothyroidism (Corrias et al, 2001, Ricardi et al. 2001). Nevertheless, the rate of hypothyroidism might be affected by other treatments combined with RT. It has been reported that a combination of

hemithyroidectomy and radiotherapy could increase the risk of hypothyroidism (Turner et al. 1995, Tell et al. 1997, Jereczek-Fossa et al. 2004, Aich et al. 2005). Higher risk of hypothyroidism might also occur if a larger volume of the thyroid is being irradiated (Tell et al. 1997, Bhandare et al. 2007). It was found that primary hypothyroidism could occur after RT with the radiation doses as low as 20 Gy (Bhandare et al. 2007). However, the development of hypothyroidism mostly occurs after irradiation of 30-45 Gy (Bhandare et al. 2007). Constine et al. (1984) reported that hypothyroidism would occur more frequently in the thyroid glands receiving mean dose of greater than 26 Gy when compared to those be irradiated with lower dose levels.

Hypothyroidism is generally considered as a late complication as it is usually seen within 5 years and with the peak occurring 2 to 3 years after the completion of RT (Tell et al. 1997, Jereczek-Fossa et al. 2004, Nishihara et al. 2006, Bhandare et al. 2007, Ulger et al. 2007). However, some studies also reported that it could occur as early as few months after the completion of RT (Tell et al. 1997, Bhandare et al. 2007, Ozawa et al. 2007, Ulger et al. 2007).

The exact pathophysiology of radiation-induced thyroid disorders has not been fully understood. However, direct damages of the thyroid parenchyma and vasculatures from radiation are believed to be the major causes (Ricardi et al. 2001, Ulger et al. 2007). It has been found that thyroid parenchymal damage is usually followed by the vascular damage (Ricardi et al. 2001). Such parenchymal and vascular damage may

happen after receiving radiation dose as low as 1.5 Gy (Bonato et al. 2008). Sinard et al. (2000) reported that direct parenchymal damage was the main cause of radiation-induced hypothyroidism because 83% of patients were found to have hypothyroid within 12 months after the completion of RT, whilst radiation-induced vascular damage of thyroid gland occurred at a later stage. Besides, associated ischemia of the thyroid gland due to radiation-induced atherosclerosis of the carotid artery, fibrosis of the gland capsule and immunological thyroidal damage are also the possible mechanisms of radiation-induced thyroid disorders or hypothyroidism (Illes et al. 2003, Jereczek-Fossa et al. 2004, Aich et al. 2005, Bhandare et al. 2007).

Hypothyroidism can be manifested by a number of symptoms including skin dryness, pleural and pericardial effusion, depression, chronic fatigue, weight gain, atherosclerosis, constipation, muscle cramps, cold intolerance and decreased motility of gastro-intestinal tract, which seriously impair patients' health and QOL (Liening et al. 1990, Turner et al. 1995, Jereczek-Fossa et al. 2004). Moreover, there is a tendency of subclinical hypothyroidism evolving into overt hypothyroidism in post-RT head and neck cancer patients (Aich et al. 2005, Bhandare et al. 2007). Persistent high TSH level in NPC survivors could also increase the risk of thyroid cancer by 15 to 53 folds when compared with the non-irradiated population (Crom et al. 1997, Tell et al. 1997, Solt et al. 2000, Jereczek-Fossa et al. 2004, Nishihara et al. 2006).

Apart from hypothyroidism, thyroid volume reduction (Stewart et al. 1989, Ricardi et al. 2001, Miller-Thomas et al. 2009) and increased number of nodules (Soberman

et al. 1991, Schneider et al. 1997) are also common morphological changes of the thyroid glands after irradiation. Hence, an early detection of radiation-induced hypothyroidism or other thyroid disorders is necessary for early disease management in order to sustain patients' health status and prevent thyroid cancer development. Currently, thyroid function test and ultrasonography are the common methods for the assessment of thyroid disorders of post-RT NPC patients.

2.3.2.3 Thyroid ultrasonography

Ultrasonography is commonly used in the assessment of thyroid glands. Grey scale ultrasound allows accurate estimation of the thyroid volume, and assessment of the thyroid morphology. It helps the characterization and detection of diffuse and focal abnormalities of the thyroid gland, and aids distinguishing solid nodules from cysts (Shapiro 2003, Hegedus et al. 2005, Loevner et al. 2008). Doppler ultrasound evaluates thyroid vasculature. Ultrasound is also helpful in guiding fine-needle aspiration and cytology (FNAC) of thyroid nodules (Hegedus et al. 2005, Ota et al. 2007). In addition, ultrasound is non-invasive, readily available, inexpensive and does not involve ionizing radiation (Andermann et al. 2007, Malago et al. 2008). Sonographically, normal thyroid gland is characterized with homogenous echotexture and is slightly hyperechoic compared with the adjacent muscles (Figure 2.11) (Muller et al. 1985, Baskin et al. 2008, Loevner et al. 2008). The transverse and anteroposterior dimensions of normal thyroid glands are less than 2cm, and the normal craniocaudal dimension of thyroid glands is around 4.5-5.5cm (Baskin et al.

2008). The normal range of the thyroid volume is 5-20cm³ in adults, and it could be influenced by body weight, age as well as physiological and environmental factors (Hegedus et al. 2005).

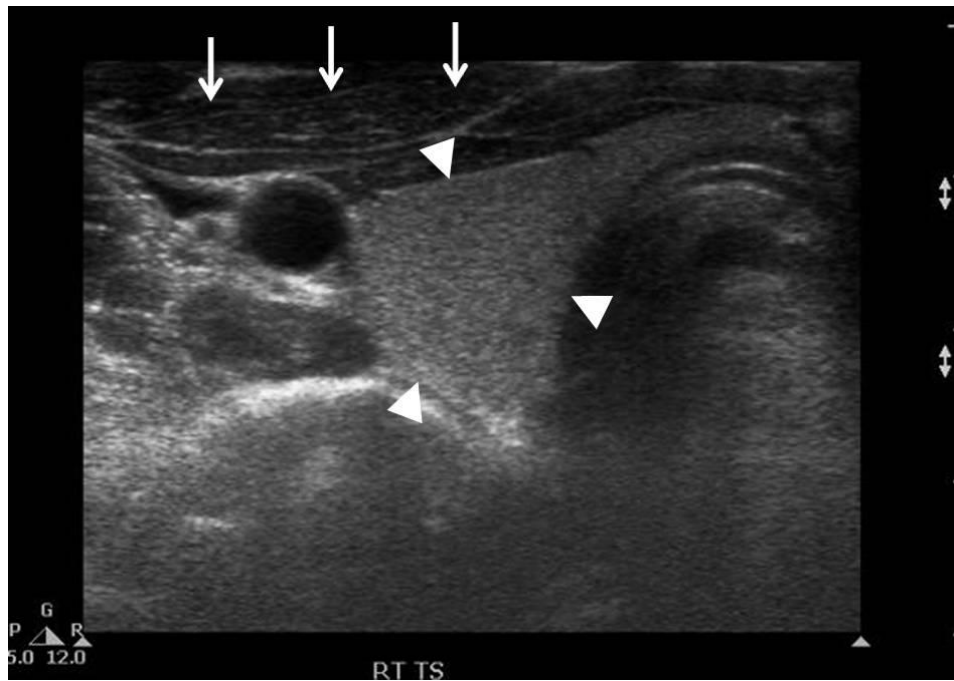


Figure 2.11: Sonogram shows a transverse scan of a normal thyroid gland with homogenous echotexture (arrowheads). It is hyperechoic compared with the adjacent sternomastoid muscle (arrows).

Reduction in thyroid size was one of the main manifestations of the irradiated thyroid glands in head and neck cancer survivors. Miller-Thomas et al. (2009) found an average decrease of 4.7mm or 13.7% in the transverse dimension of the thyroid gland in about 2 years after the completion of RT in laryngeal cancer patients. Bonato and colleagues (2008) assessed the changes of thyroid gland in 59 post-RT paediatric patients using thyroid function test and ultrasonography, and found that there was a negative correlation between the thyroid volume and the TSH levels. The

mean thyroid volume in the study group with lower TSH levels (3.1ml) was higher than that in the study group with higher TSH levels (1.36ml) (Bonato et al. 2008). Bossi et al. (1998) also showed similar finding that patients with high TSH and low free T4 levels tended to have smaller thyroid glands. As primary hypothyroidism is characterized with high TSH level, the associated reduced thyroid volume in patients with high TSH level might suggest the occurrence of primary hypothyroidism (Bonato et al. 2008). Other studies using ultrasound to measure the thyroid size also reported similar findings of thyroid volume reduction in the post-RT head and neck cancer patients (Stewart et al. 1989, Ricardi et al. 2001). Nevertheless, there was no standard method for thyroid volume measurement (Andermann et al. 2007). Volume estimation based on cross-sectional images in CT and MRI has high accuracy (90-95%) (Hegedus et al. 2005). However, CT involves ionizing radiation, and the examinations require the administration of iodinated contrast medium which imposes the risk of allergic reaction in some patients. MRI is expensive and is not widely available (Andermann et al. 2007, Malago et al. 2008). Three-dimensional (3D) ultrasonography is highly correlated with the surgical reference volume of thyroid glands and is lack of systematic error and has higher accuracy in thyroid volume estimation compared to two-dimensional (2D) ultrasonography. However, 3D ultrasound is not available in all centres, and is not commonly used in routine clinical practice of thyroid ultrasonography (Andermann et al. 2007). Hence, 2D grey scale ultrasonography is still commonly used in the clinical practice for thyroid volume estimation (Rossi et al. 2002, Andermann et al. 2007, Ruggieri et al. 2008).

The volume of each thyroid lobe can be obtained by the following equations that were previously reported:

$$\text{Thyroid lobe volume} = \pi/6 \cdot (\text{CC} \times \text{LM} \times \text{AP}) \text{ (Brown and Spencer 1978)}$$

$$\text{Thyroid lobe volume} = 0.479 \cdot (\text{CC} \times \text{LM} \times \text{AP}) \text{ (Brunn et al. 1981)}$$

$$\text{Thyroid lobe volume} = 0.529 \cdot (\text{CC} \times \text{LM} \times \text{AP}) \text{ (Shabana et al. 2006)}$$

$$\text{Thyroid lobe volume} = 0.38 \cdot (\text{CC} \times \text{LM} \times \text{AP}) + 1.76 \text{ (Ying et al. 2008)}$$

where CC is the craniocaudal dimension, LM is the lateromedial dimension and AP is the anteroposterior dimension of the thyroid lobe.

The total volume of the thyroid gland is the sum of the left and right lobes, whilst the isthmus volume is usually not included (Rossi et al. 2002, Baskin et al. 2008). Among the above equations, the ellipsoid formula suggested by Brown and Spencer (1978) is more commonly used. However, Ying et al. (2008) developed a new equation and found that the new equation is more accurate than the other equations (Brown and Spencer 1978, Brunn et al. 1981, Shabana et al. 2006) in thyroid volume estimation.

Apart from thyroid volume reduction, nodules are also commonly found in the irradiated thyroid glands (Mihailescu et al. 2005). Thyroid nodules in the post-RT patients are of particular concern because of the increased risk of cancer development (Crom et al. 1997). It has been found that thyroid nodules could be

detected in up to 87% of the irradiated patients (Schneider et al. 1997). A dose-response relationship between radiation dose to the thyroid glands and the risk of nodule formation has been found in previous studies (Crom et al. 1997, Stewart et al. 1989, Corrias et al. 2001, Ricardi et al. 2001). Crom et al. (1997) reported that the risk of thyroid nodule development in 10.8 years after RT was 6 and 8.2 times higher in patients who had received 15-30 Gy and 31-66 Gy of radiation respectively than those received less than 2 Gy of radiation. Besides, Stewart et al. (1989) found that benign and malignant thyroid nodules may develop after the irradiation of 25-41 Gy. Other studies also demonstrated higher incidence of thyroid nodules in post-RT patients (Corrias et al. 2001, Ricardi et al. 2001).

High-resolution ultrasonography has high sensitivity (94%) in the detection of thyroid nodules, and can detect nodules as small as 2-3mm in diameter (Soberman et al. 1991, Schneider et al. 1997). Ultrasonography allows thyroid nodule localization, and nodule volume estimation using ellipsoid formula (Mihailescu et al. 2005, Baskin et al. 2008). Thyroid nodules are predominantly hypoechoic to the normal thyroid parenchyma whereas others are isoechoic and with echolucent halo (Soberman et al. 1991). Ultrasonography may be helpful in differentiating benign and malignant nodules with the use of colour Doppler ultrasound since increased intranodular vascular flow is more predictive for malignancy (Ahuja et al. 2003, Soberman et al. 1991). However, thyroid cancers were only presented in about 10% of all solitary thyroid nodules (Mihailescu et al. 2005). The sonographic characteristics of the nodules such as irregular margins, intranodular vascular spots,

microcalcifications, high tall-to-width ratio are the risk factors of malignancy but the risk is usually not associated with the nodule size (Mihailescu et al. 2005, Moon et al. 2008, Popowicz et al. 2009). Although thyroid nodules are commonly found in post-RT patients, they are also common in the apparently healthy individuals, accounting for 50-70% in asymptomatic and non-irradiated population, and the incidence is higher in females and with increasing age (Mehanna et al. 2009, Hegedus et al. 2005). Therefore, it should be with caution when evaluating thyroid nodules in the post-RT patients.

Besides thyroid volume reduction and nodule formation, heterogeneous echotexture and decreased echogenicity of thyroid parenchyma, which are associated with hypothyroidism and increased TSH levels, may also be the possible sonographic features indicating radiation-induced thyroid disorders (Corrias et al. 2001, Schiemann et al. 2003, Vejbjerg et al. 2006).

2.3.2.4 Thyroid Function Test

Thyroid function test is commonly used in assessing thyroid dysfunction, especially hypothyroidism, for post-RT head and neck cancer patients. It measures the circulating thyroid hormone levels for thyroid function assessment, and TSH and free T4 (fT4) remains the common parameters for the assessment (Rose 2001). Clinical or overt hypothyroidism is characterized by decreased fT4 level and increased TSH level, whether or not the patient shows clinical manifestation of

decreased thyroid function. However, subclinical or occult hypothyroidism is defined as an asymptomatic condition characterized by normal fT4 level with increased TSH level (Bartalena et al. 1996, Sinard et al. 2000, Paulino 2002). The normal reference ranges of TSH and fT4 are 0.27-4.7 μ IU/mL and 9-20pmol/L respectively (Col et al. 2004, Surks et al. 2004). However, the exact values of thyroid hormones in defining thyroid function status depend on the laboratory because each laboratory has its own reference ranges (Alterio et al. 2007). Although the assessment of serum TSH alone is sufficient to detect most of the primary hypothyroidism cases, normal or low TSH level could occur in patients with central hypothyroidism (Bartalena et al. 1996). Also, increased TSH level could be found in patients with normal thyroid during the recovery phase of hypothyroxinemia of some critical illnesses (Brent et al. 1986). Hence, fT4 measurement in addition to TSH assessment is always required in accurate hypothyroidism diagnosis, especially when there is normal or low TSH level (Bartalena et al. 1996). Sinard et al. (2000) stated that fT4 measurement should be performed to confirm subclinical hypothyroidism or clinical hypothyroidism if the TSH level of the patients increases but is lower than 10 μ IU/mL. It was because these patients tended to have a higher risk of hypothyroidism (Sinard et al. 2000). On the other hand, TSH level at 10 μ IU/mL or above should be considered as clinical hypothyroidism, regardless of the fT4 value (Sinard et al. 2000).

Chronic elevated TSH level could lead to thyroid cancer by up to 53 folds (Crom et al. 1997, Tell et al. 1997, Solt et al. 2000, Jereczek-Fossa et al. 2004, Nishihara et al.

2006) and subclinical hypothyroidism is very likely to develop into clinical hypothyroidism over time (Aich et al. 2005, Bhandare et al. 2007). Therefore, regular thyroid function test of post-RT patients is necessary for early detection of hypothyroidism after RT. Garcia-Serra et al. (2005) found that at least 50% patients developed primary hypothyroidism after they had a neck irradiation of more than 50 Gy. Therefore, the authors suggested that TSH level should be monitored every 6 months for 5 years and then annually afterward (Garcia-Serra et al. 2005). However, Turner et al. (1995) suggested thyroid function should be monitored 1 month after treatment and followed by 3-6 months intervals for at least 5 years. Nevertheless, it is generally agreed that regular thyroid function assessment is necessary for post-RT patients in the first 5 years of post-treatment period.

Previous studies showed different incidence rates of hypothyroidism after RT. The discrepancy of the finding is probably due to the use of different methodologies in the studies, such as different time intervals of thyroid function test after RT, and the availability of pre-treatment baseline thyroid function test (Sinard et al. 2000, Aich et al. 2005, Bhandare et al. 2007). Moreover, the incidence rate could be altered by the other treatments that the patients received such as neck surgery (Liening et al. 1990, Tell et al. 1997, Jereczek-Fossa et al. 2004, Ozawa et al. 2007). Liening et al. (1990) found that 6% of patients treated with RT alone showed increased TSH level, whilst increased TSH level was found in 28% of patients treated with RT and neck surgery. Nevertheless, it has shown that chemotherapy did not increase the risk of hypothyroidism in addition to RT (Sinard et al. 2000, Solt et al. 2000, Aich et al.

2005). Hence, in the assessment of hypothyroidism of post-RT patients, it should be with caution on the treatment modalities employed to the patients.

Although thyroid function test can help assessing thyroid function and identifying clinical and subclinical hypothyroidism in patients treated with RT, it cannot assess the morphological changes and vascular damages of post-RT thyroid which can be evaluated with some medical imaging modalities such as ultrasonography. Hence, a combination of medical imaging and thyroid function assessments is necessary for a comprehensive evaluation of post-RT thyroid glands.

2.4 Basis of this study

Improvement in the radiation-induced xerostomia assessment could help investigating methods in relieving xerostomia and help improving quality of life for post-RT NPC patients. High resolution ultrasound is useful in assessing salivary glands. However, there is scant information in the literature regarding ultrasound evaluation of post-RT changes in the salivary glands. Available data is limited to the investigation of parotid glands, and the sample size of the study was small (Ying et al. 2007). A clear understanding of the sonographic appearances of irradiated salivary glands is crucial for the ultrasound assessment of salivary glands in post-RT patients, and thus the normal post-RT changes of the glands are not mis-interpreted as pathologies. Therefore, it is necessary to investigate the sonographic appearances

of the irradiated salivary glands in NPC patients treated with radiotherapy for accurate diagnosis.

Ultrasound has been widely used in assessing thyroid glands, but there is scant information in the literature about ultrasound evaluation of radiation-induced damages of thyroid glands. The post-RT changes of the sonographic appearance must be identified so that these changes would not be misinterpreted as other thyroid diseases. Besides, compared with conventional RT, IMRT might reduce possible radiation-induced damages of thyroid gland during cervical lymph node irradiation. In order to facilitate differential diagnosis, it is necessary to investigate the value of ultrasound in identifying post-RT changes of thyroid glands, and to distinguish the sonographic appearance of thyroid glands between NPC patients with their cervical lymph nodes treated with different RT techniques.

Chapter Three

Study One

Sonographic appearance of parotid glands in patients treated with intensity-modulated radiotherapy or conventional radiotherapy for nasopharyngeal carcinoma

3.1 Introduction

Nasopharyngeal carcinoma (NPC) is a common head and neck malignancy in Southeast Asia with an incidence rate of 15-50 per 100,000 population (Chan et al. 2002). Early stage of NPC is commonly treated with radical radiotherapy alone, whilst chemo-radiotherapy is recommended for patients with moderate to advanced stages (Lu and Yao 2008). With the use of appropriate treatments, the long term survival rate can be up to 90% for stage I NPC (Liu et al. 2004).

Two-dimensional conventional radiotherapy (conventional RT) has long been used for the treatment of NPC in Hong Kong. Since it has limitation in effective sparing the organs at risk such as salivary glands and spinal cord that are incidentally covered by the radiation fields, it has been reported to cause various radiation toxicities such as salivary gland damage and loss of taste (Lu and Yao 2008; King et al. 2007). High radiation dose to the normal structures would impair their function and affect the patients' quality of life (Lu and Yao 2008; Liu et al. 2004).

With the availability of modern radiotherapy techniques such as intensity-modulated radiotherapy (IMRT), accurate dose conformity to the target can be achieved and the organs at risk can be better spared from the radiation (Lu and Yao 2008; King et al. 2007; Eisbruch 2002). Previous studies revealed that IMRT not only improved the local tumour control, but also reduced treatment morbidity and hence improved patients' quality of life (Lu and Yao 2008; Gregoire et al. 2007; Eisbruch 2002).

Radiation-induced damage to salivary glands is the most common post-radiotherapy (post-RT) complication for head and neck cancer as salivary glands are usually included in the radiation fields, especially in the conventional RT. High radiation dose could damage salivary glands, leading to radiation-induced xerostomia. Xerostomia could lead to oral discomfort and oral infection, affecting patient's daily life. Parotid glands are prone to be irradiated with high dose in conventional RT due to their close proximity to the radiation field. Nevertheless, with the use of the advanced parotid sparing technique in IMRT, the radiation dose to parotid glands and the risk of xerostomia in the patients have been significantly reduced (Lu and Yao 2008; Kubicek and Machtay 2008).

As nearly all post-RT NPC patients would develop different degrees of xerostomia, early and accurate detection of radiation-induced changes in salivary gland allows early management of this complication. Moreover, improvement in the assessment of xerostomia and the understanding of its causes may help to investigate methods to relieve the conditions of xerostomia and improve patients' quality of life.

With the use of high resolution ultrasound, it is useful in assessing superficial soft tissue structures including salivary glands. However, there is scant information in the literature regarding ultrasound evaluation of post-RT changes in the salivary glands. Available data is limited to a single RT technique, and the sample size of the study was small (Ying et al. 2007). There is also lack of literature comparing the sonographic appearances of salivary glands in nasopharyngeal cancer patients treated with different radiotherapy techniques. Furthermore, it is also important to identify the sonographic appearances of post-RT salivary glands so that the normal post-RT changes of the glands are not misinterpreted as salivary gland pathologies. Therefore, this study was undertaken to investigate and compare the sonographic appearances of the parotid glands in NPC patients treated with conventional RT or IMRT. The finding of the present study would offer a basis in the application of ultrasound to identify post-RT changes of salivary glands.

3.2 Materials and methodologies

3.2.1 Subjects

A total of 81 NPC patients at stage I to III of the disease were recruited in the study. Inclusion criterion was patients who have completed either conventional RT or IMRT of the tumour between 2000 and 2007. Oncologists reviewed all NPC patients during their follow-ups and patients who fulfill the inclusion criteria were recruited. Exclusion criteria were history of earlier salivary gland diseases including salivary gland malignancy and Sjogren's syndrome. Informed written consent was obtained from each patient.

3.2.1.1 NPC patients treated with conventional RT

Among the 81 patients, 43 patients (28 males and 15 females) were treated with conventional RT for the primary tumour. The age range of the patients was 32 to 69 years old with the mean age of 52.6 ± 9.2 years. All patients received conventional RT with a radiation dose of 68 Gy to the target. A 10 Gy parapharyngeal boost was given using a 6MV posterior oblique facio-cerival field if there was parapharyngeal extension of the disease, in which the ipsilateral parotid gland would be included in the irradiated side (Kwong et al. 2004b). The mean parotid dose was 38.0 Gy.

3.2.1.2 NPC patients treated with IMRT

The remaining 38 patients (25 males and 13 females) were treated with IMRT. The age range of the patients was 33 to 71 years old with the mean age of 49.8 ± 8.3 years. Patients treated by IMRT were delivered with a total radiation dose of 66 to 76 Gy to the target. Efforts were made to spare the parotid glands, especially for early stage patients, by limiting the dose to at least one-half of the parotid glands on both sides to a dose of $< 20\text{Gy}$ (Kwong et al. 2004a). The mean parotid dose was 30.3 Gy.

3.2.1.3 Healthy subjects

A total of 58 healthy subjects (25 males and 33 females) were also recruited in the study. Exclusion criteria for the healthy subjects included smoking history and clinical history of any known cancers and earlier salivary gland diseases. The age range of the subjects was 27 to 60 years old with the mean age of $47.4 + 9.8$ years. Subjects previously received radiotherapy, chemotherapy or head and neck surgery were excluded. Informed written consent was obtained from each subject.

This study was approved by the Human Subjects Ethics Sub-committee of the Hong Kong Polytechnic University and the Institutional Review Boards of the involved hospitals.

3.2.2 Equipment

All ultrasound examinations were performed with the Philips HD11 XE or the Philips HD11 ultrasound unit in conjunction with a 12-5 MHz linear transducer (Philips Medical System, Bothell, WA, USA).

3.2.3 Parotid gland ultrasound examination

A parotid ultrasound examination was performed on the 81 NPC patients and the 58 healthy subjects by single operator (*i.e.* Cheng Chi Him). For the 43 patients treated with conventional RT, the parotid gland ultrasound examination was performed 31 to 111 months after the completion of RT (mean = 78.2 months). For the 38 patients treated with IMRT, the parotid ultrasound examination was conducted 22 to 96 months after the completion of RT (mean = 57.8 months). In the ultrasound examination, patients/subjects laid supine on the examination couch, with the neck hyperextended and shoulders supported by a pillow. The left and right parotid glands were assessed separately with the patient/subject's head turned away from the side under examination. Longitudinal and transverse scans were performed on each parotid gland, and the maximum longitudinal and transverse dimensions of the parotid glands were measured (Figures 3.1 and 3.2). Extended field-of-view ultrasound was used whenever the dimension of the parotid gland was larger than the field-of-view of the ultrasound beam (Figure 3.1).

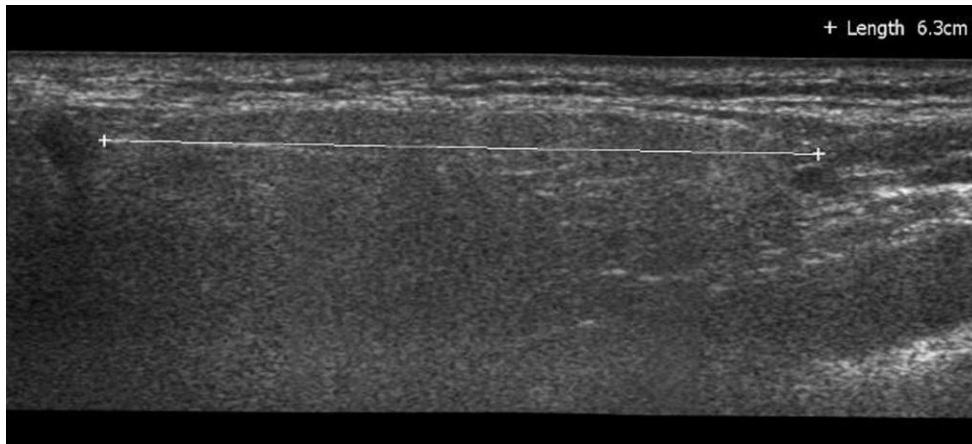


Figure 3.1: Longitudinal grey scale extended field-of-view sonogram shows the measurement of the longitudinal (LS) dimension of a parotid gland (calipers) in a patient treated with intensity-modulated radiotherapy.

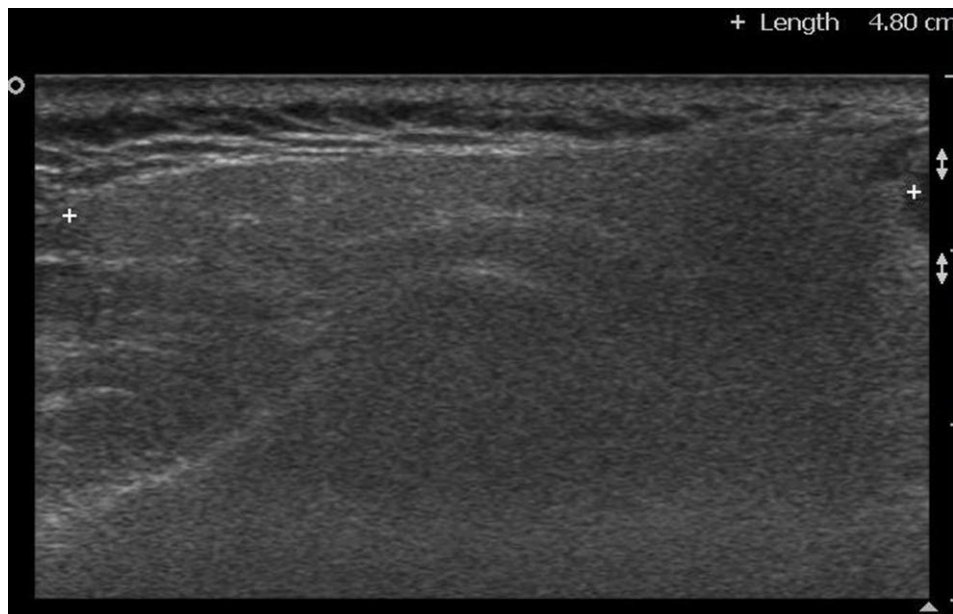


Figure 3.2: Transverse grey scale sonogram shows the measurement of the transverse (TS) dimension of a parotid gland (calipers) in a healthy subject.

The echogenicity of the parotid glands was assessed and subjectively classified into hypoechoic, isoechoic and hyperechoic when compared to the adjacent masseter muscle. Objective evaluation of the parotid gland echogenicity was also conducted.

Multiple transverse scans of the parotid glands were taken, and images were stored in the hard disk of the ultrasound unit. Archived images were retrieved after the ultrasound examination, and the echo-intensity of the parotid glands and the adjacent masseter muscles were quantified with the use of the specific software QLab™ (Philips Medical System, Bothell, WA, USA). In the quantification of the echo-intensity of the parotid glands and masseter muscles, the boundaries of parotid gland and those of the masseter muscle were outlined manually, and the value of the echo-intensity of the parotid glands and masseter muscle were then measured automatically by the QLab™ (Figure 3.3). In this quantification method, echolucent structures had lower echo-intensity values whereas echogenic structures had higher echo-intensity values. Three images with larger cross-sectional area of parotid glands and masseter muscle were selected and measured, and a mean value of the echo-intensity of parotid gland and the muscle were obtained. An echogenicity index of each parotid gland was then calculated with the following equation:

$$\text{Echogenicity index} = \frac{\text{mean parotid gland echo-intensity}}{\text{mean muscle echo-intensity}}$$

In the assessment of the echogenicity index of parotid glands, hypoechoic parotid glands tended to have a lower echogenicity index, whereas hyperechoic parotid glands tended to have a higher echogenicity index.

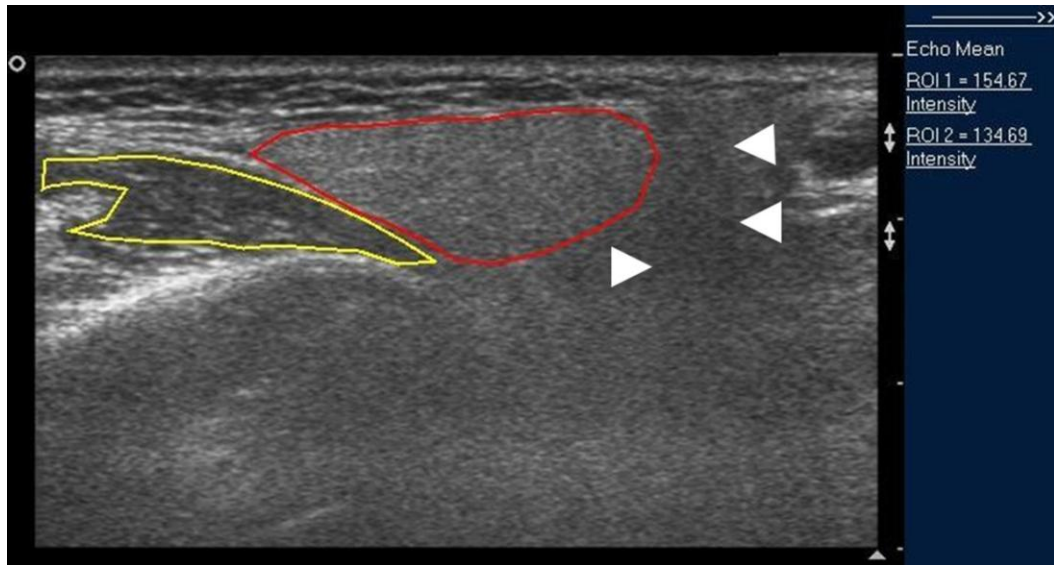


Figure 3.3: Transverse grey scale sonogram shows the measurement of the echo-intensity of a normal parotid gland (red line) and the adjacent masseter muscle (yellow line) by outlining their boundaries using the software QLab™. Note the artifacts (arrowheads) are not included in the region of interest (ROI). The echo-intensity of the parotid gland (ROI 1) and the masseter muscle (ROI 2) are shown in the right upper corner of the image.

The echogeneity of parotid glands was assessed. The gland was considered to be homogeneous when its parenchyma had a uniform echogenicity, whereas it was considered heterogeneous when it showed non-uniform parenchymal echogenicity. For the heterogeneous parotid glands, they were further evaluated with the previously described criteria for chronic fibrotic sialadenitis: multiple hypoechoic areas and multiple hyperechoic lines (Shimizu et al. 2006). The hyperechoic lines within the parotid gland were considered to be the intra-parotid ducts, and the conspicuity of the intra-parotid ducts was also assessed, which were classified into categories:

Obviously seen – the intra-parotid ducts were obviously seen with the echogenicity of the ducts substantially higher than that of the parenchyma of the gland.

Marginally seen – the intra-parotid ducts could be seen but not as obvious as in “obviously seen”. The echogenicity of the ducts was just slightly higher than that of the parenchyma of the gland.

Not seen – intra-parotid ducts were not seen within the gland.

3.2.4 Evaluation of parotid dose

For NPC patients treated with conventional RT, the total mean parotid dose was evaluated with the use of isodose display. For NPC patients treated with IMRT, the RT treatment plan was retrieved from the treatment planning system (TPS). The treatment plans were computed according to the planning criteria of the corresponding techniques. The total mean dose to the parotid gland was evaluated using isodose display, dose volume histogram and associated dosimetric parameters provided by the TPS.

3.2.5 Xerostomia questionnaire

Each patient was asked to complete a validated structured questionnaire, which was adopted from Zimmerman et al (1997) (Appendix I). It was used to assess the condition of xerostomia of the patients. The questions in the questionnaire asked the

patients about their subjective feelings of the changes due to salivary secretion and the impacts on their daily life. With the use of visual analog scale, patients were asked to put a vertical mark along the answering bar of each question in which the mark near the right end indicated better condition. The position of the mark relative to the whole length of the bar was expressed as a numerical value in which higher value indicated better condition of that question. The sum of all values of all questions yielded a xerostomia score of each patient that higher score indicated better (*i.e.* less severe) overall xerostomia condition.

3.2.6 Statistical analysis

The level of significance of the difference in size and echogenicity index of parotid glands between healthy subjects, the patients treated with IMRT and the patients treated with conventional RT were calculated by Kruskal-Wallis Test with Dunn's Multiple Comparison Test as the post-hoc test. Fisher's Exact Test was used to calculate the level of significance of the difference in echogenicity, echogeneity, conspicuity of intra-parotid ducts, and incidence of hypoechoic areas of parotid glands between healthy subjects, the patients treated with IMRT and the patients treated with conventional RT. Mann-Whitney Test was used to calculate the level of significance of the difference in xerostomia score between the patients treated with IMRT and the patients treated with conventional RT.

P-value smaller than 0.05 was considered to be statistically significant. GraphPad InStat software was used for all the statistical analyses (GraphPad Software Inc., San Diego, CA, USA).

3.3 Results

A total of 278 parotid glands were evaluated with ultrasonography in the 43 NPC patients treated with conventional RT (n = 86), the 38 NPC patients treated with IMRT (n = 76) and the 58 healthy subjects (n = 116). The present study found that the mean xerostomia score in the patients treated with IMRT (73.4 ± 15.4) was significantly greater than that of the patients treated with conventional RT (58.3 ± 23.7) ($p < 0.05$).

Results showed that there was a significant difference in the mean transverse (TS) dimension of the parotid glands among the healthy subjects, patients treated with conventional RT and those treated with IMRT ($p < 0.05$, Table 3.1). However, there was no significant difference in the mean longitudinal (LS) dimension of the parotid glands among the three study groups ($p > 0.05$, Table 3.1). Further evaluation using post hoc Dunn's Multiple Comparisons Tests indicated that the mean TS dimensions of the parotid glands in patients treated with conventional RT (4.61 cm) and in those treated with IMRT (4.53 cm) were significantly smaller than that in the healthy subjects (5.69 cm) ($p < 0.05$). However, there were no significant differences in the

mean TS dimension of parotid glands between patients treated with conventional RT and those treated with IMRT ($p > 0.05$).

There was a significant difference in the echogenicity index of the parotid glands among the three study groups ($p < 0.05$, Table 3.1). Further evaluation with the post hoc test found that the mean echogenicity index of parotid glands in the patients treated with conventional RT (1.13) was significantly smaller than that in the IMRT group (1.21) ($p < 0.05$). Likewise, the mean echogenicity indices of parotid glands in the patients treated with conventional RT and those treated with IMRT were significantly smaller than that in the healthy subjects (1.31) ($p < 0.05$).

Table 3.1: Comparison of the mean transverse and longitudinal dimensions and the mean echogenicity index of the parotid glands in healthy subjects, and patients treated with conventional RT and those treated with IMRT

Sonographic parameters	Mean \pm SD			p-value
	Healthy Subjects	NPC patients with IMRT	NPC patients with conventional RT	
Transverse dimension (cm)	5.69 \pm 1.20	4.53 \pm 1.02	4.61 \pm 1.32	< 0.05
Longitudinal dimension (cm)	6.32 \pm 0.77	6.48 \pm 1.02	6.20 \pm 0.80	0.10
Echogenicity index	1.31 \pm 0.22	1.21 \pm 0.15	1.13 \pm 0.25	< 0.05

SD = Standard deviation, RT = Radiotherapy, IMRT = Intensity-modulated radiotherapy

The p-value indicates the level of significance between the overall comparison of the 3 study groups (i.e. healthy subjects, NPC patients with IMRT and NPC patients with conventional RT) using Kruskal-Wallis Test.

All parotid glands in the healthy subjects (Figure 3.4A) and the majority of the parotid glands (93%) in the IMRT group were hyperechoic (Figure 3.4B), whilst 51% of the parotid glands in the patients treated with conventional RT were either isoechoic or hypoechoic (Figure 3.4C) when compared to the adjacent masseter muscles (Table 3.2). Result indicated that the differences in echogenicity of parotid glands between conventional RT and IMRT groups, between conventional RT group and healthy subjects, and between IMRT group and healthy subjects were statistically significant ($p < 0.05$).

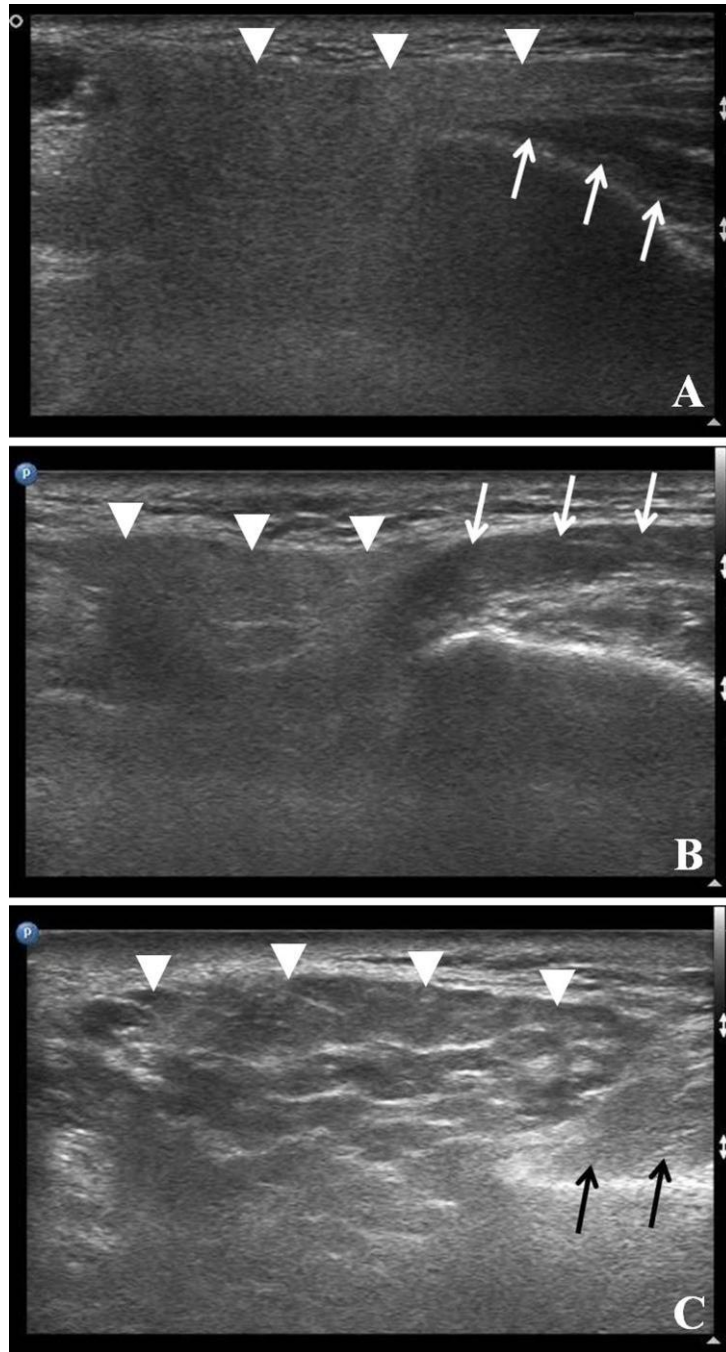


Figure 3.4: Transverse grey scale sonograms show the parotid glands and the adjacent masseter muscles of a healthy subject (A), a patient treated with intensity-modulated radiotherapy (B) and a patient treated with conventional radiotherapy (C). Note the parotid gland (arrowheads in A and B) in the healthy subject and patient treated with intensity-modulated radiotherapy is hyperechoic when compared to the adjacent masseter muscle (white arrows). However, in the patient treated with conventional radiotherapy, the parotid gland particularly the glandular parenchyma (arrowheads in C) is relatively hypoechoic to the adjacent masseter muscle (black arrows).

Table 3.2: Comparison of echogenicity, echogeneity, incidence of hypoechoic areas and conspicuity of intra-parotid ducts of parotid glands in healthy subjects, and patients treated with conventional RT and those treated with IMRT

	Number of parotid glands (%)			p-value		
	Healthy Subjects	NPC patients with IMRT	NPC patients with conventional RT	Healthy subjects vs NPC patients with IMRT	Healthy subjects vs NPC patients with conventional RT	NPC patients with IMRT vs NPC patients with conventional RT
Echogenicity						
<i>Hypoechoic</i>	116 (100%)	71 (93%)	42 (49%)	0.01	< 0.05	< 0.05
<i>Isoechoic</i>	0 (0%)	4 (5%)	31 (36%)			
<i>Hypoechoic</i>	0 (0%)	1 (2%)	13 (15%)			
Echogeneity						
<i>Homogenous</i>	112 (97%)	47 (62%)	2 (2%)	< 0.05	< 0.05	< 0.05
<i>Heterogeneous</i>	4 (3%)	29 (38%)	84 (98%)			
Hypoechoic areas						
<i>Present</i>	4 (3%)	27 (36%)	81 (94%)	< 0.05	< 0.05	< 0.05
<i>Absent</i>	112 (97%)	49 (64%)	5 (6%)			
Conspicuity of intra-parotid ducts						
<i>Obviously seen</i>	3 (3%)	8 (11%)	55 (64%)	0.03	< 0.05	< 0.05
<i>Marginally seen</i>	113 (97%)	68 (89%)	31 (36%)			

NPC = Nasopharyngeal carcinoma, RT = Radiotherapy, IMRT = Intensity-modulated radiotherapy

Majority of the parotid glands (97%) in the healthy subjects appeared homogenous on ultrasound (Figure 3.5A). In the IMRT group, 62% of parotid glands were homogenous (Figure 3.5B) whereas 38% of them were heterogeneous. However, in the patients treated with conventional RT, majority of the parotid glands (98%) were heterogeneous (Figure 3.5C). Result showed that the differences in the echogeneity of parotid glands among the patients treated with conventional RT, the patients treated with IMRT, and the healthy subjects were significant ($p < 0.05$, Table 3.2).

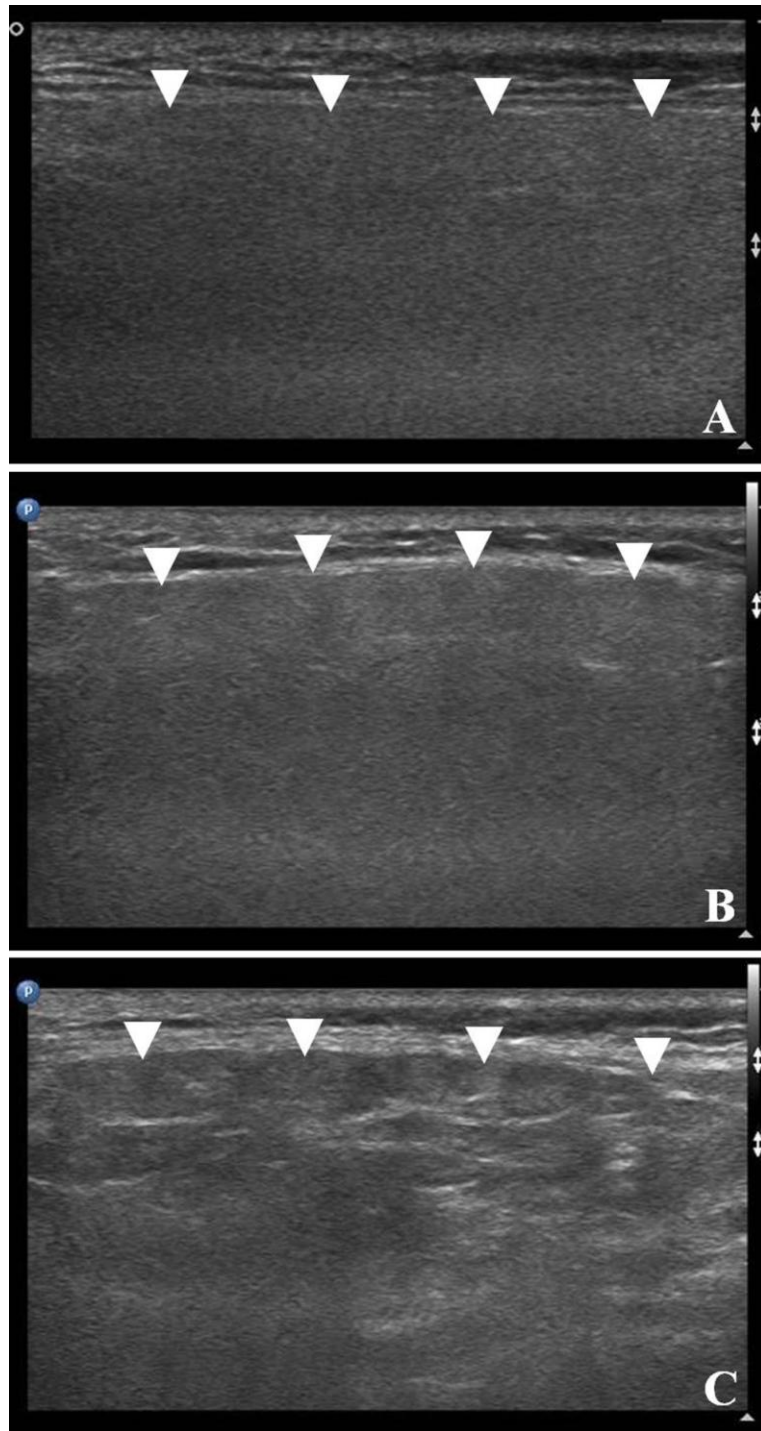


Figure 3.5: Longitudinal grey scale sonograms show the parotid glands of a healthy subject (A), a patient treated with intensity-modulated radiotherapy (B) and a patient treated with conventional radiotherapy (C). The parotid gland (arrowheads in A and B) of the healthy subject and that of the patient treated with intensity-modulated radiotherapy appear homogenous, whilst the parotid gland (arrowheads in C) of the patient treated with conventional radiotherapy is heterogeneous with non-uniform echogenicity of the gland.

This study found that majority of the parotid glands in healthy subjects (97%) (Figure 3.6A) and in patients treated with IMRT (64%) (Figure 3.6B) did not show hypoechoic areas. However, hypoechoic areas were commonly found in the parotid glands of patients treated with conventional RT (94%) (Figure 3.6C). The differences in the incidence of hypoechoic areas in the parotid glands among the two groups of patients and the healthy subjects were statistically significant ($p < 0.05$, Table 3.2).

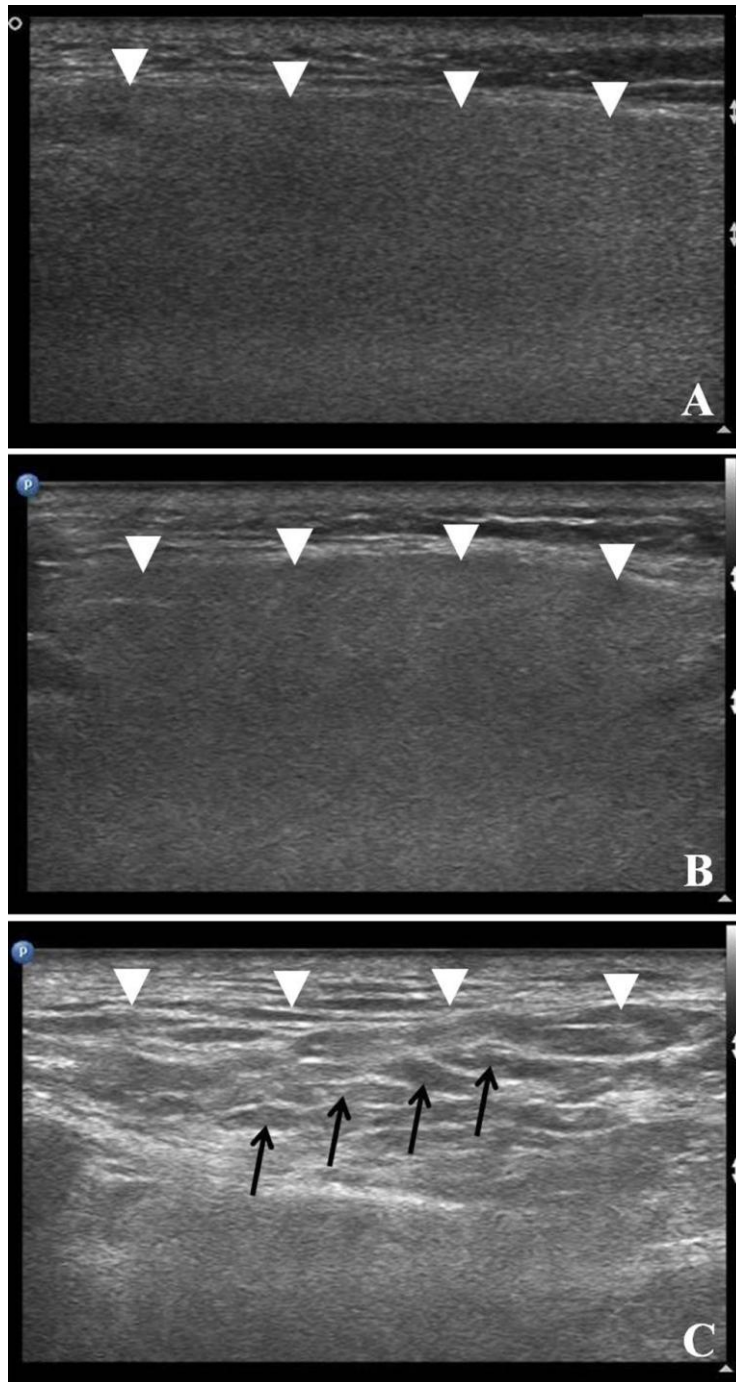


Figure 3.6: Longitudinal grey scale sonograms show the parotid glands (arrowheads) in a healthy subject (A), a patient treated with intensity-modulated radiotherapy (B) and a patient treated with conventional radiotherapy (C). Note the hypoechoic areas (arrows) are common in the parotid glands of patients treated with conventional radiotherapy, whilst they are uncommon in the parotid glands of healthy subjects and patients treated with intensity-modulated radiotherapy.

In the ultrasound images, intra-parotid ducts appeared as echogenic linear structures within the parotid gland. Intra-parotid ducts were demonstrated in the parotid glands of both NPC patients and healthy subjects, with various degree of conspicuity. Table 3.2 shows the conspicuity of intra-parotid ducts on ultrasound of the three study groups. The majority of intra-parotid ducts in the healthy subjects (97%) and the patients treated with IMRT (89%) were marginally seen in the ultrasound images (Figures 3.7A and B). However, in the patients treated with conventional RT, 64% of the intra-parotid ducts were obviously seen on ultrasound (Figure 3.7C) whereas 36% of them were marginally seen. The differences in the conspicuity of intra-parotid ducts among patients treated with conventional RT, patients treated with IMRT, and healthy subjects were significant ($p < 0.05$).

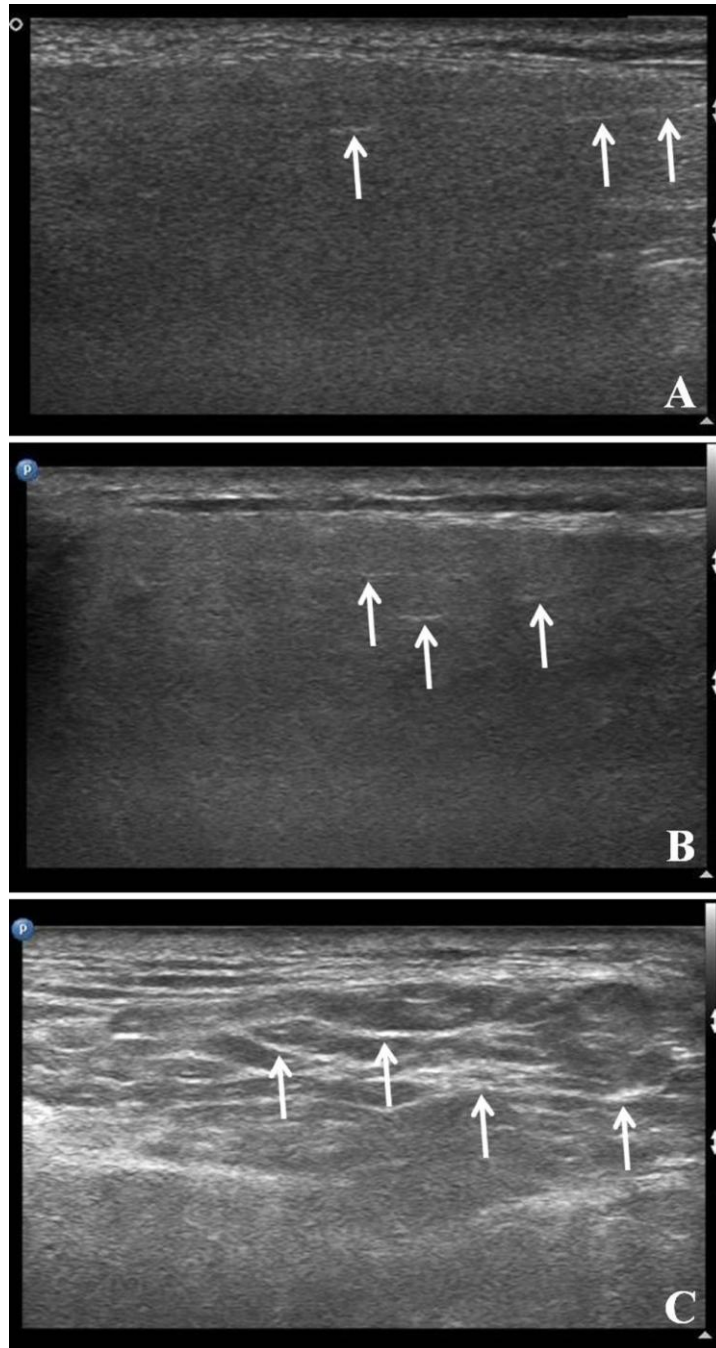


Figure 3.7: Longitudinal grey scale sonograms show the parotid glands and the intra-parotid ducts in a healthy subject (A), a patient treated with intensity-modulated radiotherapy (B) and a patient treated with conventional radiotherapy (C). Note the intra-parotid ducts in the healthy subject and the patient treated with intensity-modulated radiotherapy appear as fine echogenic linear structures and are marginally seen on ultrasound (arrows in A and B). However, in the patient treated with conventional radiotherapy, the intra-parotid ducts are obviously seen and appear as extensive hyperechoic linear structures (arrows in C).

3.4 Discussion

With the use of high resolution ultrasound, parotid glands can be easily visualized and assessed. In the present study, the sonographic appearances of parotid glands were different in the healthy subjects, NPC patients treated with conventional RT and those treated with IMRT. Results showed that normal parotid glands were homogenous (Figure 3.5A) and hyperechoic compared to the adjacent masseter muscle (Figure 3.4A), which was consistent with the findings in previous literatures (Katz et al. 2009; Ying et al. 2007). Histological studies reported that normal parotid glands were filled with homogenous pure serous acinar cells with densely packed translucent secretory granules, and did not have parenchymal loss, acinar atrophy or fibrosis (Eisbruch et al. 2003a; Henriksson et al. 1994; Radfar and Sirois 2003). Those densely packed cells and granules provided uniform and highly reflective interfaces for ultrasound beam, accounting for the homogeneous and hyperechoic appearance of the normal parotid glands. Intra-parotid ducts of the normal parotid glands were often marginally seen and appeared as fine hyperechoic linear structures (Figure 3.7A), which was comparable to our previous pilot study (Ying et al. 2007). Histologically, the intercalated ducts were branching between acini of the parotid glands (Henriksson et al. 1994), which might provide reflective interfaces for ultrasound beam and thus were shown as fine hyperechoic linear structures sonographically.

The present study found that the size of the parotid glands in the NPC patients treated with conventional RT and those with IMRT was significantly smaller than that of the healthy subjects. The smaller size of parotid glands found in post-RT NPC patients was due to acinar cell loss and acinar atrophy after irradiation (Henriksson et al. 1994; Radfar and Sirois 2003). Volume reduction of parotid glands after radiotherapy had been documented in previous studies using computed tomography (CT) (Barker et al. 2004; Lee et al. 2008a) and magnetic resonance imaging (MRI) (Nomayr et al. 2001; Wada et al. 2009). Nevertheless, the result of the present study only showed significant difference in the mean transverse dimension of the glands among the three study groups but not in the mean longitudinal dimension, which was consistent with the finding of our pilot study (Ying et al. 2007). The reason for that is not clear, but we postulate that this may be due to the anatomical location of the parotid gland, which is inferior to zygomatic arch, superior and posterior to angle of mandible and anteriorly overlaps with masseter muscle (Shah 2002). In the transverse orientation, the elastic muscular structure (i.e. masseter muscle) would exert an extrinsic force on the gland. When there were acinar cell loss and atrophy after irradiation, the parotid gland might be further “squeezed” by the masseter muscle transversely, leading to a substantial reduction in the transverse dimension. However, in the longitudinal orientation, the parotid gland is mainly in contact with the inelastic bony structures that would not exert an extrinsic force on it. Therefore, the reduction in the longitudinal dimension of the gland was more subtle and insignificant compared to the transverse dimension.

Hence, the result indicated that transverse dimension could better reflect the parotid gland size reduction after radiotherapy in ultrasound examinations.

In a histological study, Grehn et al. (1997) reported that the loss of acinar cells was dose dependent (i.e. higher radiation dose to the gland, greater the cell loss). Moreover, Nomayr et al. (2001) in a MRI study also showed that parotid gland volume reduction was dose dependent, in which the average volume of parotid glands was reduced by 26% and 40% following 30 Gy and 70 Gy of radiation respectively. In addition, volume recovery of parotid glands was not found after irradiation of more than 60 Gy (Nomayr et al. 2001). In the present study, we hypothesized that the degree of size reduction of parotid glands in the patients treated with IMRT was smaller than that in the patients treated with conventional RT, because of the better parotid sparing in IMRT which, in turn, leads to a lower parotid dose. However, results showed that there was no significant difference on the mean transverse and longitudinal dimensions of the parotid glands between the two groups of patients. The insignificant difference in the size of parotid glands between the two groups of patients might be due to the fact that this study only included two-dimensional measurements of the parotid glands, which might not be able to fully reflect the three-dimensional volume changes of the glands. Moreover, this study evaluated the superficial lobe of the parotid gland, whereas the deep lobe of the parotid gland was obscured by the mandible and could not be assessed with ultrasound. Therefore, the difference between IMRT and conventional RT in the post-RT changes of the deep lobe of the parotid gland was not fully evaluated, and

further studies using other cross-sectional imaging methods such as CT and MRI are suggested.

In the present study, the parotid glands in patients treated with IMRT and in healthy subjects tended to be hyperechoic (93% and 100% respectively), whereas parotid glands in patients treated with conventional RT were usually isoechoic or hypoechoic (51%), comparing with the echogenicity of adjacent masseter muscle. Therefore, in routine clinical practices, healthy individuals and NPC patients treated with IMRT with isoechoic or hypoechoic parotid glands may be suspicious of salivary gland diseases such as Sjögren's syndrome (Tzioufas and Moutsopoulos 2008). However, in NPC patients treated with conventional RT, decreased echogenicity of parotid gland may not be a useful criterion in identifying salivary gland pathologies as it is a common post-RT change in this group of patients. Radiation-induced chronic sialadenitis had been reported in the salivary glands of post-RT head and neck cancer patients, which was characterized by inflammatory infiltration and fibrosis histopathologically (Seifert 1995; Radfar and Sirois 2003; Teymoortash et al. 2005). The hypoechoic inflammatory infiltrate could lower the echogenicity of the parotid glands, leading to decreased echogenicity in post-RT glands (Radfar and Sirois 2003; Teymoortash et al. 2005; Ying et al. 2007), especially in the glands received high dose in conventional RT.

In the routine clinical practice, the echogenicity of parotid gland is commonly determined according to the operator's perception subjectively. However, subtle

changes of the echogenicity may not be easily identified with this method. In order to accurately evaluate and quantify the echogenicity of the parotid gland, echogenicity index of the gland was used in the present study. The echogenicity index is a relative value of echo-intensities of glands and muscles on the same image, and hence the value should not be significantly affected by the change of different settings like time gain compensation and overall gain of the ultrasound machines. Nevertheless, the variation of ultrasound settings had been minimized in order to minimize the potential alteration in echogenicity index. Result showed that the echogenicity index of parotid glands in the healthy subjects (mean = 1.31) was significantly higher than that in the patients treated with IMRT (mean = 1.21), and the parotid echogenicity indexes in the healthy subjects and patient treated with IMRT were significantly higher than that in the patients received conventional RT (mean = 1.13). The result of the parotid echogenicity index in the healthy subjects and the two patients groups was consistent with that of the subjective assessment of the parotid echogenicity, which indicated that the echogenicity index may be useful in differentiating normal and post-RT parotid glands. However, before the echogenicity index can be used in the routine clinical practice, further studies to investigate the optimal cut-off value of the index to distinguish normal and post-RT parotid glands are needed.

Results of the present study showed that the parotid glands in healthy subjects had a higher echogenicity than those in post-RT patients regardless of the RT technique used. The decreased echogenicity in post-RT parotid glands was probably due to reduced reflective interfaces for ultrasound beam because of the loss of secretory granules and acinar cells after irradiation (Price et al. 1995). Moreover, the presence

of inflammatory infiltrate due to radiation-induced chronic sialadenitis in the post-RT glands tended to be hypoechoic, which would also lower the overall echogenicity of the glands (Radfar and Sirois 2003; Teymoortash et al. 2005; Ying et al. 2007). In the present study, parotid glands in patients treated with IMRT had a higher echogenicity than those in patients received conventional RT. Since the parotid glands in patients treated with IMRT were irradiated with lower radiation dose compared to those in patients received conventional RT, lesser acinar cell loss or inflammatory infiltrates may account for the higher echogenicity of the parotid glands in the IMRT group. In the present study, the echogenicity of the parotid gland was compared with the adjacent masseter muscle. The advantage of comparing the echogenicity of the gland with the masseter muscle was that both structures were closely located and thus they could be demonstrated in the same ultrasound image, which was convenient and efficient for comparison clinically (Howlett 2003; Kotecha et al. 2008). It should be noted that the echogenicity change in parotid gland and masseter muscle might not be in linear or proportional, which could affect the comparison of echogenicity. Nevertheless, the radiation tolerance of muscle was found significantly higher than that of parotid gland and hence the echogenicity variation of muscle after irradiation should not be as much as that in the parotid glands (Emami et al. 1991; Ying et al. 2007).

Parotid glands in the healthy subjects and the patients treated with IMRT tended to be more homogenous, whereas parotid glands in the patients treated with conventional RT were predominantly heterogeneous. The heterogeneous echopattern

of the parotid gland was probably due to the presence of non-uniform ultrasound reflective interfaces from the disorganized acinar cell arrangement after parenchymal loss and acinar atrophy in the high-dose irradiated glands (Grehn et al. 1997; Nagler 2002; Ying et al. 2007). Moreover, the presence of patches of inflammatory infiltrates due to radiation-induced chronic sialadenitis would appear as multiple hypoechoic areas within the gland, leading to the heterogeneous echopattern. The results of the present study also showed that there was higher incidence of hypoechoic areas in the parotid glands of the patients treated with conventional RT when compared to that of the patients treated with IMRT and the healthy subjects. As the parotid glands in the IMRT group generally received lower dose when compared to that in the conventional RT group, the acinar cells of the gland in the IMRT group were arranged in a more organized manner with lesser inflammatory infiltration. Therefore, intra-parotid hypoechoic areas were uncommon, and the parotid glands tended to be homogenous. Nevertheless, 38% of the parotid glands in the IMRT group were heterogeneous and 36% of them had intra-parotid hypoechoic areas. Although it was found that 24 Gy and 26 Gy were the threshold dose for recovery of un-stimulated and stimulated parotid salivary flow respectively (Eisbruch et al. 1999), these thresholds could not be always achieved clinically. Kwong et al. (2004a) reported that the parotid glands could receive a mean dose of 38.8 Gy with a range of 32.0-46.1 Gy for early stage NPC patients receiving IMRT. Hence, those parotid glands receiving higher doses may appear heterogeneous and/or have hypoechoic areas sonographically. Nevertheless, the relationship between dose and sonographic appearances of post-RT glands should be further investigated.

The present study found that intra-parotid ducts, which appeared as echogenic linear structures within the parotid gland, were found in all the parotid glands of the three study groups. Nevertheless, the conspicuity of the intra-glandular ducts varied in different study groups. In the patients treated with IMRT and in the healthy subjects, intra-parotid ducts tended to be marginally seen (89% and 97% respectively). However, intra-parotid ducts are usually more echogenic and obviously seen in the patients treated with conventional RT (64%). The increased echogenicity of the intra-parotid ducts in the patients treated with conventional RT might be due to the proliferation or dilation of the ducts after high dose of irradiation. Radfar and Sirois (2003) found dilated striated and intercalated ducts as well as duct proliferation in the parotid glands irradiated with 70Gy in a minipig study. The proliferated and dilated ducts provide a highly reflective interface for ultrasound, showing as hyperechoic linear structures (Ying et al. 2007). The increased echogenicity of intra-parotid ducts might be also due to the presence of fibrosis of the ducts after irradiation, and such fibrotic changes could lead to reduced elasticity of the ducts and the ductal lumen, which restrain the salivary flow (Ying et al. 2007). Besides, the reduced echogenicity of the irradiated parotid glands would make the intra-parotid duct become more obvious sonographically.

Results of the present study showed that the mean xerostomia score of the patients treated with IMRT was higher than that of the patients treated with conventional RT. Higher xerostomia score in the IMRT group indicated less severe xerostomia

condition compared with the conventional RT group. It should be due to the fact that parotid glands were spared from high radiation dose during IMRT, preserving the acinar cells and hence the salivary function of the glands. However, it should be noted that xerostomia score is a subjective measurement, which does not provide quantitative analysis of the salivary function. Moreover, the oral sensation and perception of oral dryness may change after radiotherapy that patients may not be able to detect the slight improvement of the salivary flow (Fox 1987). As the present study is lack of the correlation between xerostomia score and sonographic appearance of the post-RT parotid glands, further study is suggested in this area.

The present study compared the sonographic appearances of parotid glands in NPC patients treated with different RT techniques, and used the findings of healthy subjects as the control. However, the dose delivered to individual parotid gland was not fully evaluated in the study. Further studies to correlate the sonographic appearance of parotid glands and their radiation dose in different RT techniques are suggested.

To conclude, ultrasound is a useful imaging tool in the evaluation of radiation-induced changes of parotid glands in NPC patients. For more accurate diagnosis, the sonographic appearances of post-RT parotid glands should be noted in ultrasound examination of patient with previous radiotherapy for NPC or other head and neck cancers.

Chapter Four

Study Two

Sonographic appearance of submandibular glands in patients treated with external beam radiotherapy for nasopharyngeal carcinoma

4.1 Introduction

Nasopharyngeal carcinoma (NPC) is a common head and neck malignancy in Southern China and Southeast Asia, with an incidence rate of 15-50 per 100,000 population (Chan et al. 2002). Radical radiotherapy (RT) is the treatment of choice and combined with chemotherapy for patients with more advanced stages (Lu and Yao 2008). With the use of appropriate treatments, the 3-year survival rate of the patients of stage I disease can be up to 90% (Cheng et al. 1998).

External beam radiotherapy including two-dimensional conventional radiotherapy (conventional RT) and intensity-modulated radiotherapy (IMRT) are commonly used to treat NPC in Hong Kong. Conventional RT has the limitation in effectively sparing the organs at risk that are incidentally covered by the radiation fields. High radiation dose to the normal structures would impair their function and affect patients' quality of life. IMRT, on the other hand, is an advanced radiotherapy modality allowing accurate dose conformity to the target and better sparing the organs at risk from

radiation, which improves local tumour control and patients' quality of life. As there is a high incidence (60-96%) of associated cervical lymph node metastases in NPC patients (Glastonbury 2007), irradiation of the neck lymphatics is necessary. Since the submandibular glands are situated next to the jugulodigastric node which is commonly involved in NPC, the submandibular glands are usually irradiated to high dose and radiation-induced damage is expected (Figure 4.1).

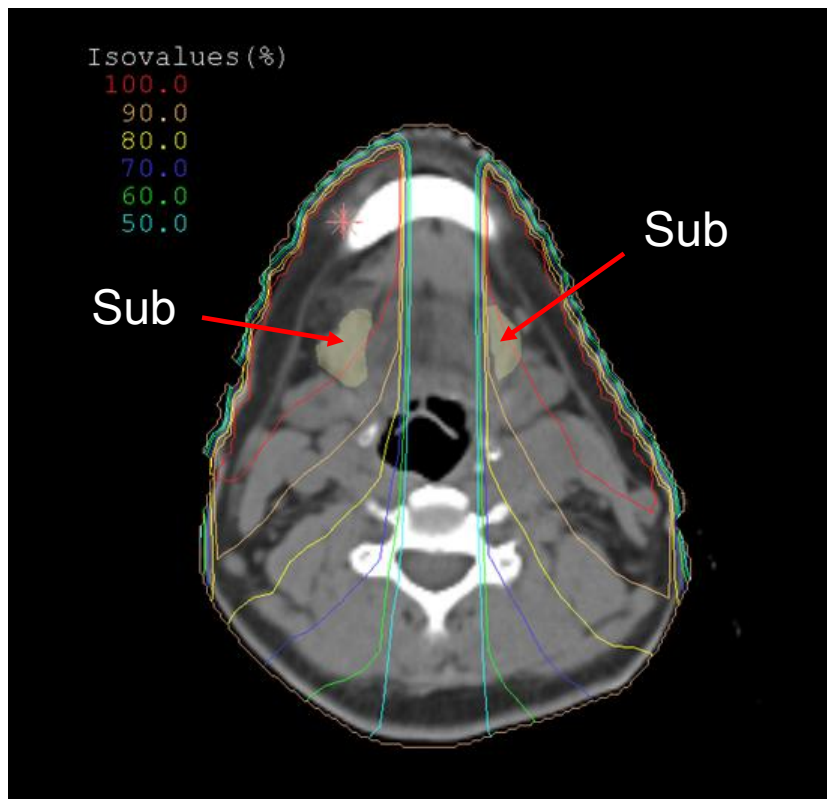


Figure 4.1: Computed tomography image shows that submandibular glands (Sub) are within the high dose region (90-100% of the prescribed dose) in the anterior cervical field.

Radiation-induced damage to salivary glands is a common post-radiotherapy (post-RT) complication for head and neck cancer resulting in xerostomia. Xerostomia could lead to oral discomfort and oral infection, affecting patient's daily life. Although saliva secretion in eating status is predominantly contributed by parotid glands, submandibular glands secrete more than 60% of saliva in the non-eating status, and hence the impairment of its function (i.e. reduction of submandibular gland secretion) could adversely affect patient's quality of life after radiotherapy especially when they are not eating.

As most post-RT NPC patients develop different degrees of xerostomia, early detection of radiation-induced changes in salivary gland allows early management of this complication. Wada and colleagues reported that reduced function of the irradiated submandibular glands was the most influential reason for the severity of radiation-induced xerostomia (Wada et al. 2009). Hence, understanding the post-RT changes of submandibular gland could help understanding the cause and improving the assessment of xerostomia, which in turn, may help investigate methods to relieve the symptom and improve patients' quality of life.

High resolution ultrasound is useful in assessing superficial soft tissue structures including salivary glands. However, there is scant information in the literature regarding ultrasound evaluation of post-RT changes in the salivary glands. Available data is limited to the investigation of irradiated parotid gland (Ying et al. 2007), and literature is devoid of any information about the sonographic appearances of

irradiated submandibular glands. Furthermore, it is also important to identify the sonographic appearances of post-RT submandibular glands so that the normal post-RT changes of the glands are not mis-interpreted as submandibular gland pathologies. Therefore, this study was undertaken to investigate the sonographic appearances of the submandibular glands in NPC patients treated with radiotherapy, and compare those in healthy subjects. The finding of this study would provide the basis in the application of ultrasound to identify post-RT changes of the submandibular glands.

4.2 Materials and methodologies

4.2.1 Subjects

4.2.1.1 Patients

A total of 81 stages I to III NPC patients (53 males and 28 females), who have completed a course of radical external beam radiotherapy between 2000 and 2007, were recruited. Patients with history of salivary gland diseases including salivary gland malignancy and Sjogren's syndrome were excluded. Informed written consent was obtained from all patients.

All patients were treated with external beam radiotherapy by either conventional radiotherapy (n = 43) or IMRT (n = 38). The age range of the patients was 32 to 71 years old with the mean age of 51.3 ± 8.8 years. Patients received radiotherapy with a mean radiation dose of 73.4 Gy to the target and a mean dose of 65.0 Gy to the neck lymphatics. As submandibular glands are within the high dose zone in both the conventional and IMRT techniques, it received doses closed to the prescribed dose. For the 81 patients, 67 patients (47 males and 20 females, mean age 50.9 ± 8.8 years) with palpable cervical lymph node(s), the submandibular glands were irradiated by a mean dose of 66 Gy. For the remaining 14 patients (6 males and 8 females, mean age 53.3 ± 8.5 years) without palpable cervical node, the mean submandibular gland dose was about 60 Gy.

For each patient, the submandibular gland ultrasound examination was performed at 22 to 111 months after the completion of RT (mean = 68.6 months).

4.2.1.2 Healthy subjects

A total of 66 healthy subjects (33 males and 33 females) were also recruited in the study. Healthy subjects with smoking history and clinical history of any cancers and salivary gland diseases were excluded. The age range of the subjects was 27 to 82 years old with the mean age of 46.8 ± 9.8 years. Informed written consent was obtained from all subjects.

This study was approved by the Human Subjects Ethics Sub-committee of the Hong Kong Polytechnic University and the Institutional Review Boards of the involved hospitals.

4.2.2 Equipment

All ultrasound examinations were performed with the Philips HD11 XE or the Philips HD11 ultrasound unit in conjunction with a 5-12 MHz linear transducer (Philips Medical System, Bothell, WA, USA).

4.2.3 Submandibular gland ultrasound examination

A submandibular ultrasound examination was performed on the 81 NPC patients and 66 healthy subjects by single operator (*i.e.* Cheng Chi Him). In the ultrasound examination, patients/subjects laid supine on the examination couch with the neck hyperextended and shoulders supported by a pillow. The left and right submandibular glands were assessed separately with the patient/subject's head turned to opposite side. Transverse scans were performed on each submandibular gland, and the maximum transverse dimension of the submandibular gland was measured (Figure 4.2).

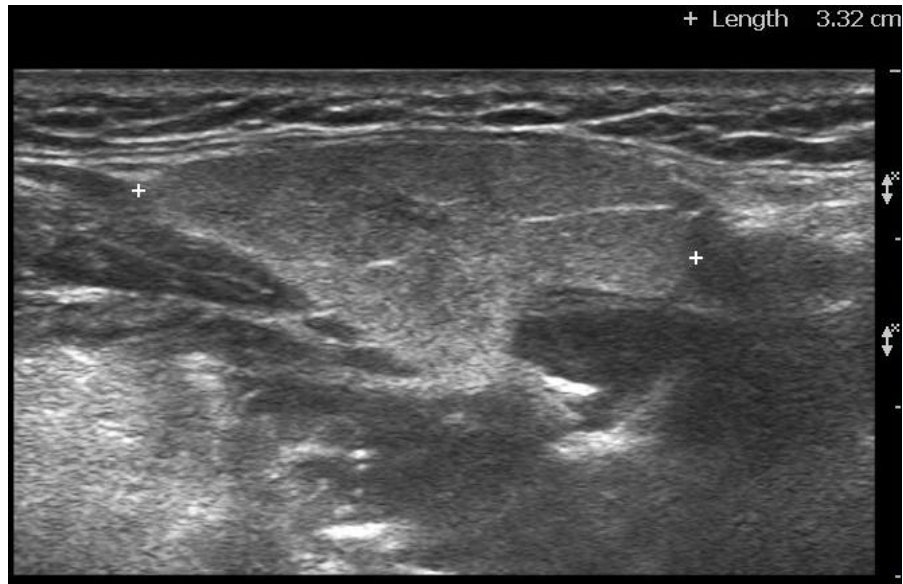


Figure. 4.2: Transverse grey scale sonogram shows the measurement of the transverse (TS) dimension of a normal submandibular gland (calipers).

The echogenicity of the submandibular glands was assessed, and subjectively classified into hypoechoic, isoechoic and hyperechoic when compared to the adjacent mylohyoid muscle. Objective evaluation of the submandibular gland echogenicity was also conducted. Multiple transverse scans of the submandibular glands were taken, and images were stored in the hard disk of the ultrasound unit. Archived images were retrieved after the ultrasound examination, and the echo-intensity of the submandibular glands and the adjacent mylohyoid muscles were quantified with the use of the specific software QLabTM (Philips Medical System, Bothell, WA, USA). In the quantification of the echo-intensity of the submandibular glands and mylohyoid muscles, the boundaries of submandibular gland and those of the mylohyoid muscle were outlined manually, and the value of the echo-intensity of the submandibular glands and mylohyoid muscle were then measured automatically by the QLabTM (Figure 4.3). In this quantification method, echolucent structures had

lower echo-intensity values whereas echogenic structures had higher echo-intensity values. Three images with larger cross-sectional area of submandibular glands and mylohyoid muscle were selected and measured, and a mean value of the echo-intensity of submandibular gland and the muscle were obtained. An echogenicity index of each submandibular gland was then calculated with the following equation:

$$\text{Echogenicity index} = \frac{\text{mean submandibular gland echo-intensity}}{\text{mean mylohyoid muscle echo-intensity}}$$

In the assessment of the echogenicity index of submandibular glands, hypoechoic submandibular glands tended to have a lower echogenicity index, whereas hyperechoic submandibular glands tended to have a higher echogenicity index.

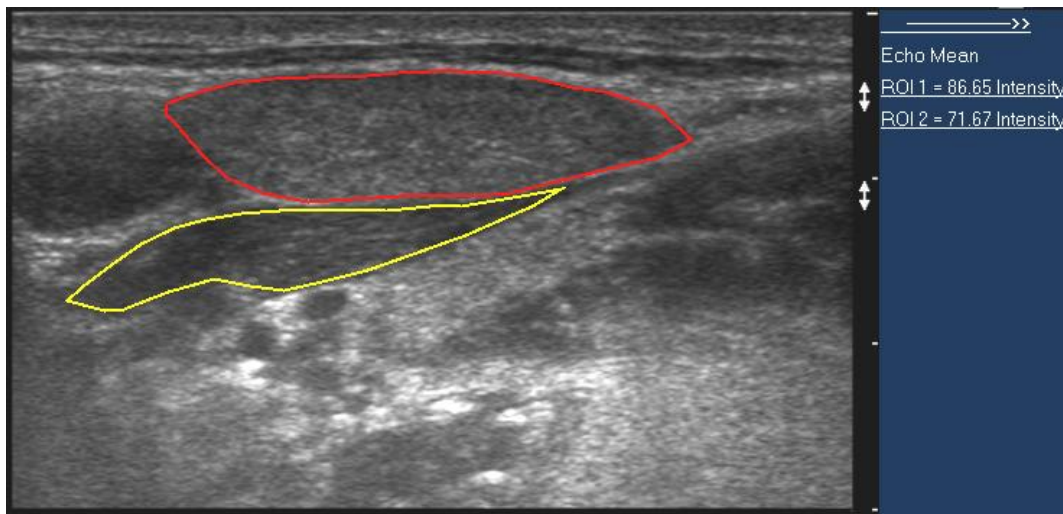


Figure 4.3: Transverse grey scale sonogram shows the measurement of the echo-intensity of a normal submandibular gland (red line) and the adjacent mylohyoid muscle (yellow line) by outlining their boundaries using software QLab™. The echo-intensity of the submandibular gland (ROI 1) and the mylohyoid muscle (ROI 2) are shown in the right upper corner of the image.

In the assessment of echogeneity, the gland was considered to be homogeneous when its parenchyma had a uniform echogenicity, whereas it was considered heterogeneous when it showed non-uniform parenchymal echogenicity. For the heterogeneous submandibular glands, they were further evaluated with the previously described criteria for chronic fibrotic sialadenitis: multiple hypoechoic areas and multiple hyperechoic lines (Shimizu et al. 2006). The hyperechoic lines within the submandibular gland were considered to be the intra-glandular ducts, and the conspicuity of the intra-glandular ducts was also assessed, which was classified into the following 3 categories:

Obviously seen – the intra-glandular ducts were obviously seen with the echogenicity of the ducts substantially higher than that of the parenchyma of the gland.

Marginally seen – the intra-glandular ducts could be seen but not as obvious as in “obviously seen”. The echogenicity of the ducts was just slightly higher than that of the parenchyma of the gland.

Not seen – intra-glandular ducts were not seen within the gland.

The border sharpness of submandibular glands was also assessed, and was categorized into well-defined or ill-defined. The submandibular gland was considered as well-defined when a clear or sharp border surrounding the gland was observed sonographically; whilst the gland was considered as ill-defined when an unclear or blurred border was observed.

4.2.4 Evaluation of submandibular gland dose

The total mean submandibular gland dose of the NPC patients treated with RT was evaluated with the use of isodose display.

4.2.5 Statistical analysis

Mann-Whitney Test was used to calculate the level of significance of the difference in the size and echogenicity index between the submandibular glands of the healthy subjects and of the post-RT NPC patients, and between the submandibular glands of the patients with the mean submandibular gland dose of 66 Gy and 60 Gy.

Fisher's Exact Test was used to calculate the level of significance of the difference in the echogenicity, echogeneity, conspicuity of intra-glandular ducts, the incidence of hypoechoic areas and the border sharpness between the submandibular glands of the healthy subjects and of the post-RT NPC patients, and between the submandibular glands of the patients with the mean submandibular gland dose of 66 Gy and 60 Gy.

4.3 Results

A total of 294 (162 from patients and 132 from healthy subjects) submandibular glands were evaluated with ultrasonography. Results showed that the mean transverse (TS) dimension of the submandibular glands of the healthy subjects (3.28 cm) was significantly greater than that of post-RT NPC patients (2.53 cm) ($p < 0.05$, Table 4.1).

Table 4.1: Comparison of the mean transverse dimension and the mean echogenicity index of submandibular glands between healthy subjects and post-RT NPC patients; between left and right sides (normal and irradiated); and between irradiated by 66 Gy and 60 Gy

	Healthy Subjects	NPC Patients	p-value	66 Gy Patients	60 Gy Patients	p-value
	Mean±SD	Mean±SD		Mean±SD	Mean±SD	
TS (cm)	3.28 ± 0.39	2.53 ± 0.42	< 0.05	2.50 ± 0.39	2.67 ± 0.51	0.14
Echogenicity index	1.54 ± 0.32	1.48 ± 0.29	0.28	1.49 ± 0.29	1.46 ± 0.28	0.53

TS = Transverse dimension of submandibular gland, SD = Standard deviation, NPC = Nasopharyngeal carcinoma, RT = Radiotherapy

Majority of the submandibular glands in the healthy subjects (99%) and in the post-RT NPC patients (97%) were hyperechoic when compared with the adjacent mylohyoid muscles (Table 4.2, Figures 4.4 and 4.5). The difference in the echogenicity of the submandibular glands between the two study groups was not statistically significant ($p = 0.23$). In the quantitative assessment of the submandibular gland echogenicity, there was also no significant difference in the mean echogenicity index of the submandibular glands between the two study groups ($p = 0.28$, Table 4.1).

Table 4.2: Comparison of echogenicity, echogeneity, incidence of hypoechoic areas, conspicuity of intra-glandular ducts and border sharpness of submandibular glands in healthy subjects and post-RT NPC patients

	Number of submandibular glands (%)		p-value
	Healthy Subjects	Post-RT NPC patients	
Echogenicity			
<i>Hyperechoic</i>	131 (99%)	157 (97%)	0.23
<i>Isoechoic</i>	1 (1%)	5 (3%)	
<i>Hypoechoic</i>	0 (0%)	0 (0%)	
Echogeneity			
<i>Homogenous</i>	119 (90%)	45 (28%)	< 0.05
<i>Heterogenous</i>	13 (10%)	117 (72%)	
Hypoechoic areas			
<i>Present</i>	6 (5%)	75 (46%)	< 0.05
<i>Absent</i>	126 (95%)	87 (54%)	
Conspicuity of intra-glandular ducts			
<i>Obviously seen</i>	3 (2%)	7 (5%)	0.52
<i>Marginally seen</i>	123 (93%)	153 (94%)	
<i>Not seen</i>	6 (5%)	2 (1%)	
Border sharpness			
<i>Well-defined</i>	69 (52%)	18 (11%)	< 0.05
<i>Ill-defined</i>	63 (48%)	144 (89%)	

RT = Radiotherapy, NPC = Nasopharyngeal carcinoma

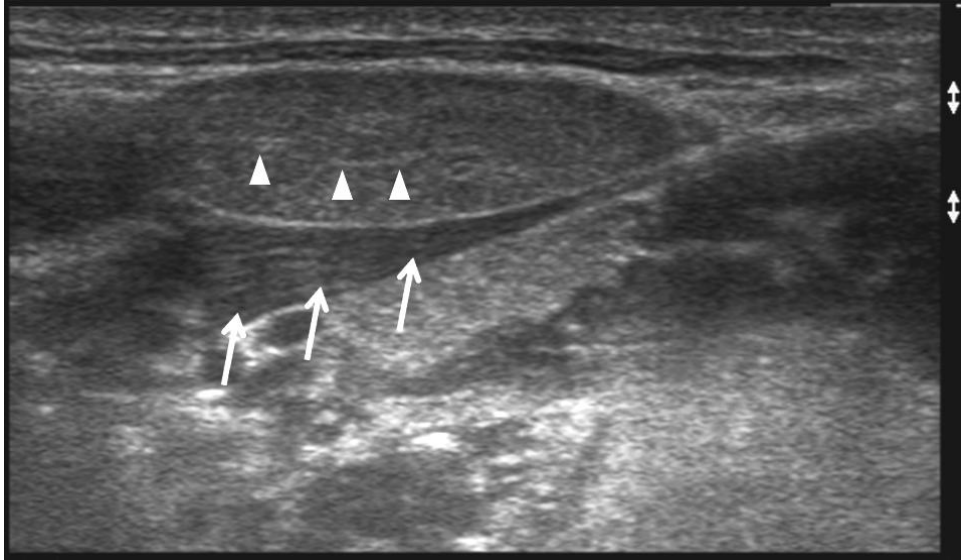


Figure 4.4: Transverse grey scale sonogram shows a normal submandibular gland which is characterized with homogenous echotexture, well-defined border, marginally seen intra-glandular ducts (arrowheads) and hyperechogenicity when compared with the adjacent mylohyoid muscle (arrows).

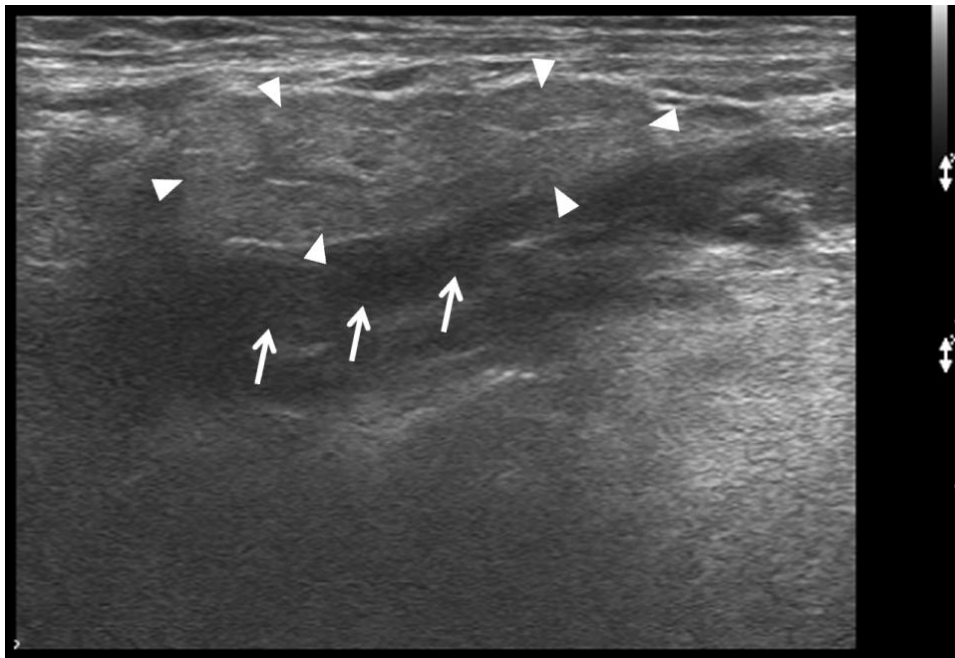


Figure 4.5: Transverse grey scale sonogram shows an irradiated submandibular gland (arrowheads). The gland is with ill-defined border, and it is hyperechoic when compared with the adjacent mylohyoid muscle (arrows).

The majority of the submandibular glands (90%) in the healthy subjects appeared homogenous on ultrasound (Figure 4.4). In the post-RT NPC patients, only 28% of submandibular glands were homogenous whereas 72% of them were heterogeneous (Figure 4.6). Result showed that the difference in the echogeneity of submandibular glands between the healthy subjects and the post-RT NPC was statistically significant ($p < 0.05$, Table 4.2).

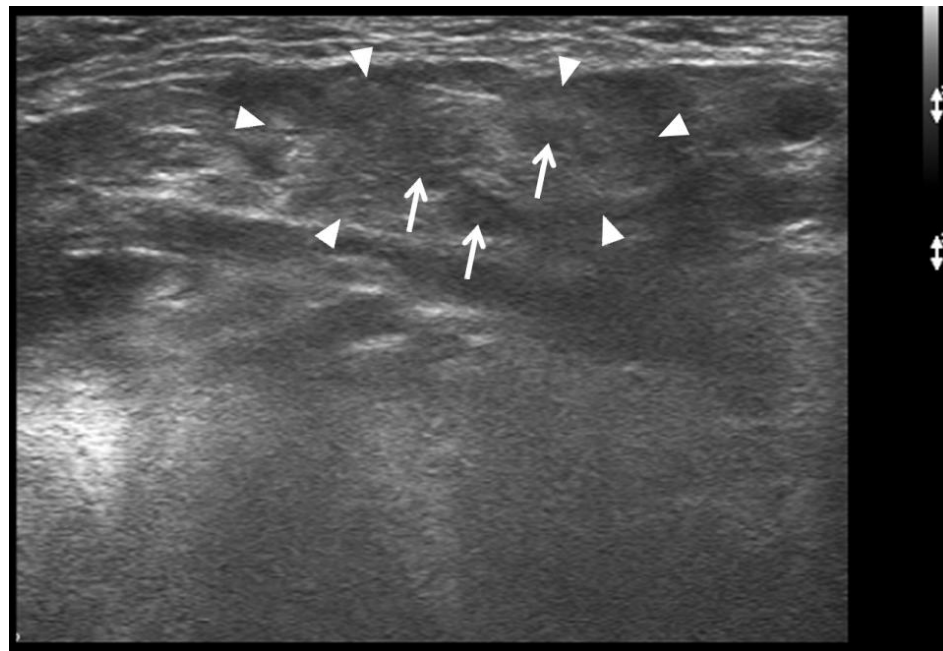


Figure 4.6: Transverse grey scale sonogram shows an irradiated submandibular gland (arrowheads), which demonstrates with hypoechoic areas (arrows) and is heterogeneous in echotexture.

Majority of the submandibular glands in healthy subjects (95%) did not show hypoechoic areas (Figure 4.4). However, 46% of the submandibular glands in the post-RT NPC patients showed intra-glandular hypoechoic areas (Figure 4.6). The

difference in the incidence of hypoechoic areas in the submandibular glands between the two study groups was statistically significant ($p < 0.05$, Table 4.2).

In the ultrasound images, intra-glandular ducts appeared as echogenic linear structures within the submandibular gland. Intra-glandular ducts were demonstrated in the submandibular glands of the healthy subjects and the post-RT NPC patients, with various degrees of conspicuity. Table 4.2 shows the conspicuity of intra-glandular ducts on ultrasound of the two study groups. The majority of intra-glandular ducts in the healthy subjects (93%) and the post-RT NPC patients (94%) were marginally seen in the ultrasound images (Figures 4.4 and 4.7). The difference in the conspicuity of intra-glandular ducts between the healthy subjects and the post-RT NPC patients was not significant ($p = 0.52$).

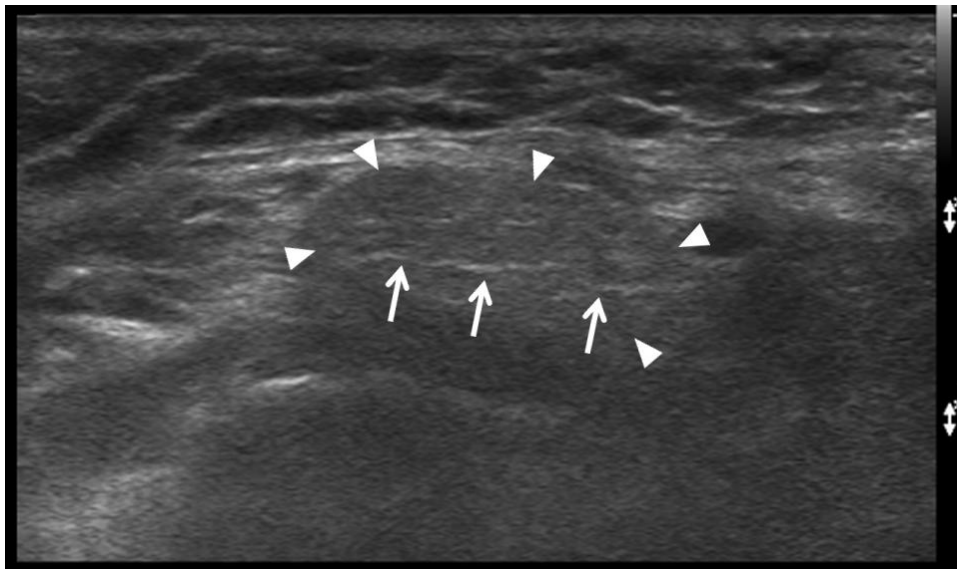


Figure 4.7: Transverse grey scale sonogram shows a small irradiated submandibular gland (arrowheads) with marginally seen intra-glandular ducts (arrows).

More than half (52%) of the submandibular glands in the healthy subjects were well-defined with sharp borders (Figure 4.4), whilst the majority of the submandibular glands (89%) in the post-RT NPC patients were ill-defined (Figure 4.5). The difference in the border sharpness in the submandibular glands between the two study groups was statistically significant ($p < 0.05$, Table 4.2).

No significant differences were found in the mean TS dimension, mean echogenicity index, echogenicity, incidence of hypoechoic areas, conspicuity of intra-glandular ducts and border sharpness of the submandibular glands between post-RT NPC patients with mean submandibular gland dose of 66 Gy and 60 Gy ($p > 0.05$, Table 4.1).

4.4 Discussion

In the present study, the mean transverse dimension of the submandibular glands in the post-RT NPC patients was significantly smaller than that of the healthy subjects, which was consistent with the findings of the previous studies (Gritzmann et al. 2003, Price et al. 1995). Smaller submandibular gland size in the post-RT NPC patients is probably due to the cellular change of the gland after irradiation. Price et al. (1995) found significant loss of both serous and mucous acini in the irradiated submandibular glands following fractionated exposure over 50 Gy. Henriksson et al. (1994) also found that there was significant serous acinar cell loss of submandibular

glands at 180 days after irradiation, but the loss of mucous acinar cells was less pronounced. Henriksson et al. (1994) also reported that the radiation-induced acinar cell loss was dose dependent, in which higher radiation dose caused greater reduction in the acinar cell density. On the other hand, Radfar and Sirois (2003) found significant parenchymal loss and acinar atrophy in the submandibular glands of Hanford minipigs at one month following fractionated irradiation of a total dose of 70 Gy to the glands. Such mass parenchymal loss and acinar atrophy could lead to shrinkage of the gland, and the reduction of the transverse dimension.

Results of the present study showed that the submandibular glands in the healthy subjects tended to be more homogenous, whilst those in the post-RT NPC patients were predominantly heterogeneous. Similar findings were also reported in the previous studies (Gritzmann et al. 2003, King et al. 2007). The heterogeneous appearance of the submandibular glands should be due to the disorganized acinar cell arrangement from parenchymal loss and acinar atrophy after high dose irradiation, resulting in uneven distribution of intra-glandular reflective interfaces for ultrasound beam (Nagler 2002, Ying et al. 2007). Besides, over half of the submandibular glands in the post-RT NPC patients presented with multiple hypoechoic areas on ultrasound. The multiple hypoechoic areas might be the patches of hypoechoic inflammatory infiltrates due to radiation-induced sialadenitis. Radiation-induced sialadenitis had been widely reported in the irradiated salivary glands in the patients who received head and neck radiotherapy, which was histopathologically characterized by inflammatory infiltration and fibrosis (Radfar

and Sirois 2003, Seifert 1995, Teymoortash et al. 2005). Such multiple hypoechoic areas could give rise heterogeneous echotexture of the irradiated submandibular glands.

In the present study, the submandibular gland echogenicity was compared with the adjacent mylohyoid muscle because both structures were closely located, which allowed convenient comparison of echogenicity in a single sonogram clinically. The echogenicity of submandibular glands is routinely and clinically determined by subjective operator's perception; however, slight echogenicity variations may not be easily identified by naked eyes. To achieve accurate evaluation and quantification, echogenicity index of submandibular gland was utilized in this study. Although Ying et al. (2007) found that the parotid glands of the post-RT head and neck cancer patients tended to be hypoechoic when compared to the adjacent masseter muscle, the submandibular glands in the post-RT NPC patients were predominantly hyperechoic when compared to the adjacent mylohyoid muscle in the present study (97%). Both subjective echogenicity assessment and quantitative echogenicity index showed hyperechogenicity in the irradiated submandibular glands and there was no significant difference in echogenicity between irradiated and normal submandibular glands. Although irradiation could lead to submandibular parenchymal loss resulting in reduced reflective interfaces for ultrasound beam (Ying et al. 2007), fatty infiltration had also been found in the irradiated salivary glands (King et al. 2007) which increased the echogenicity of the glands. During the comparison of echogenicity, it should be noted that the echogenicity change in submandibular gland

and mylohyoid muscle might not be in linear or proportional, which could affect the comparison of echogenicity. Nevertheless, the radiation tolerance of muscle was found significantly higher than that of submandibular gland and hence the echogenicity variation of muscle after irradiation should not be as much as that in the submandibular glands (Emami et al. 1991).

Results of the present study showed that the intra-glandular ducts of submandibular glands were in general marginally seen in both post-RT NPC patients (94%) and healthy subjects (93%), and there was no significant difference between the two study groups. The result of the present study was different from the findings on the parotid glands in a previous study. Ying et al. (2007) found obviously seen intra-glandular ducts in the irradiated parotid glands sonographically, which was believed due to the post-RT ductal proliferation and fibrosis in the glands. Although Radfar and Sirois (2003) reported similar histological changes including ductal proliferation, ductal dilation and fibrosis in both irradiated parotid and submandibular glands, the intra-glandular ducts of submandibular glands were marginally seen in the present study. The reason for the discrepancy of findings is not clear, but we postulate that this may be due to the radiosensitivity difference between parotid glands and submandibular glands. Previous studies reported that submandibular glands were less radiosensitive than parotid glands (Cooper et al. 1995, Liem et al. 1996, Vissink et al. 1990), and thus to the post-RT ductal proliferation and fibrosis in the irradiated submandibular glands were subtle, which were then not obvious on ultrasound. This

may account for the similar conspicuity of intra-glandular ducts between irradiated and non-irradiated submandibular glands in the present study.

In the present study, the borders of the normal submandibular glands were generally well-defined (52%), whilst the majority of the irradiated glands were ill-defined (89%) sonographically. A normal submandibular gland is anatomically surrounded by a tight capsule (Larsson et al. 1987) providing a highly reflective interface for ultrasound beam, which account for the well-defined borders demonstrated on ultrasound. Although there is lack of study documenting the cellular changes of the capsules of irradiated submandibular glands, we postulate that high dose of radiation could destroy the capsule resulting in ill-defined borders of the irradiated glands. However, further histological and ultrasound studies are necessary to investigate the post-RT changes in the capsules of the irradiated submandibular glands.

For the comparison of the submandibular glands in the patients with the mean gland dose of 66 Gy and 60 Gy, there were no significant differences in mean transverse dimension, mean echogenicity index, echogenicity, echogeneity, incidence of hypoechoic areas, conspicuity of the intra-glandular ducts and border sharpness between the two study groups. This might be due to the fact that the radiation dose difference (i.e. 6 Gy) was not great enough to cause an obvious variation in the sonographic appearance of the submandibular glands. Several previous studies reported permanent damage of salivary gland or irreversible impaired salivary flow in the salivary glands received ionizing radiation of 24 Gy or more (Eisbruch et al.

1999, Leek and Albertsson 2002, Shiboski et al. 2007). As all the post-RT submandibular glands in the present study received a radiation dose of 60 Gy or above, permanent damage of the glands was expected.

A limitation of this study was that unlike the IMRT technique, the dose delivered to submandibular gland was an estimation (by retrospectively superimposing the treatment fields on the CT slices) for the patients treated by conventional technique, as their treatment plans were not directly performed on CT. This might result in a reduced accuracy in the determination of the submandibular gland dose. Besides, further studies are suggested to evaluate the correlation of the absorbed dose of submandibular glands with the sonographic appearance of the glands.

To conclude, ultrasound is an effective imaging modality in assessing radiation-induced changes of submandibular glands in the post-RT NPC patients. The irradiated submandibular glands are characterized with reduced gland size, heterogeneous, multiple hypoechoic areas and ill-defined glandular border. For more accurate diagnosis, the sonographic appearances of the irradiated submandibular glands should be noted in ultrasound examination for patients treated with radiotherapy for NPC or other head and neck cancers that involve upper neck irradiation.

Chapter Five

Study Three

Sonographic appearance of thyroid glands in patients treated with intensity-modulated radiotherapy or conventional radiotherapy for nasopharyngeal carcinoma

5.1 Introduction

External beam radiotherapy including two-dimensional conventional radiotherapy (RT) and intensity-modulated radiotherapy (IMRT) are commonly used to treat nasopharyngeal carcinoma (NPC) in Hong Kong. As there is a high incidence of associated cervical lymph node metastases (around 60-96%) (Glastonbury 2007), an anterior cervical field is also employed to irradiate cervical lymph nodes for all patients. Since the anterior cervical field to the neck involved irradiation of thyroid glands which are radiosensitive (Figure 5.1), post-RT thyroid disorders are common in the patients (Ulger et al 2007). Hypothyroidism is the most common manifestation of post-RT head and neck cancer patients, in which around 20-30% of the patients would develop primary hypothyroidism (Alterio et al. 2007, Ulger et al. 2007, Bonato et al. 2008). Patients with higher thyroid dose tend to have higher risk of hypothyroidism (Tell et al. 1997, Bhandare et al. 2007). It was found that primary hypothyroidism could occur with the radiation doses as low as 20 Gy, but mostly occur after 30-50 Gy of irradiation (Tell et al. 1997, Garcia-Serra et al. 2005,

Bhandare et al. 2007). Hypothyroidism is a late complication as it is usually occurred within 5 years, with the peak incidence at 2-3 years after RT (Tell et al. 1997, Jereczek-Fossa et al. 2004, Nishihara et al. 2006, Bhandare et al. 2007, Ulger et al 2007). The exact pathophysiology of radiation-induced hypothyroidism is still unclear. However, direct damages of the thyroid parenchyma and vasculatures by radiation are believed to be the main causes of the thyroid disorder (Ricardi et al. 2001, Ulger et al 2007).

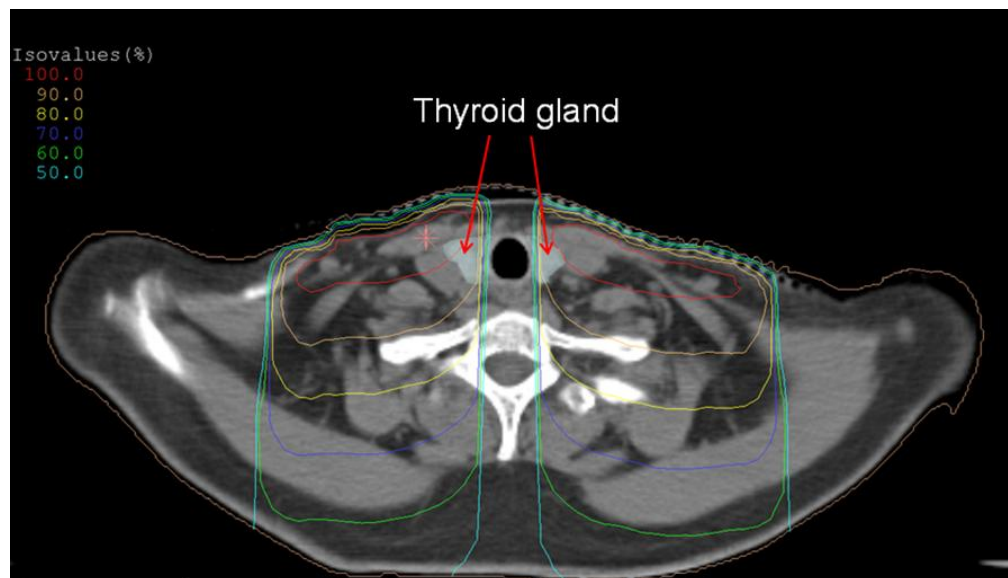


Figure 5.1: Computed tomography image shows that thyroid gland is within the high dose region (90-100% of the prescribed dose) in the anterior cervical field.

Hypothyroidism could be manifested by a number of symptoms including skin dryness, depression, chronic fatigue, weight gain, constipation and cold intolerance, which seriously impair patient's health and quality of life (Liening et al. 1990, Turner et al. 1995, Jereczek-Fossa et al. 2004). Moreover, there is a tendency of evolving subclinical hypothyroidism into clinical hypothyroidism in post-RT head

and neck cancer patients (Aich et al. 2005, Bhandare et al. 2007). Persistent high thyrotropin (TSH, thyroid stimulating hormone) level in patients could also increase the risk of thyroid cancer by 15-53 folds compared with the non-irradiated population (Stewart et al. 1989, Crom et al. 1997, Tell et al. 1997, Solt et al. 2000, Jereczek-Fossa et al. 2004, Nishihara et al. 2006). Apart from hypothyroidism, thyroid size reduction (Ricardi et al. 2001, Miller-Thomas et al. 2009) and increased number of thyroid nodules (Stewart et al. 1989, Soberman et al. 1991, Schneider et al. 1997) are also common morphological changes of the thyroid glands after irradiation. Hence, an early detection of radiation-induced hypothyroidism or other associated thyroid disorders is necessary for early disease management in order to sustain patient's health status and prevent thyroid cancer development.

Thyroid function test is a common method to assess thyroid dysfunction, especially hypothyroidism, for post-RT head and neck cancer patients. It measures the circulating serum thyroid hormone levels for thyroid function assessment. TSH and free thyroxine (fT4) are the common parameters for assessing thyroid function (Rose 2001). Although thyroid function test could help assessing thyroid function, and identifying clinical and subclinical hypothyroidism in patients treated with RT, it cannot assess the morphological changes and vascular damages of post-RT thyroid glands, which could be evaluated by medical imaging such as ultrasonography.

Ultrasonography has been widely used for the assessment of thyroid glands. However, it is not commonly used to evaluate radiation-induced damages of thyroid

glands, and there is a lack of systematic evaluation of the post-RT sonographic appearance of the thyroid glands. The post-RT changes of the sonographic appearance must be identified so that these changes would not be misinterpreted as other thyroid gland diseases. On the other hand, IMRT has the advantage of effective sparing of the organ at risks and, at the same time, providing accurate dose conformity to the tumour, which might reduce possible radiation-induced damages of thyroid gland during cervical lymph node irradiation. Therefore, this study aimed to determine the value of ultrasonography in identifying post-RT changes of thyroid glands, and to distinguish the sonographic appearance of thyroid gland between NPC patients with their cervical lymph nodes treated with conventional anterior cervical field and those treated with IMRT. The information in this study provided baseline information for further sonographic investigations on radiation-induced damages of thyroid glands.

5.2 Materials and methodologies

5.2.1 Subjects

5.2.1.1 Part I: Comparison between patients with normal thyroid function and those with abnormal thyroid function

A total of 103 NPC patients (70 males and 33 females) who had finished radiotherapy, with the cervical lymph nodes treated with anterior cervical field, between 2000 and 2008 in Queen Mary Hospital (QMH) were recruited in the study. The age range of the patients was 24 to 71 years old with the mean age of 50.2 ± 9.1 years. Another 30 NPC patients (20 males and 10 females) who had completed radiotherapy, with the cervical lymph nodes treated with IMRT, between 2006 and 2008 in Princess Margaret Hospital (PMH) were also recruited. The age range of these 30 patients was 29 to 81 years old with the mean age of 53.0 ± 13.0 years. Based on the results of the thyroid function test, the patients were categorized into normal thyroid function (normal TSH and fT4 levels) and abnormal thyroid function (abnormal TSH and/or fT4 level) groups. The sonographic appearance of thyroid glands in patients with normal thyroid function and those with abnormal thyroid function were evaluated and compared.

In the present study, patients with recurrent disease or block dissection of the neck were excluded. Patients with previous thyroidectomy or known thyroid diseases

were also excluded. All the patients were recruited when they attended the follow-ups in the hospitals, and the clinical history of patients was reviewed by oncologists for the recruitment.

5.2.1.2 Part II: Comparison between healthy subjects and patients treated with different radiotherapy techniques

For the 103 NPC patients recruited in QMH, 39 of them (30 males and 9 females) who had finished radiotherapy between 2005 and 2007 were involved in this part of the study. The age range of these 39 patients was 32 to 62 years old with the mean age of 47.8 ± 7.8 years. The 30 NPC patients recruited in PMH were also involved in the study.

Besides, a total of 61 healthy subjects (32 males and 29 females) were also recruited as the control group. Subjects with clinical history of any cancers or thyroid gland diseases were excluded. The age range of the healthy subjects was 27 to 82 years old with the mean age of 47.0 ± 9.8 years.

Informed written consent was obtained from all patients and healthy subjects. Each patient and healthy subject received a thyroid ultrasound examination, and a blood test for thyroid function evaluation. The thyroid ultrasound examination and blood test for all patients were arranged so that the time of the ultrasound examination and the blood test was around 2 to 3 years after the completion of RT.

This study was approved by the Human Subjects Ethics Sub-committee of the Hong Kong Polytechnic University and the Institutional Review Boards of the involved hospitals.

5.2.2 Thyroid ultrasound examination

A thyroid ultrasound examination was performed on all NPC patients and healthy subjects by single operator (*i.e.* Cheng Chi Him). All ultrasound examinations were performed with the Philips HD11 XE or the Philips HD11 ultrasound unit in conjunction with a 5-12 MHz linear transducer (Philips Medical System, Bothell, WA, USA).

In the ultrasound examination, patients/subjects laid supine on the examination couch with the neck hyperextended and shoulders supported by a pillow. The right and left thyroid lobes were scanned separately with the patient/subject's head turned to the opposite side. Transverse and longitudinal scans of the thyroid lobes were performed. Patients/subjects with incidental detection of thyroid nodule(s) in the ultrasound examination, and the thyroid lobes with nodule(s) were identified and recorded. To measure the thyroid lobe volume, the maximum craniocaudal (CC), lateromedial (LM) and anteroposterior (AP) dimensions of the thyroid lobe were measured. The LM and AP dimensions were measured in the transverse scan plane with a maximum cross-sectional area of the thyroid lobe (Figure 5.2). The CC dimension was measured in the longitudinal scan of the thyroid lobe (Figure 5.3).

All the dimensions of the thyroid lobe were measured using the built-in electronic callipers of the ultrasound unit. The thyroid volume was the sum of the volume of left and right thyroid lobes, and the thyroid lobe volume was calculated by the equation described in a previous report (Ying et al. 2008):

$$\text{Thyroid lobe volume} = 0.38 \cdot (\text{CC} \cdot \text{LM} \cdot \text{AP}) + 1.76$$

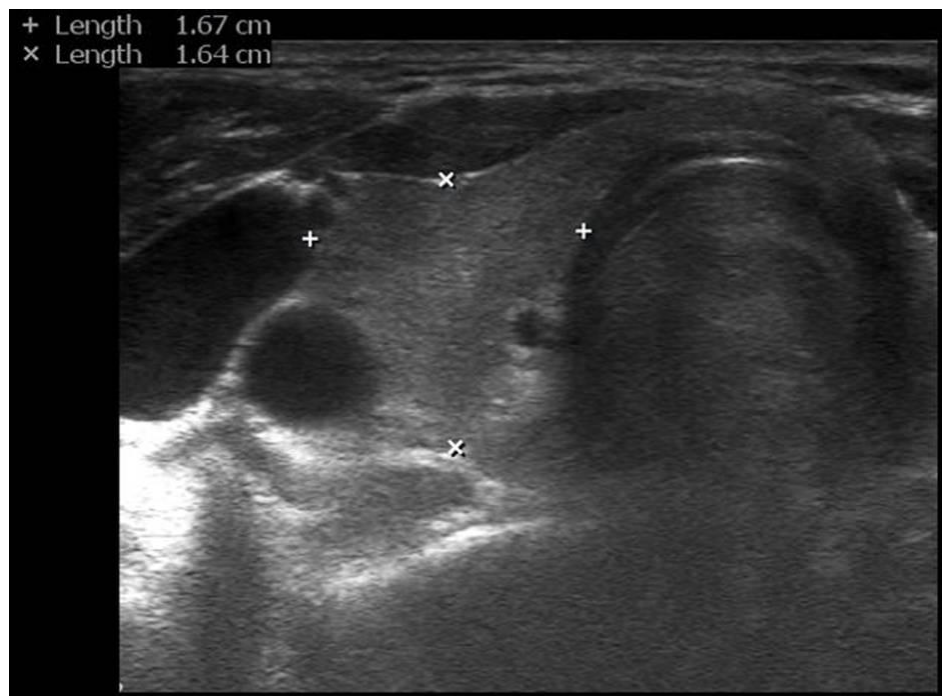


Figure 5.2: Transverse grey scale sonogram shows the measurement of the lateromedial (LM) dimension (calipers “+”) and anteroposterior (AP) dimension (calipers “x”) of the thyroid lobe in a patient with the neck treated with intensity-modulated radiotherapy.



Figure 5.3: Longitudinal grey scale sonogram shows the measurement of the longitudinal (LS) dimension (calipers) of the thyroid lobe in a patient with the neck treated with intensity-modulated radiotherapy.

The echogenicity of the thyroid gland was assessed and subjectively classified into hypoechoic, isoechoic and hyperechoic when compared with the adjacent sternomastoid muscle. Multiple images of the transverse scan of the thyroid gland were taken. Archived images were retrieved after the ultrasound examination, and the echo-intensity of the thyroid gland and sternomastoid muscle was quantified with the specific software QLabTM (Philips Medical System, Bothell, WA, USA). In the quantification of the echo-intensity of the thyroid gland and muscle, the boundaries of the thyroid gland and the boundaries of the muscle were outlined manually, and the value of the echo-intensity of the thyroid gland and muscle were measured automatically by the inbuilt software (Figure 5.4). In each side of the neck, three images with relative homogenous echopattern and larger cross-sectional area of the thyroid lobe were selected and measured. The mean value of the echo-intensity of

the thyroid lobe, and that of the sternomastoid muscle were obtained. The echogenicity index of the thyroid lobe was then calculated with the following equation:

$$\text{Echogenicity index} = \frac{\text{mean echo-intensity of the thyroid lobe}}{\text{mean echo-intensity of the sternomastoid muscle}}$$

The mean echogenicity index of the entire thyroid gland was the mean value of the echogenicity indexes of the left and right thyroid lobes. In the assessment of the echogenicity index of thyroid glands, hypoechoic thyroids tended to have a lower echogenicity index, whereas hyperechoic thyroids tended to have a higher echogenicity index.

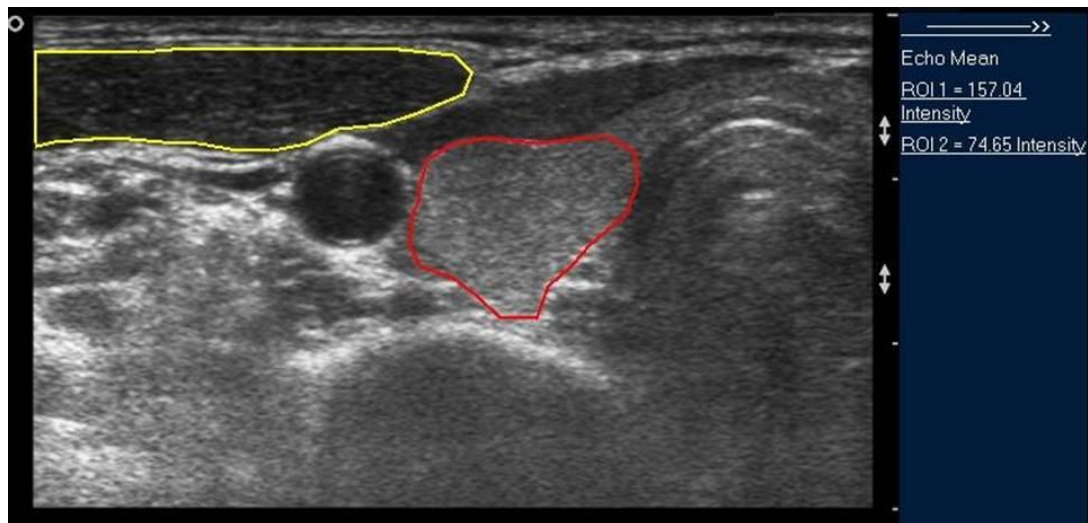


Figure 5.4: Transverse grey scale sonogram shows the measurement of the echo-intensity of a normal thyroid gland (red line) and the adjacent sternomastoid muscle (yellow line) by outlining their boundaries using the software QLabTM. The echo-intensity of the thyroid gland (ROI 1) and the sternomastoid muscle (ROI 2) are shown in the right upper corner of the image.

The echogeneity of the thyroid glands was assessed. The thyroid gland was considered to be homogeneous when its parenchyma showed a uniform echogenicity, whereas the thyroid was considered heterogeneous when it demonstrated a non-uniform parenchyma.

Power Doppler sonography was used to assess the thyroid vascularity (Figure 5.5). The Doppler setting was standardized for high sensitivity in the detection of blood vessels and with minimum artifact: medium wall filter, pulse repetition frequency (PRF) 700Hz, medium persistence. The colour gain was first increased to a level which shows colour noise, and then decreased until the noise disappears (Ying et al. 2007). Multiple Doppler ultrasound images were taken at different parts of the thyroid gland. In each thyroid lobe, three images with the most abundant thyroid vascularity were assessed. For each ultrasound image, the degree of thyroid vascularity was assessed by a customized algorithm using the software MATLAB[®] (Ying et al. 2009).

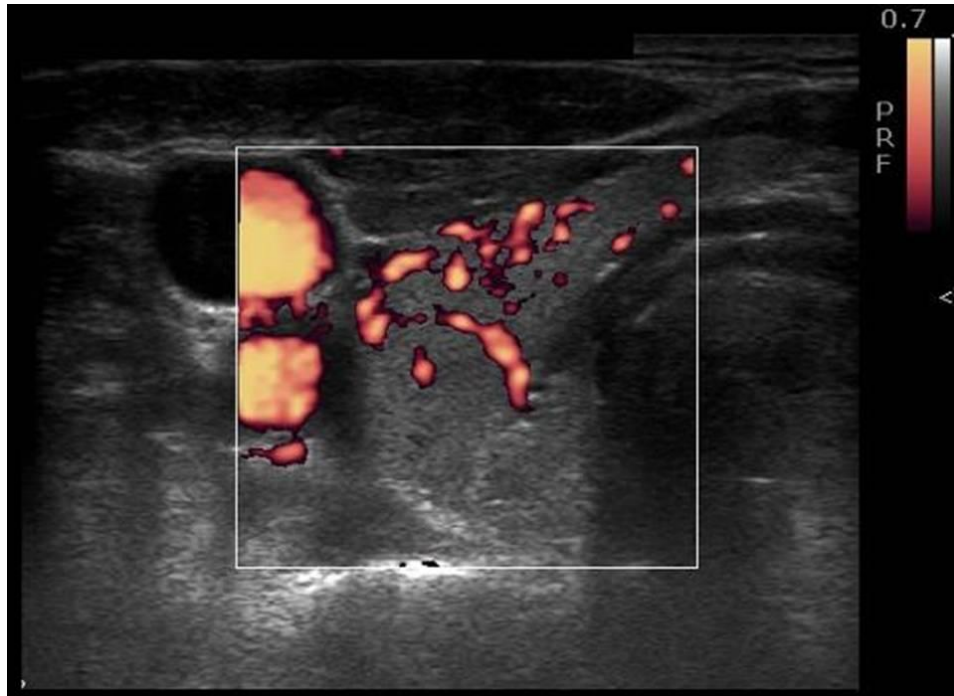


Figure 5.5: Transverse Power Doppler sonogram shows the vascularity measurement of the thyroid lobe in a patient with his neck treated with intensity-modulated radiotherapy.

In the evaluation of the degree of thyroid vascularity, the boundaries of the thyroid lobe (i.e. the region of interest, ROI) were outlined manually on the ultrasound image. The junction of the right and left lobes and the thyroid isthmus was approximately of the lateral border of the trachea. The customized algorithm extracted the ROI from the ultrasound image and the total number of pixels of the ROI was measured by the algorithm. Subsequently, the colour pixels (i.e. pixels other than grey scale) were extracted from the ROI and the number of colour pixels was measured (Figure 5.6). The vascularity index (degree of vascularity) of each thyroid lobe was then calculated by the following equation:

$$\text{Vascularity index} = \frac{\text{Number of colour pixels within the ROI}}{\text{Total number of pixels within the ROI}}$$

The mean thyroid vascularity index of the whole thyroid gland was the mean value of the vascularity indexes of the left and right thyroid lobes.

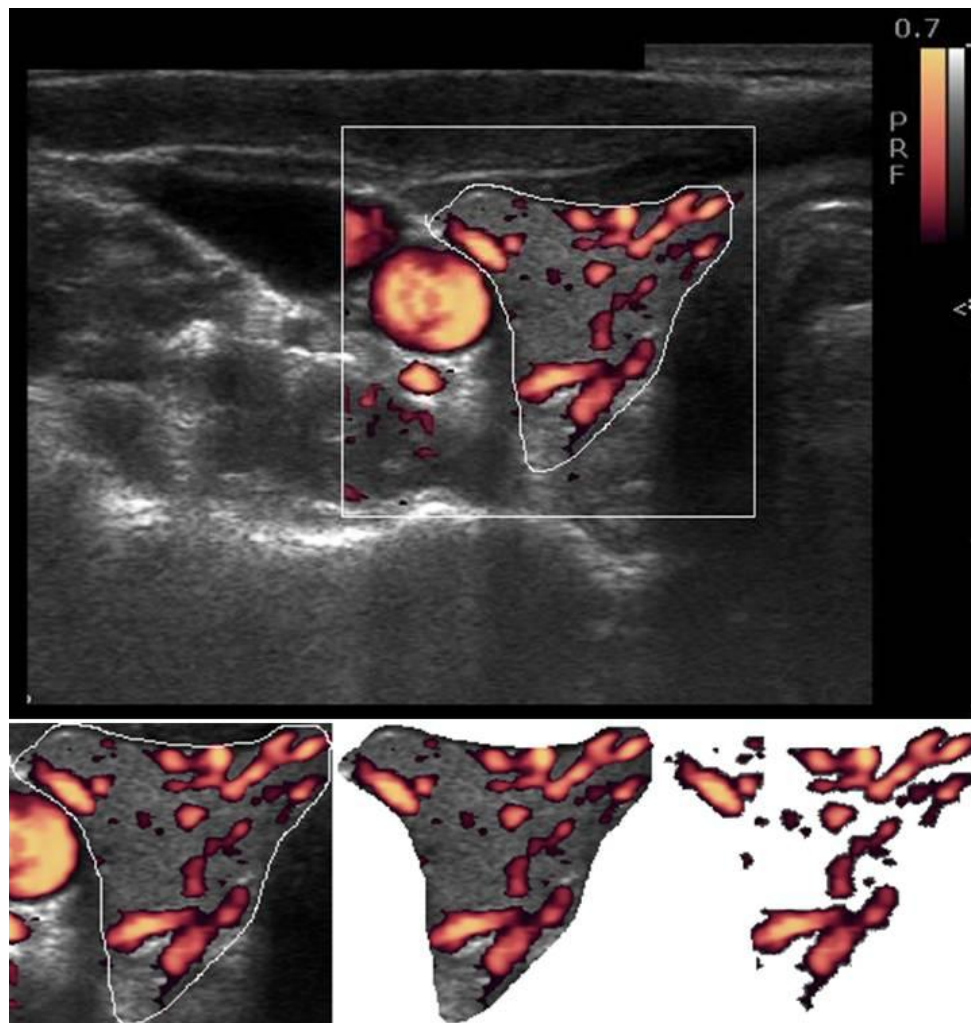


Figure 5.6: Sonograms demonstrated the extraction of colour pixel in the region of interest (ROI) for the measurement of vascularity index of thyroid gland.

5.2.3 *Thyroid function test*

For each NPC patient and healthy subject, 5 ml of blood sample was drawn by venipuncture and put into a heparin tube. Plasma was extracted after centrifugation at 2500 rpm for 10 minutes at 4 C°, and was then stored in the refrigerator at -25 C° until being tested. Before the test, the plasma was thawed at room temperature for 30 minutes. An automated VIDAS® analyzer (bioMerieux, France) was used to measure the thyroid hormone levels. Plasma TSH level was assayed by analytical reagent kits for TSH (VIDAS® TSH, bioMerieux China Ltd., Jiangmen, Guangdong, China), and plasma fT4 level was evaluated by analytical reagent kits for fT4 (VIDAS® fT4, bioMerieux China Ltd., Jiangmen, Guangdong, China). Subjects with a TSH level between 0.27 and 4.7 µUI/mL, and a fT4 level between 9 and 20 pmol/L were considered to be normal (Col et al. 2004, Surks et al. 2004). Subjects with either TSH or fT4 levels out of the aforementioned range were considered as abnormal.

5.2.4 *Evaluation of thyroid gland dose*

For NPC patients with cervical lymph nodes treated with anterior cervical field in QMH, the total mean thyroid dose was evaluated with the use of isodose display. For NPC patients with cervical lymph nodes treated with IMRT in PMH, the RT treatment plan was retrieved from the treatment planning system (TPS). The treatment plans were computed according to the planning criteria of the corresponding techniques. The total mean dose to the thyroid gland was evaluated

using isodose display, dose volume histogram and associated dosimetric parameters provided by the TPS.

5.2.5 Statistical analysis

In the data analysis, findings of the study were compared between patients / subjects with normal thyroid function and those with abnormal thyroid function, and were compared between healthy subjects and patients treated with different RT techniques.

In the comparison between patients with normal thyroid function and those with abnormal thyroid function, the level of significance of the difference in thyroid volume, thyroid echogenicity index, thyroid vascularity index, number of nodules, the level of TSH and fT4 between the normal and abnormal thyroid function groups were calculated by Mann-Whitney Test. Fisher's Exact Test was used to calculate the level of significance of the difference in thyroid echogenicity and echogeneity, and the incidence of thyroid nodules between the two groups.

In the comparison between healthy subjects and patients treated with different RT techniques, the level of significance of the difference in thyroid volume, thyroid echogenicity index, thyroid vascularity index, number of nodules, the level of TSH and fT4 among healthy subjects, patients with cervical nodes treated with anterior cervical field, and patients with cervical nodes treated with IMRT were calculated by Kruskal-Wallis Test. When a significant difference ($p < 0.05$) was found in the

Kruskal-Wallis Test, Dunn's Multiple Comparison Test was used as the post-hoc test. Fisher's Exact Test was used to calculate the level of significance of the difference in thyroid echogenicity and echogeneity, and the incidence of thyroid nodules among the three study groups.

P-value smaller than 0.05 was considered to be statistically significant. GraphPad InStat software was used for the statistical analyses (GraphPad Software Inc., San Diego, CA, USA).

Optimal cut-off value of thyroid volume and echogenicity index for distinguishing normal and abnormal thyroid function were evaluated. A total of 36 cut-off values with an interval of 0.5 cm³ for thyroid volume (from 5.0 to 22.5 cm³), and 25 cut-off values with an interval of 0.2 for echogenicity index (from 0.8 to 5.6) were evaluated for the sensitivity and specificity in the differential diagnosis. A thyroid gland with abnormal thyroid function (i.e. either TSH or fT4 levels out of the aforementioned range) showing a thyroid volume smaller than the selected cut-off value was considered as a true positive finding, whilst the thyroid volume equal to or greater than the selected cut-off value was considered as a false negative finding. Likewise a thyroid gland with normal thyroid function (i.e. TSH and fT4 levels within the aforementioned range) showing a thyroid volume equal to or greater than the selected cut-off value was considered as a true negative finding, whilst the thyroid volume smaller than the selected cut-off value was considered as a false positive

finding. The sensitivity and specificity were calculated and used to plot the receiver operating characteristic (ROC) curve.

In the assessment of thyroid echogenicity index, a thyroid gland with abnormal thyroid function showing an echogenicity index smaller than the selected cut-off value was considered as a true positive finding, whilst the echogenicity index equal to or greater than the selected cut-off value was considered as a false negative finding. Likewise a thyroid gland with normal thyroid function showing an echogenicity index equal to or greater than the selected cut-off value was considered as a true negative finding, whilst the echogenicity index smaller than the selected cut-off value was considered as a false positive finding. The sensitivity and specificity were calculated and used to plot the ROC curve.

5.3 Results

5.3.1 Part I: Comparison between patients with normal thyroid function and those with abnormal thyroid function

A total of 133 thyroid glands (266 thyroid lobes) were evaluated with ultrasonography and thyroid function test in the 133 NPC patients from QMH and PMH. Thyroid function test demonstrated that 38 patients had abnormal thyroid function who were categorized into the abnormal thyroid function group, whilst 95

patients showed normal thyroid function who were included into the normal thyroid function group. Results indicated that the mean TSH level of the abnormal thyroid function group (9.32 μ UI/mL) was significantly greater than that of the normal thyroid function group (2.55 μ UI/mL) ($p < 0.05$, Table 5.1); whilst the mean fT4 level of abnormal thyroid function group (8.67 pmol/L) was significantly lower than that of the normal thyroid function group (11.35 pmol/L) ($p < 0.05$, Table 5.1). For the 38 patients with abnormal thyroid function, the mean thyroid dose was 62.6 ± 4.9 Gy, whilst the mean thyroid dose of the 95 patients with normal thyroid function was 62.6 ± 5.6 Gy. There was no significant difference of mean thyroid dose between the two groups ($p = 0.79$).

Results showed that the mean thyroid volume of normal thyroid function group (9.57 cm^3) was significantly greater than that of the abnormal thyroid function group (8.06 cm^3) ($p < 0.05$, Table 5.1). In addition, the mean thyroid echogenicity index of the normal thyroid function group (2.32) was significantly greater than that of the abnormal thyroid function group (2.03) ($p = 0.02$, Table 5.1). However, there was no significant difference in the mean thyroid vascularity index between the two groups ($p = 0.86$, Table 5.1).

Table 5.1: Comparison of the mean thyroid volume, mean echogenicity index, mean vascularity index, mean number of thyroid nodules, mean TSH level and mean fT4 level of the thyroid glands in the post-RT NPC patients with normal thyroid function and those with abnormal thyroid function

Sonographic appearance	Mean \pm SD		p-value
	Normal thyroid function group	Abnormal thyroid function group	
Thyroid volume (cm ³)	9.57 \pm 2.60	8.06 \pm 2.39	< 0.05
Echogenicity index	2.32 \pm 0.88	2.03 \pm 0.99	0.02
Vascularity index	29.64 \pm 11.31	29.28 \pm 12.14	0.86
Number of nodules	0.45 \pm 0.82	0.58 \pm 0.86	0.46
TSH level (μ UI/mL)	2.55 \pm 0.99	9.32 \pm 9.87	< 0.05
fT4 level (pmol/L)	11.35 \pm 1.53	8.67 \pm 1.50	< 0.05

SD = Standard deviation

The p-value indicates the level of significance between the overall comparison of the 2 study groups (i.e. post-RT NPC patients with normal thyroid function, and those with abnormal thyroid function) using Mann-Whitney Test.

Majority of thyroid glands in the normal thyroid function group (63%) were homogenous (Figure 5.7A), but thyroid glands tended to be heterogeneous (Figure 5.7B) in the abnormal thyroid function group (66%). The difference in the thyroid echogeneity between the two groups was statistically significant ($p < 0.05$, Table 5.2).

In the subjective assessment of thyroid echogenicity, results indicated that the thyroid glands in both normal thyroid function (100%) and abnormal thyroid function (97%) groups tended to be hyperechoic when compared with the adjacent sternomastoid muscles ($p = 0.29$, Table 5.2). Results also showed that nodules were found in 31% and 37% of thyroid glands in the normal and abnormal thyroid function groups respectively, and the difference was not statistically significant ($p = 0.54$, Table 5.2). For the number of thyroid nodules, results indicated that there was no significance difference in the mean number of nodules between normal (0.45 nodules) and abnormal (0.58 nodules) thyroid function groups ($p = 0.46$, Table 5.1).

Table 5.2: Comparison of echogenicity, echogeneity, incidence of nodules of thyroid glands in the post-RT NPC patients with normal thyroid function and those with abnormal thyroid function

Sonographic appearance	Number of thyroid glands (%)		p-value
	Normal thyroid function group	Abnormal thyroid function group	
Echogenicity			
<i>Hyperechoic</i>	95 (100%)	37 (97%)	0.29
<i>Isoechoic</i>	0 (0%)	1 (3%)	
<i>Hypoechoic</i>	0 (0%)	0 (0%)	
Echogeneity			
<i>Homogenous</i>	60 (63%)	13 (34%)	< 0.05
<i>Heterogeneous</i>	35 (37%)	25 (66%)	
Incidence of nodules			
<i>Present</i>	29 (31%)	14 (37%)	0.54
<i>Absent</i>	66 (69%)	24 (63%)	

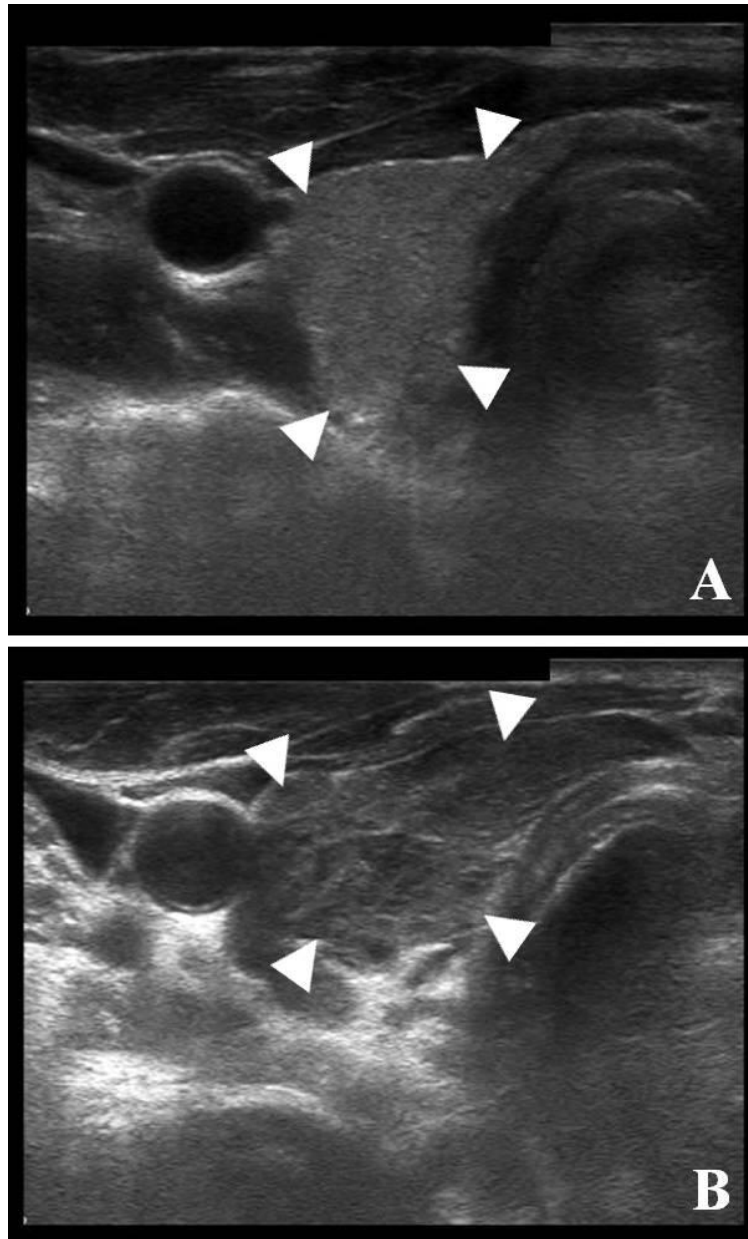


Figure 5.7: Transverse grey scale sonograms show the thyroid lobes (arrowheads) of a post-RT patient with normal thyroid function (A) and of a post-RT patient with abnormal thyroid function (B). Note the thyroid lobe of the patient with normal thyroid function appears homogenous, whilst the thyroid lobe of the patient with abnormal thyroid function appears heterogeneous.

For the ROC curves, the point nearest to the top left corner is the cut-off value of the thyroid volume or echogenicity index with the best sensitivity and a high specificity (Altman, 1991). The ROC curve for thyroid volume showed that the optimum cut-off was 7.0 cm³ with a sensitivity of 50% and specificity of 94.7% (Figure 5.8). On the other hand, the ROC curve for echogenicity index showed that the optimum cut-off was 1.8 with a sensitivity of 55.3% and specificity of 69.5% (Figure 5.9).

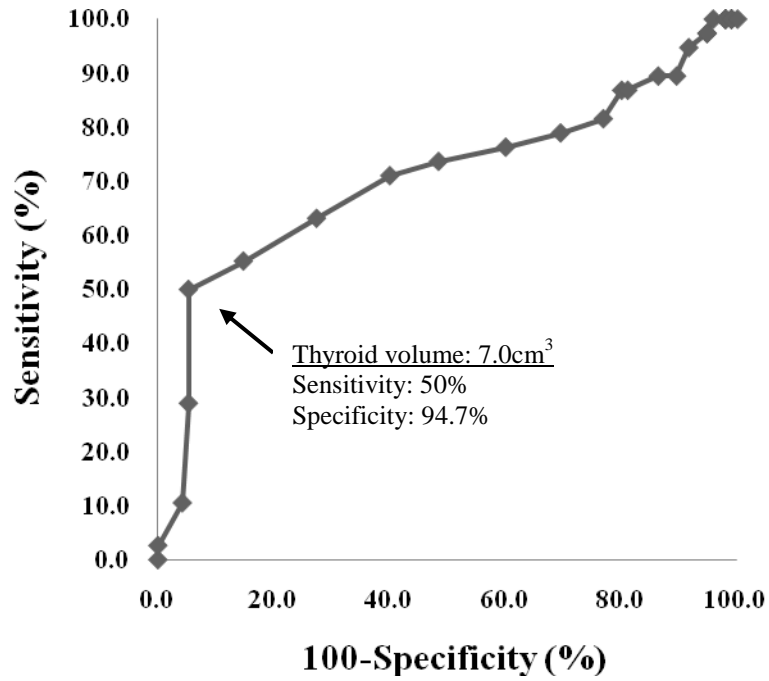


Figure 5.8: ROC curve of the thyroid volume of the post-RT NPC patients

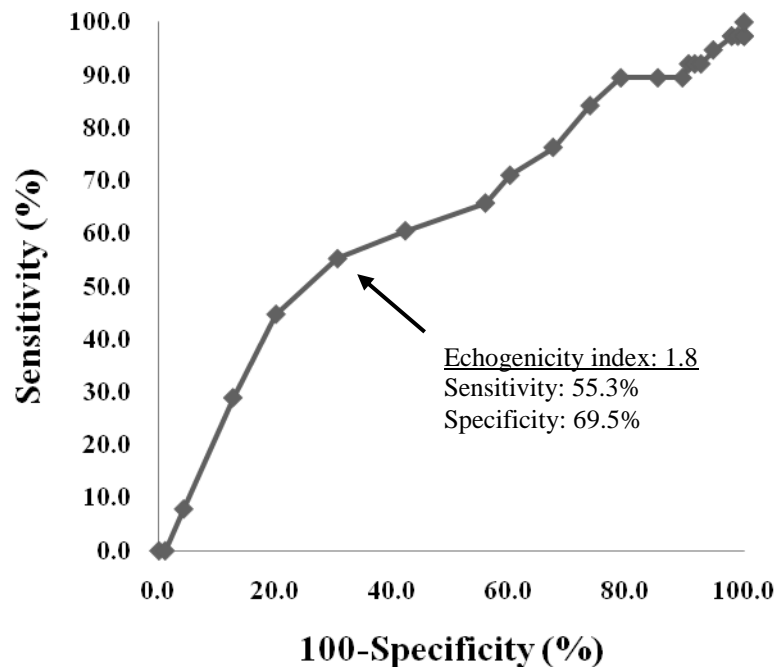


Figure 5.9: ROC curve of the thyroid echogenicity index of the post-RT NPC patients

5.3.2 Part II: Comparison between healthy subjects and patients treated with different radiotherapy techniques

For the 39 patients with the neck treated with anterior cervical field, the mean thyroid dose was 65.0 ± 3.1 Gy, whilst the mean thyroid dose of the 30 patients treated with IMRT was 54.7 ± 5.0 Gy. There was a significant difference of mean thyroid dose between the two groups ($p < 0.05$). A total of 130 thyroid glands (260 thyroid lobes) were evaluated with ultrasonography and thyroid function test in the 61 healthy subjects, and in the 39 and 30 NPC patients treated with anterior cervical field (conventional RT group) and IMRT (IMRT group) respectively. All healthy subjects showed normal thyroid function, whilst 32 patients (82%) in the conventional RT group and 21 patients (70%) in the IMRT group had normal thyroid function. The mean numbers of months after radiotherapy in the conventional RT and IMRT groups were 35.5 ± 8.6 months and 34.0 ± 6.8 months respectively. Results showed that there was a significant difference in the mean volume of the thyroid glands among the healthy subjects, conventional RT group and IMRT group ($p < 0.05$). Further evaluation using post hoc Dunn's Multiple Comparisons Tests indicated that the mean volume of the thyroid glands in the conventional RT group (9.56 cm^3) and IMRT group (9.47 cm^3) were significantly smaller than that in the healthy subjects (12.2 cm^3) ($p < 0.05$, Table 5.3). However, there was no significant difference in the mean thyroid volume between the two patient groups ($p > 0.05$).

Table 5.3: Comparison of the mean thyroid volume, mean echogenicity index, mean vascularity index, mean number of thyroid nodules, mean TSH level and mean ft4 level of the thyroid glands in healthy subjects, and NPC patients with their necks treated with IMRT and those with anterior cervical field

Sonographic appearance	Mean \pm SD			p-value
	Healthy Subjects	IMRT group	Conventional RT group	
Thyroid volume (cm³)	12.2 \pm 4.41	9.47 \pm 3.34	9.56 \pm 2.44	< 0.05
Echogenicity index	2.11 \pm 0.71	3.15 \pm 0.98	2.08 \pm 0.82	< 0.05
Vascularity index	17.05 \pm 8.80	24.38 \pm 6.90	32.09 \pm 12.73	< 0.05
Number of nodules	1.61 \pm 1.74	0.50 \pm 0.78	0.44 \pm 0.75	< 0.05
TSH level (μUI/mL)	1.62 \pm 0.71	5.49 \pm 7.96	4.53 \pm 7.79	< 0.05
ft4 level (pmol/L)	12.60 \pm 2.06	10.30 \pm 1.79	11.23 \pm 2.21	< 0.05

SD = Standard deviation, IMRT group = NPC patients with their necks treated with intensity-modulated radiotherapy, Conventional RT group = NPC patients with their necks treated with anterior cervical field, TSH = Thyroid stimulating hormone, ft4 = free thyroxine
The p-value indicates the level of significance between the overall comparison of the 3 study groups (i.e. healthy subjects, NPC patients with their necks treated with IMRT and those with anterior cervical field) using Kruskal-Wallis Test.

There was a significant difference in the mean echogenicity index of the thyroid glands among the three study groups ($p < 0.05$, Table 5.3). Post hoc test indicated that the mean echogenicity indexes of thyroid glands in the conventional RT group (2.08) and health subjects (2.11) were significantly smaller than that in the IMRT group (3.15) ($p < 0.05$). However, there was no significant difference in the mean echogenicity index between conventional RT group and healthy subjects ($p > 0.05$).

Result showed that there was a significant difference in the mean vascularity index of the thyroid glands among the three study groups ($p < 0.05$, Table 5.3). Further evaluation with the post hoc test found that the mean vascularity indexes of thyroid glands in the conventional RT group (32.1) and IMRT group (24.4) were significantly greater than that in the healthy subjects (17.1) ($p < 0.05$) (Figure 5.10A-C). However, there was no significant difference in the mean vascularity index between the two patient groups ($p > 0.05$).

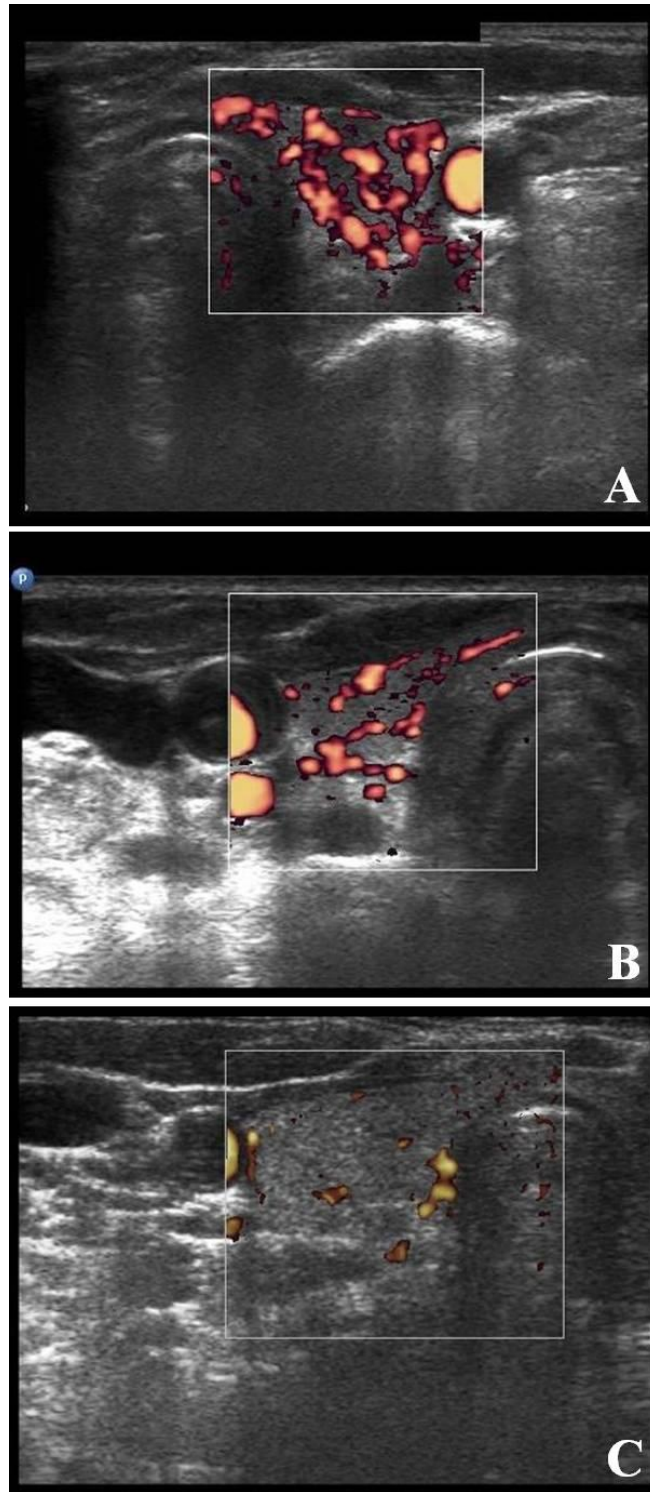


Figure 5.10: Transverse power Doppler sonograms show the measurement of the thyroid vascularity in a patient with the neck treated with anterior cervical field (A), a patient with the neck treated with intensity-modulated radiotherapy (B) and a healthy subject (C). Note the thyroid vascularity is higher in the patients when compared to the healthy subject.

Majority of thyroid glands in the conventional RT group (97%) and all thyroid glands in the IMRT group (100%) and healthy subjects (100%) were hyperechoic compared with the adjacent sternomastoid muscle (Figure 5.11A-C). Result showed that the difference in the echogenicity of thyroid glands among the three study groups were not statistically significant ($p > 0.05$, Table 5.4).

Over half of the thyroid glands in the conventional RT (54%) and IMRT groups (57%) appeared homogenous on ultrasound (Figure 5.11A&B). However, only 39% of thyroid glands in healthy subjects were homogenous (Figure 5.11C). Nevertheless, results indicated that the difference in echogeneity of thyroid glands among the three study groups were not statistically significant ($p > 0.05$, Table 5.4).

Table 5.4: Comparison of echogenicity, echogeneity, incidence of nodules of thyroid glands in healthy subjects, and patients with their neck treated with IMRT and those treated with anterior cervical field

Sonographic appearance	Number of thyroid glands (%)			p-value		
	Healthy Subjects	IMRT Group	Conventional RT group	Healthy subjects vs IMRT group	Healthy subjects vs conventional RT group	IMRT group vs conventional RT group
Echogenicity						
<i>Hyperechoic</i>	61 (100%)	30 (100%)	38 (97%)	1.00	1.00	1.00
<i>Isoechoic</i>	0 (0%)	0 (0%)	1 (3%)			
<i>Hypoechoic</i>	0 (0%)	0 (0%)	0 (0%)			
Echogeneity						
<i>Homogenous</i>	24 (39%)	17 (57%)	21 (54%)	0.18	0.22	1.00
<i>Heterogeneous</i>	37 (61%)	13 (43%)	18 (46%)			
Incidence of nodules						
<i>Present</i>	37 (61%)	11 (37%)	13 (33%)	0.04	0.01	0.80
<i>Absent</i>	24 (39%)	19 (63%)	26 (67%)			

IMRT group = NPC patients with their necks treated with intensity-modulated radiotherapy, Conventional RT group = NPC patients with their necks treated with anterior cervical field

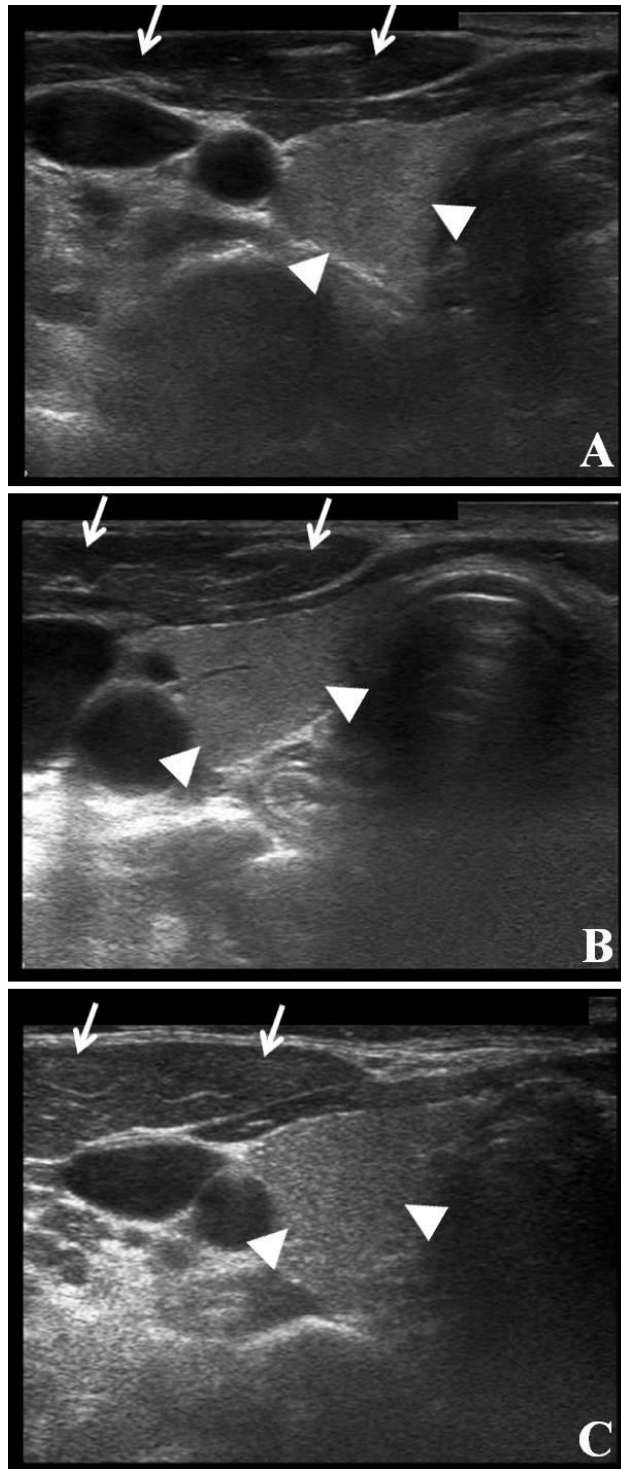


Figure 5.11: Transverse grey scale sonograms show the thyroid lobes (arrowheads in A to C) in a patient with the neck treated with anterior cervical field (A), in a patient with the neck treated with intensity-modulated radiotherapy (B) and in a healthy subject (C). Note the thyroid lobes are homogenous in echogeneity and are hyperechoic compared with the adjacent sternomastoid muscles (arrows).

Results showed that nodules were present in 33% and 37% of the thyroid glands in conventional RT and IMRT groups respectively (Figure 5.12A&B). However, 61% of thyroid glands in healthy subjects were with nodules (Figure 5.12C). The incidence of thyroid nodules in healthy subjects was significantly higher than that of the conventional RT and IMRT groups ($p = 0.01$ and $p = 0.04$ respectively, Table 5.4), but there was no significant difference between conventional RT and IMRT groups ($p = 0.80$, Table 5.4). For the number of thyroid nodules, results indicated that there was a significant difference in the mean number of nodules among the three study groups ($p < 0.05$, Table 5.3). Further evaluation using post hoc Dunn's Multiple Comparisons Tests showed that the mean number of nodules in the conventional RT group (0.4) and IMRT group (0.5) were significantly less than that in the healthy subjects (1.6) ($p < 0.05$ and $p = 0.01$ respectively). However, there was no significant difference in the mean number of nodules between the two patient groups ($p > 0.05$).

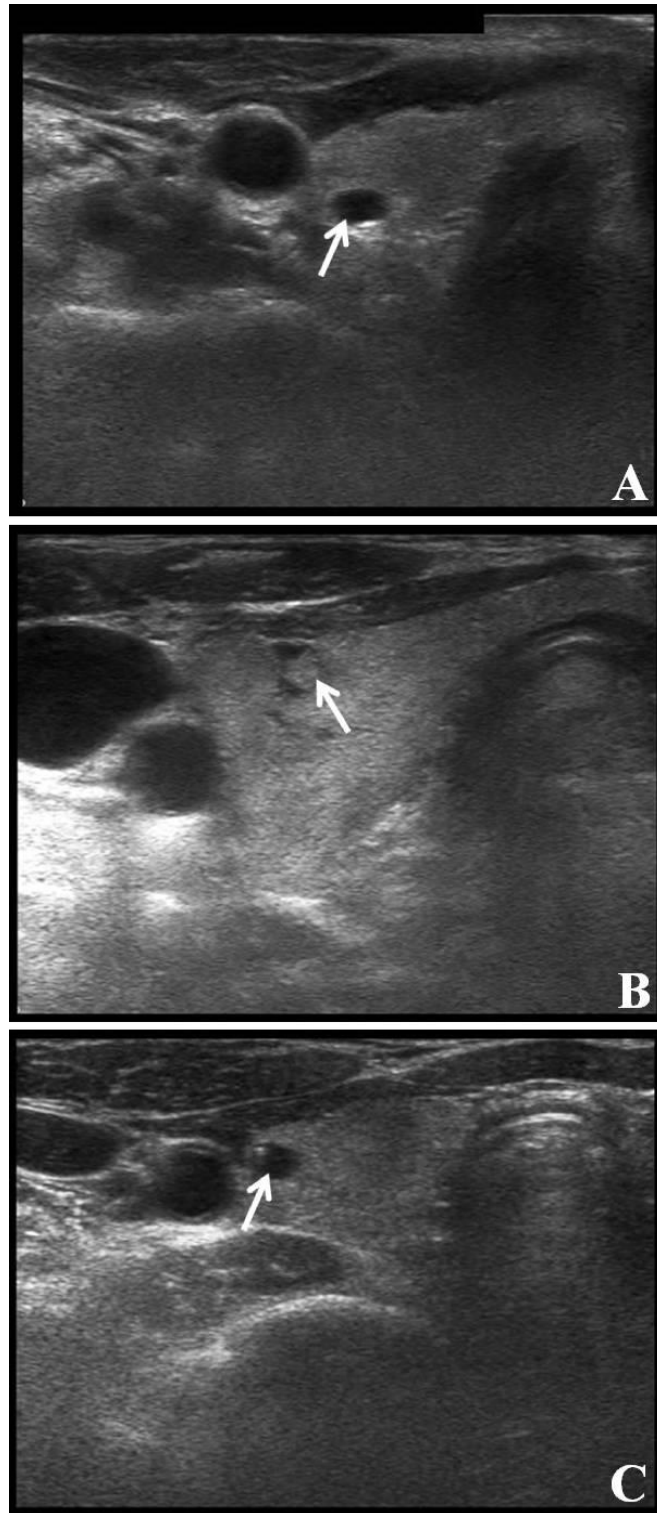


Figure 5.12: Transverse grey scale sonograms show the thyroid lobes in a patient with the neck treated with anterior cervical field (A), in a patient with the neck treated with intensity-modulated radiotherapy (B) and in a healthy subject (C). Note a nodule (arrows in images A to C) is present in the thyroid lobe of each patient/subject.

For the thyroid function test, there was a significant difference in the mean TSH level among the three study groups ($p < 0.05$, Table 5.3). Post hoc test indicated that the mean TSH levels of conventional RT group (4.53 $\mu\text{UI/mL}$) and IMRT group (5.49 $\mu\text{UI/mL}$) were significantly higher than that of the healthy subjects (1.62 $\mu\text{UI/mL}$) ($p < 0.05$). On the other hand, there was a significant difference in the mean fT4 level among the three study groups ($p < 0.05$, Table 5.3). Post hoc test showed that the mean fT4 levels of conventional RT group (11.23 pmol/L) and IMRT group (10.30 pmol/L) were significantly lower than that of the healthy subjects (12.60 pmol/L) ($p < 0.05$ and $p < 0.05$ respectively). However, there was no significant difference in the mean TSH and mean fT4 levels between the two patient groups ($p > 0.05$).

5.4 Discussion

The thyroid volume in the abnormal thyroid function group was lower than that of the normal thyroid function group, which was consistent with the findings from the previous studies which reported that reduced thyroid volume was found in patients with reduced thyroid function (Bonato et al. 2008, Lin et al. 2011). Bonato et al. (2008) found that the thyroid volume decreases with the TSH level increases in the post-RT patients with thyroid dysfunction. However, Miller-Thomas et al. (2009) did not find any significant difference in average size change between hypothyroid and euthyroid patients after RT. The inconsistent finding between two studies might

be due to different methodologies used, in which the former used ultrasound to measure thyroid volume, whilst the latter study only measured the thyroid width with the use of computed tomography. In the present study, with the use of ROC curve, it was found that thyroid volume of 7.0 cm³ was the optimum cut-off to identify thyroid reduced function with the sensitivity and specificity of 50% and 94.7% respectively. Although using this cut-off value had a low sensitivity, it achieved a high specificity in the differential diagnosis. While the evaluation of thyroid hormones level is a routine clinical practice for assessing thyroid function, ultrasound measurement of thyroid volume could have the potential to be used as a complementary method in the assessment of thyroid function. Nevertheless, studies with larger sample size are needed to further validate the accuracy of this cut-off value in the clinical practice.

In the present study, significant lower echogenicity index was found in the abnormal thyroid function group. Although there is a lack of literature correlating thyroid echogenicity with thyroid function in post-RT patients, the association between reduced echogenicity and thyroid hypofunction had been documented in patients with other thyroid diseases, and the findings of these previous studies were consistent with the result of the present study. Schiemann et al. (2003) noted that hypoechogenicity of thyroid glands was associated with increased level of TSH in the patients with Hashimoto's thyroiditis. Vejbjerg et al. (2006) also found a strong negative association between TSH level and thyroid echogenicity (i.e. higher the TSH level, lower the thyroid echogenicity). In the present study, with the use of

ROC curve, it was found that an echogenicity index of 1.8 was the optimum cut-off to identify thyroid glands with reduced function, with the sensitivity and specificity of 55.3% and 69.5% respectively. Although using this cut-off had a low sensitivity and moderate specificity, it could provide complementary information about thyroid status in addition to thyroid function test. Similar to the thyroid volume, studies with larger sample size are needed to further validate the accuracy of this cut-off value in the clinical practice.

Although the thyroid echogenicity index in the abnormal thyroid function group was significantly lower than that in the normal thyroid function group, there was no significant difference between the two groups when the thyroid echogenicity was assessed subjectively. The insignificant result might be due to the fact that the subjective assessment method might not be able to identify subtle changes of the thyroid echogenicity.

In present study, the thyroid glands in the abnormal thyroid function group tended to be heterogeneous whilst those in the normal thyroid function group tended to be homogenous. The finding of the present study was consistent with that of a previous study which found that heterogeneous echopattern of thyroid glands was associated with increased TSH level (Vebjerg et al., 2006).

The present study found that there was no significant difference in the vascularity index between normal and abnormal thyroid function groups, although thyroid

glands in post-RT patients had a significantly higher vascularity index than thyroid glands in healthy subjects (Table 5.3). Increased thyroid vascularity had been found in the patients with increased thyroid hormone levels such as Grave's disease and thyroiditis (Ralls et al. 1988, Bogazzi et al. 1999, Ota et al. 2007), but such correlation was not found in the post-RT patients. Although the actual reason for the different result in the post-RT patients is unclear and there are lack of studies on investigating thyroid vascularity in the post-RT head and neck cancer patients, the increased vascularity in the post-RT patients might be due to angiogenesis induced by increased TSH level (Bogazzi et al. 1999, Tseng et al. 1993, Viglietto et al. 1996). And we postulated that the similar thyroid vascularity in the normal and abnormal thyroid functions groups may be because the changes of thyroid hormones in the abnormal thyroid function group was not large enough to induce a substantial alteration in the thyroid vascularity.

Besides, insignificant differences in both the incidence and number of thyroid nodules between normal and abnormal thyroid function groups were also found in the present study, which indicated that the development of thyroid nodules might not be associated with the altered thyroid function after RT.

The present study found that the sonographic appearances of thyroid glands were different between the healthy subjects and the post-RT NPC patients. However, similar sonographic appearances of the thyroid were found in the patients with their neck treated with anterior cervical field and those treated with IMRT. Although there

is not an agreed thyroid tolerance dose (Jereczek-Fossa et al. 2004, Alterio et al. 2007), a number of studies found that thyroid disorders including hypothyroidism were commonly developed after thyroid glands received 30-50 Gy of radiation (Tell R et al. 1997, Garcia-Serra et al. 2005, Bhandare et al. 2007). In the present study, the mean thyroid doses of conventional RT and IMRT groups were 65.0 Gy and 54.7 Gy respectively, which exceeded the aforementioned dose range. In the conventional RT group, thyroid glands were within the anterior cervical field receiving full prescribed dose, and hence substantial radiation-induced damage to the glands was expected. On the other hand, Alterio et al. (2007) pointed out that sparing of thyroid glands has not yet been routinely performed in IMRT. In the present study, a portion of the thyroid gland in each patient might be encompassed within the planning target volume (PTV) in the IMRT, which brought the glands still received fairly high dose of radiation. Therefore, similar degree of radiation-induced damage and hence similar sonographic appearance of the thyroid glands were observed in the two patient groups. Nevertheless, there are lack of information of the dose response relationship about the severity of thyroid gland damage and the sonographic appearance of thyroid glands at different dose levels, and further studies in this area are suggested.

Higher TSH and lower fT4 levels (hypothyroidism) were found in the two post-RT patient groups when compared with the healthy subjects, which indicated possible reduced thyroid function in the patient groups. Reduced thyroid function, including clinical and subclinical hypothyroidism, had been reported (Tami TA, et al. 1992,

Mercado et al. 2001, Bhandare et al. 2007). The mechanism of radiation-induced hypothyroidism was believed due to direct thyroid parenchymal damage from radiation, radiation-induced vascular injury and autoimmune-mediated damage (Mercado et al. 2001, Illes et al. 2003, Ulger et al. 2007).

Results of the present study showed that thyroid volume of the post-RT patients (both conventional RT and IMRT groups) was smaller than that of the healthy subjects. Volume or size reduction of the irradiated thyroid glands had been documented in other studies using ultrasound and computed tomography for the thyroid size measurement (Bossi G et al. 1998, Bonato et al. 2008, Miller-Thomas et al. 2009, Lin et al. 2011). Previous histological studies demonstrated that thyroid follicular cell destruction and vascular damage could occur following radiation dose as low as 1.5-2.25 Gy (Turner et al. 1995, Bonato et al. 2008), and these two factors could lead to thyroid size reduction (Miller-Thomas et al. 2009). Bossi et al. (1998) found that thyroid volume was significantly smaller in the patients received cervical dose more than 20 Gy. As the thyroid glands in the both patient groups of the present study received a mean dose of more than 50 Gy, the reduction of thyroid volume might be related to the massive parenchymal cell loss of the thyroid gland after irradiation.

In the present study, the normal thyroid glands were hyperechoic when compared to the adjacent sternomastoid muscle, which was consistent with the findings in the previous literatures (Crom et al. 1997, Loevner et al. 2008, Ying et al. 1998). A

previous histological study showed that normal thyroid glands are characterized with densely packed colloid with relatively low portion of follicular cells (Muller et al. 1985). The cell-colloid interfaces provide highly reflective interfaces for ultrasound beam, which accounts for the hyperechoic appearance of the normal thyroid glands (Muller et al. 1985, Ying et al. 1998). On the other hand, results showed that the thyroid glands in the two post-RT patient groups also tended to be hyperechoic when compared to the adjacent sternomastoid muscle. Although we hypothesized decreased echogenicity in the irradiated thyroid glands owing to the reduced ultrasound reflective interfaces from parenchymal loss, results showed that thyroid glands of both patient groups tended to be hyperechoic. This might be due to the fact that the echogenicity of the irradiated thyroid glands was still higher than that of the muscle even though it had reduced. In the routine clinical practice, the echogenicity of thyroid gland is determined by the operator's subjective perception. However, subtle changes of the echogenicity may not be easily identified by naked eyes. Hence, echogenicity index of the gland was introduced in the present study for more accurate evaluation and quantification of the thyroid echogenicity. Results of the present study showed that the mean echogenicity index of the thyroid glands in the IMRT group was higher than that of the conventional RT group, indicating that the thyroid glands in the IMRT group were more echogenic than those in the conventional RT group. The higher echogenicity might be due to the lower mean thyroid dose of the IMRT group (54.7 Gy) and hence destruction of parenchyma and reduction of ultrasound reflective interfaces were less pronounced compared with the conventional RT group (65.0 Gy). However, the mean echogenicity index of the

IMRT group was surprisingly higher than that of the healthy subjects, and the mean echogenicity indexes of the healthy subjects and conventional RT group were not significantly different. The reason for this finding is unclear but we postulated that this might be due to the research method used in the study. This was a cross-sectional study which was lack of pre-RT baseline information of thyroid echogenicity, and comparison between pre-RT and post-RT echogenicity of thyroid glands was not possible. Hence, although the echogenicity index of the thyroid glands in the IMRT group was higher than the other two groups, there might be a reduction in echogenicity index after RT but could not be reflected in the present study. Further studies assessing the pre-RT and post-RT thyroid echogenicity index are suggested.

During the comparison of echogenicity, it should be noted that the echogenicity change in thyroid gland and sternomastoid muscle might not be in linear or proportional, which could affect the comparison of echogenicity. Nevertheless, the radiation tolerance of muscle was found significantly higher than that of thyroid gland and hence the echogenicity variation of muscle after irradiation should not be as much as that in the thyroid glands (Emami et al. 1991).

In the present study, the echogenicity of the thyroid gland was compared with the adjacent sternomastoid muscle. The advantage of comparing the echogenicity of the gland with the sternomastoid muscle was that both structures were closely located and thus they could be demonstrated in the same ultrasound image, which was

convenient and efficient for comparison clinically (Ying et al. 1998). Although the echogenicity of the muscle might change after irradiation, the radiation tolerance of muscle was much higher than that of the thyroid gland, and hence the echogenicity variation of muscle after irradiation should not be as much as that in the thyroid glands (Emami et al. 1991).

Although a number of studies found higher risk of nodule (both benign and malignant) development in the irradiated thyroid glands especially after high dose irradiation (Crom et al. 1997, Mihailescu et al. 2005, Schneider et al. 2009), results of the present study showed that both the incidence and the number of thyroid nodules in the healthy subjects were higher than that of the two patient groups. Thyroid nodules are common in the normal population. A study reported that nodules could exist in the thyroid glands of 50-70% of the non-irradiated people (Mehanna et al. 2009), which was comparable with our findings in the healthy subjects with 61% of incidence rate of thyroid nodules. Besides, the present study was a cross-sectional study without baseline information of pre-RT condition of patients' thyroid glands, and thus the rate of thyroid nodule development after RT could not be assessed. Further studies incorporating the pre-RT and post-RT ultrasound assessment of thyroid glands are suggested to investigate the change in sonographic appearance (including nodule development) of thyroid gland after RT.

In the present study, over 40% of the thyroid glands in the two patient groups and 61% of the normal thyroid glands tended to be heterogeneous. Nevertheless,

previous studies found that normal thyroid glands were characterized with homogenous speckled pattern (Muller et al. 1985, Ying et al. 1998). The higher incidence of heterogeneous echopattern of thyroid glands in the healthy subjects of the present study might be due to the high incidence rate of thyroid nodules in the group. In the two patient groups, some thyroid glands appeared heterogeneous but did not have thyroid nodules (15.3% and 6.7% in conventional RT and IMRT groups, respectively). Heterogeneous echopattern in the irradiated thyroid glands had also been documented in other studies (Soberman et al. 1991, Crom et al. 1997, Corrias et al 2001). The heterogeneous echopattern might be due to the diffuse lymphocytic infiltration in the irradiated glands that the infiltrate appeared hypoechoic and unevenly distributed within the thyroid gland, leading to an overall decreased echogenicity and heterogeneous echopattern of the gland (Vejbjerg et al. 2006).

In the assessment of the thyroid vascularity, the present study found that the thyroid glands of the two patient groups were more vascular than the thyroid glands of the healthy subjects. Although there is scant information about the vascularity of irradiated thyroid glands, increased thyroid vascularity had been reported in the patients with thyroid disorders such as Grave's disease and thyroiditis (Ralls et al. 1988, Bogazzi et al. 1999, Ota et al. 2007). Nevertheless, the mechanism of the increased vascularity in irradiated thyroid glands is still unclear, and further histopathological studies are needed for better understanding of post-radiation changes of thyroid vascularity.

To conclude, ultrasound is a useful imaging tool in the evaluation of radiation-induced changes of thyroid glands in NPC patients. Reduced thyroid volume, reduced thyroid echogenicity index and heterogeneous echogeneity might be useful indicators for reduced thyroid function in the post-RT head and neck cancer patients. Reduced thyroid volume and increased vascularity index might be the useful indicators in identifying thyroid glands of the post-RT head and neck cancer patients. For more accurate diagnosis, the sonographic appearances of irradiated thyroid glands should be noted in the ultrasound examination of patients with previous radiotherapy for NPC or other head and neck cancers.

Chapter Six

Summary of the thesis

This thesis describes the sonographic appearances of salivary and thyroid glands in NPC patients treated with external beam radiotherapy.

Chapter 1 gives a brief introduction of the background and objectives of the present study. Chapter 2 includes a review of the epidemiology of NPC, a review of radiotherapy including conventional RT and IMRT for NPC, a review of radiation-induced complications in salivary and thyroid glands, a description of the anatomy and function of salivary and thyroid glands, a review of the roles of different diagnostic imaging modalities and functional tests for assessing post-RT changes of salivary glands, and a review of ultrasonography and thyroid function test for assessing post-RT changes of thyroid glands.

Radiation-induced xerostomia is common in head and neck cancer patients treated with radical external beam radiotherapy, and this complication could adversely affect patients' quality of life. High resolution ultrasound has been widely used in the evaluation of parotid glands, but there is scant information in the literature about its role on post-RT changes in the glands. Available data is only limited to a single radiotherapy technique, and the sample size of the study was small. In order to facilitate the investigation of radiation-induced xerostomia and aid differential

diagnosis, a better understanding of the role of ultrasound in assessing radiation-induced changes of salivary glands is necessary. An investigation of the sonographic appearances of parotid glands in NPC patients treated with conventional RT and IMRT has been undertaken (Chapter 3). Forty-three NPC patients treated with conventional RT, 38 NPC patients treated with IMRT and 58 healthy subjects were involved in the study. Parotid ultrasound examination was performed on each patient/subject. Parotid glands were assessed for their size, echogenicity, echogeneity, incidence of hypoechoic areas and conspicuity of intra-parotid ducts. An objective measurement of echogenicity named echogenicity index of parotid gland was also introduced in this study. The results in this study showed that the mean transverse dimension of the glands in patients treated with conventional RT and those treated with IMRT were significantly smaller than that in healthy subjects. Parotid glands of the IMRT group tended to be hyperechoic (93%), homogenous (62%), without hypoechoic areas (64%) and with marginally-seen intra-parotid ducts (89%), which were similar to those in healthy subjects. On the other hand, parotid glands in the conventional RT group tended to be hypoechoic (51%), heterogeneous (98%), with hypoechoic areas (94%) and had obviously-seen intra-parotid ducts (64%). The main findings are summarized in Table 6.1.

Although submandibular glands only secrete around 20-40% of saliva during eating, they contribute more than 60% of total salivary output at the resting state. Hence, radiation-induced damage of submandibular glands after radiotherapy could lead to xerostomia affecting patients' quality of life, especially at rest. Ultrasound technique on submandibular gland evaluation has been well established. However, there is a lack of studies investigating the role of ultrasound in evaluating post-RT changes of the glands. In order to facilitate the investigation of radiation-induced xerostomia and aid differential diagnosis, an investigation of the sonographic appearances of submandibular glands in NPC patients treated external beam radiotherapy has been undertaken (Chapter 4). Eighty-one NPC patients treated with external beam radiotherapy and 66 healthy subjects were involved in the study. Submandibular gland ultrasound examination was performed on each patient/subject. Submandibular glands were assessed for their size, echogenicity, echogenicity index, echogeneity, incidence of hypoechoic areas, conspicuity of intra-glandular ducts and border sharpness. The results of this study showed that the mean transverse dimension of submandibular glands in patients treated with radiotherapy was significantly smaller than that of the healthy subjects. Submandibular glands in patients treated with radiotherapy tended to be heterogeneous (72%) with hypoechoic areas (46%) and have ill-defined borders (89%). However, there were no significant differences in the echogenicity and conspicuity of intra-glandular ducts of submandibular glands between patients and healthy subjects, in which the glands in both study groups tended to be hyperechoic and with marginally seen intra-glandular ducts. The main findings are summarized in Table 6.1

Since there is a high incidence of associated cervical lymph node metastases in NPC patients, an additional anterior cervical field is usually employed to irradiate the cervical lymph nodes for NPC patients. However, the anterior cervical field to the neck involved irradiation of thyroid glands, and thus radiation-induced thyroid disorders especially hypothyroidism are common in the patients. Although thyroid function test can help in assessing post-RT thyroid functional changes, it cannot assess the morphological changes and vascular damages of thyroid glands. Ultrasound has been widely used for thyroid assessment, but it is not commonly used to evaluate radiation-induced damages of the gland. In order to prevent misinterpretation of post-RT changes as other thyroid diseases and aid differential diagnosis, the sonographic appearances of thyroid glands in NPC patients treated external beam radiotherapy has now been undertaken (Chapter 5). One hundred and three NPC patients who had finished radiotherapy of cervical lymph nodes using anterior cervical field, 30 NPC patients who had finished radiotherapy of cervical lymph nodes using IMRT, and 61 healthy subjects were included in this study. Thyroid ultrasound examination was performed on each patient/subject. Thyroid glands were sonographically assessed for their size, echogenicity, echogenicity index, echogeneity, vascularity index, and incidence and number of nodules. Thyroid function test was also performed on each patient/subject. Compared with the patients with abnormal thyroid function, thyroid glands of the patients with normal thyroid function tended to be homogenous and bigger and have higher echogenicity index. However, there were no significant differences in the vascularity index, incidence

and number of nodules, and echogenicity of thyroid glands between the two patient groups. On the other hand, compared with the healthy subjects, the thyroid glands of patients treated with IMRT and those treated with anterior cervical field showed significantly lower thyroid volume, lower incidence and number of nodules, and higher vascularity index. However, there were no significant differences in the thyroid echogenicity and echogeneity between the healthy subjects and patients. The main findings are summarized in Table 6.2.

In the present study, it can be seen that size is a more sensitive predictor than other sonographic appearances for post-RT changes because size reduction happened in the irradiated parotid, submandibular and thyroid glands. However, the infiltration of inflammatory cells may not be as pronounced as parenchymal cell reduction after RT and mild infiltration may not be noted in ultrasound. Hence, echogenicity and echogeneity as well as other sonographic appearances were the less sensitive predictors compared with size reduction for post-RT changes. Nevertheless, further study is necessary to investigate the threshold dose or dose-response relationship for gland echogenicity and echogeneity.

All in all, the present study provided the information about sonographic appearances of salivary and thyroid glands in NPC patients treated with external beam radiotherapy. For more accurate diagnosis, the sonographic appearances of irradiated salivary and thyroid glands should be noted during ultrasound examination of patients with previous radiotherapy for NPC or other head and neck cancer.

Table 6.1: Summary of the sonographic appearance of parotid glands and submandibular glands in healthy subjects and NPC patients after radiotherapy

	Parotid gland			Submandibular gland	
	Healthy	IMRT	CRT	Healthy	Post-RT
Mean dose	N/A	30.3 Gy	38.0 Gy	N/A	65 Gy
Size	greater	smaller	Smaller	greater	smaller
Echogenicity	hyperechoic	hyperechoic	iso/hypoechoic	hyperechoic	hyperechoic
Echogenicity index	higher	moderate	Lower	no difference	no difference
Hypoechoic areas	absent	generally absent	Present	absent	present
Echotexture	homogenous	generally homogenous	Heterogeneous	homogenous	heterogeneous
Duct conspicuity	marginally seen	marginally seen	obviously seen	marginally seen	marginally seen
Border sharpness	N/A	N/A	N/A	well-defined	ill-defined

Healthy = healthy subjects, IMRT = NPC patients treated with intensity-modulated radiotherapy, CRT = NPC patients treated with conventional radiotherapy, Post-RT = NPC patients treated with external beam radiotherapy

Table 6.2: Summary of the sonographic appearance of thyroid glands in healthy subjects and NPC patients after radiotherapy; and in the post-radiotherapy NPC patients with normal and abnormal thyroid functions

	Thyroid function		Healthy	IMRT	CRT
	Normal	Abnormal			
Mean dose	62.6 Gy	62.6 Gy	N/A	54.7 Gy	65.0 Gy
Mean TSH level	lower	higher	Lower	higher	higher
Mean fT4 level	higher	lower	Higher	lower	lower
Thyroid volume	greater	smaller	Greater	smaller	smaller
Echogenicity	hyperechoic	hyperechoic	hyperechoic	hyperechoic	hyperechoic
Echogenicity index	higher	lower	Lower	higher	lower
Echogeneity	homogenous	heterogeneous	heterogeneous	homogenous	homogenous
Incidence of nodules	no difference	no difference	Higher	higher	lower
Number of nodules	no difference	no difference	Higher	higher	lower

Healthy = healthy subjects, IMRT = NPC patients with cervical lymph nodes treated with intensity-modulated radiotherapy, CRT = NPC patients with cervical lymph nodes treated with conventional radiotherapy, TSH = thyroid stimulating hormone, fT4 = free thyroxine

References

Ahuja A, Evans R, King A, van Hasselt C. Imaging in head and neck cancer: a practical approach. London: Greenwich Medical Media, 2003.

Aich RK, Ranjan DA, Pal S, Naha BL, Amitabh R. Iatrogenic hypothyroidism: a consequence of external beam radiotherapy to the head & neck malignancies. *J Cancer Res Ther* 2005; 1: 142-146.

Alterio D, Jereczek-Fossa BA, Franchi B, D'Onofrio A, Piazzini V, Rondi E, et al. Thyroid disorders in patients treated with radiotherapy for head-and-neck cancer: a retrospective analysis of seventy-three patients. *Int J Radiat Oncol Biol Phys* 2007; 67: 144-150.

Andermann P, Schlogl S, Mader U, Luster M, Lassmann M, Reiners C. Intra- and interobserver variability of thyroid volume measurements in healthy adults by 2D versus 3D ultrasound. *Nuklearmedizin* 2007; 46: 1-7.

Anjos DA, Etchebehere EC, Santos AO, Lima MC, Ramos CD, Paula RB, et al. Normal values of [^{99m}Tc]pertechnetate uptake and excretion fraction by major salivary glands. *Nucl Med Commun* 2006; 27: 395-403.

Astreinidou E, Raaymakers CPJ, Roesink JM, Terhaard CH, Lagendijk JJ, Bartels LW. 3D MR sialography protocol for postradiotherapy follow-up of the salivary duct system. *J Magn Reson Imaging* 2006; 24: 556-562.

Astreinidou E, Roesink JM, Raaijmakers CP, Bartels LW, Witkamp TD, Lagendijk JJ, et al. 3D MR sialography as a tool to investigate radiation-induced xerostomia: feasibility study. *Int J Radiat Oncol Biol Phys* 2007; 68: 1310-1319.

Barker JL, Garden AS, Ang KK, O'Daniel JC, Wang H, Court LE, et al. Quantification of volumetric and geometric changes occurring during fractionated radiotherapy for head-and-neck cancer using an integrated CT/linear accelerator system. *Int J Radiat Oncol Biol Phys* 2004; 59: 960-970.

Bartalena L, Bogazzi F, Brogioni S, Burelli A, Scarcello G, Martino E. Measurement of serum free thyroid hormone concentrations: an essential tool for the diagnosis of thyroid dysfunction. *Horm Res* 1996; 45: 142-147.

Baskin HJ, Duick DS, Levine RA. Thyroid ultrasound and ultrasound-guided FNA. 2nd ed. New York: Springer, 2008.

Baum BJ. Evaluation of stimulated parotid saliva flow rate in different age groups. *J Dent Res* 1981; 60: 1292-1296.

Becker M, Schroth G, Zbaren P, Delavelle J, Greiner R, Vock P, et al. Long-term changes induced by high-dose irradiation of the head and neck region: imaging findings. *Radiographics* 1997; 17: 5-26.

Bernal J, Refetoff S. The action of thyroid hormone. *Clin Endocrinol* 1977; 6: 227-249.

Bhandare N, Kennedy L, Malyapa RS, Morris CG, Mendenhall WM. Primary and central hypothyroidism after radiotherapy for head-and-neck tumors. *Int J Radiat Oncol Biol Phys* 2007; 68: 1131-1139.

Bialek EJ, Jakubowski W, Zajkowski P, Szopinski KT, Osmolski A. US of the major salivary glands: anatomy and spatial relationships, pathologic conditions, and pitfalls. *Radiographics* 2006; 26: 745-763.

Bogazzi F, Bartalena L, Brogioni S, Burelli A, Manetti L, Tanda ML, et al. Thyroid vascularity and blood flow are not dependent on serum thyroid hormone levels: studies in vivo by color flow doppler sonography. *Eur J Endocrinol* 1999; 140: 452-456

Bonato C, Severino RF, Elnecave RH. Reduced thyroid volume and hypothyroidism in survivors of childhood cancer treated with radiotherapy. *J Pediatr Endocrinol Metab* 2008; 21: 943-949.

Bossi G, Larizza D, Sommaruga G, Corbella F, Klersy C, Arico M. Thyroid volume is progressively reduced as a sequel of neck irradiation for childhood Hodgkin's disease. *Haematologica* 1998; 83: 754-756.

Brent GA, Hershman JM, Braunstein GD. Patients with severe nonthyroidal illness and serum thyrotropin concentrations in the hypothyroid range. *Am J Med* 1986; 81: 463-468.

Bronstein AD, Nyberg DA, Schwartz AN, Shuman WP, Griffin BR. Increased salivary gland density on contrast-enhanced CT after head and neck radiation. *AJR Am J Roentgenol* 1987; 149: 1259-1263.

Brown MC, Spencer R. Thyroid gland volume estimated by use of ultrasound in addition to scintigraphy. *Acta Radiol Oncol Radiat Phys Biol* 1978; 17: 337-341.

Brunn J, Block U, Ruf G, Bos I, Kunze WP, Scriba PC. Volumetric analysis of thyroid lobes by real-time ultrasound. *Dtsch Med Wochenschr* 1981; 106: 1338-1340.

Bryan RN, Miller RH, Ferreyro RI, Sessions RB. Computed tomography of the major salivary glands. *AJR Am J Roentgenol* 1982; 139:547-554.

Calcaterra TC, Stern F, Ward PH. Dilemma of delayed radiation injury of the larynx. *Ann Otol Rhinol Laryngol* 1972; 81: 501-507.

Chambers MS, Garden AS, Kies MS, Martin JW. Radiation-induced xerostomia in patients with head and neck cancer: pathogenesis, impact on quality of life and management. *Head Neck* 2004; 26: 796-807.

Chan ATC, Teo PML, Johnson PJ. Nasopharyngeal carcinoma. *Annals of Oncology* 2002; 13: 1007-1015.

Cheng SH, Jian JJ, Tsai SY. Prognostic features and treatment outcome in locoregionally advanced nasopharyngeal carcinoma following concurrent chemotherapy and radiotherapy. *Int J Radiat Oncol Biol Phys* 1998;41:755-762.

Chikui T, Okamura K, Tokumori K, Nakamura S, Shimizu M, Koga M, et al. Quantitative analyses of sonographic images of the parotid gland in patients with Sjogren's syndrome. *Ultrasound Med Biol* 2006; 32: 617-622.

Ching ASC, Chong VFH, Khoo JBK. CT evaluation of nasolacrimal relapse of nasopharyngeal carcinoma. *Clinical Radiology* 2003; 58:642-647.

Chong VFH, Ong CK. Nasopharyngeal carcinoma. *European Journal of Radiology* 2008; 66: 437-447.

Col NF, Surks MI, Daniels GH. Subclinical thyroid disease: clinical applications. *JAMA* 2004; 291: 239-243.

Constine LS, Donaldson SS, McDougall IR, Cox RS, Link MP, Kaplan HS. Thyroid dysfunction after radiotherapy in children with Hodgkin's disease. *Cancer* 1984; 53: 878-883.

Cooper JS, Fu K, Marks J, Silverman S. Late effects of radiation therapy in the head and neck region. *Int J Radiat Oncol Biol Phys* 1995; 31: 1141-1164.

Cooper RA, Cowan RA, Owens SE, Jeans SP, Roberts JK, Hillel PG, et al. Dose salivary gland scintigraphy predict response to pilocarpine in patients with post-radiotherapy xerostomia? *Eur J Nucl Med* 1999; 26: 220-225.

Coppes RP, Vissink A, Konings AWT. Comparison of radiosensitivity of rat parotid and submandibular glands after different radiation schedules. *Radiother Oncol* 2002; 63: 321-328.

Corrias A, Einaudi S, Ricardi U, Besenon L, Altare F, Artesani L, et al. Thyroid diseases in patients treated during pre-puberty for medulloblastoma with different radiotherapeutic protocols. *Endocrinol Invest* 2001; 24: 387-392.

Criswell MA, Sinha CK. Hyperthermic, supersaturated humidification in the treatment of xerostomia. *Laryngoscope* 2001; 111: 992-996.

Crom DB, Kaste SC, Tubergen DG, Greenwald CA, Sharp GB, Hudson MM. Ultrasonography for thyroid screening after head and neck irradiation in childhood cancer survivors. *Med Pediatr Oncol* 1997; 28: 15-21.

Eisbruch A. Clinical aspects of IMRT for head-and-neck cancer. *Med Dosim* 2002; 27: 99-104.

Eisbruch A, Kim HM, Terrell JE, Marsh LH, Dawson LA, Ship JA. Xerostomia and its predictors following parotid-sparing irradiation of head-and neck cancer. *Int J Radiat Oncol Biol Phys* 2001; 50: 695-704.

Eisbruch A, Rhodus N, Rosenthal D, Murphy B, Rasch C, Sonis S, et al. How should we measure and report radiotherapy-induced xerostomia? *Semin Radiat Oncol* 2003a; 13: 226-234.

Eisbruch A, Ship JA, Dawson LA, Kim HM, Bradford CR, Terrell JE, et al. Salivary gland sparing and improved target irradiation by conformal and intensity modulated irradiation of head and neck cancer. *World J Surg* 2003b; 27: 832-837.

Eisbruch A, Ten Haken RK, Kim HM, Marsh LH, Ship JA. Dose, volume, and function relationships in parotid salivary glands following conformal and intensity-modulated irradiation of head and neck cancer. *Int J Radiat Oncol Biol Phys* 1999; 45: 577-587.

El Miedany YM, Ahmed I, Mourad HG, Mehanna AN, Aty SA, Gamal HM, et al. Quantitative ultrasonography and magnetic resonance imaging of the parotid gland: can they replace histopathologic studies in patients with Sjogren's syndrome. *Joint Bone Spine* 2004; 71: 29-38.

Emami B, Lyman J, Brown A, Coia L, Goitein M, Munzenrider JE, Shank B, Solin LJ, Wesson M. Tolerance of normal tissue to therapeutic irradiation. *Int J Radiat Oncol Biol Phys* 1991; 21: 109-122.

Eneroth CM, Henrikson CO, Jakobsson PA. Effects of fractionated radiotherapy on salivary gland function. *Cancer* 1972; 30: 1147-1153.

Fox PC, Busch KA, Baum BJ. Subjective reports of xerostomia and objective measures of salivary gland performance. *J Am Dent Assoc* 1987; 115: 581-584.

Franzen L, Funegard U, Ericson T, Henriksson R. Parotid gland function during and following radiotherapy of malignancies in the head and neck: a consecutive study of salivary flow and patient discomfort. *Eur J Cancer* 1992; 28: 457-462.

Garcia-Serra A, Amdur RJ, Morris CG, Mazzaferri E, Mendenhall WM. Thyroid function should be monitored following radiotherapy to the low neck. *Am J Clin Oncol* 2005; 28: 255-258.

Glastonbury CM. Nasopharyngeal carcinoma: the role of magnetic resonance imaging in diagnosis, staging, treatment, and follow-up. *Top Magn Reson Imaging* 2007; 18: 225-235.

Gregoire V, De Neve W, Eisbruch A, Lee N, Van den Weyngaert D, Van Gestel D. Intensity-modulated radiation therapy for head and neck carcinoma. *Oncologist* 2007; 12: 555-564.

Grehn AL, Gustafsson H, Franzen L, Thornell LE, Henriksson R. Ultrastructural morphometry of parotid acinar cells following fractionated irradiation. *Oral Oncol* 1997; 33: 23-28.

Gritzmann N, Rettenbacher T, Hollerweger A, Macheiner P, Hubner E. Sonography of the salivary glands. *Eur Radiol* 2003; 13: 964-975.

Gritzmann N. Sonography of the salivary glands. *AJR Am J Roentgenol* 1989; 153: 161-166.

Hegedus L, Bennedbaek FN. Nonisotopic techniques of thyroid imaging. In LE Braverman & RD Utiger editors. *Werner & Ingbar's the thyroid: a fundamental & clinical text*. 9th ed. Philadelphia: Lippincott Williams & Wilkins; 2005. p.374-484.

Henriksson R, Frojd O, Gustafsson H, Johansson S, Yi-Qing C, Franzen L, et al. Increase in mast cells and hyaluronic acid correlates to radiation-induced damage and loss of serous acinar cells in salivary glands: the parotid and submandibular glands differ in radiation sensitivity. *Br J Cancer* 1994; 69: 320-326.

Heo MS, Lee SC, Lee SS, Choi HM, Choi SC, Park TW. Quantitative analysis of normal major salivary glands using computed tomography. *Oral Surg Oral Med Oral Pathol Oral Radiol Endod* 2001; 92: 240-244.

Hermann GA, Vivino FB, Shnier D, Krumm RP, Mayrin V. Diagnostic accuracy of salivary scintigraphic indices in xerostomic populations. *Clin Nucl Med* 1999; 24: 167-172.

Heussinger N, Buttner M, Ott G, Brachtel E, Pilch BZ, Kremmer E, et al. Expression of the Epstein-Barr virus (EBV) Yencoded latent membrane protein 2A (LMP2A) in EBV-associated nasopharyngeal carcinoma. *J Pathol* 2004; 203: 696-699.

Hong Kong Cancer Registry. *Hong Kong Cancer Stat* 2007. Hospital Authority 2009.

Howlett DC. High resolution ultrasound assessment of the parotid gland. *Br J Radiol* 2003; 76: 271-277.

Illes A, Biro E, Miltenyi Z, Keresztes K, Varoczy L, Andras C, et al. Hypothyroidism and thyroiditis after therapy for Hodgkin's disease. *Acta Haematol* 2003; 109: 11-17.

Jereczek-Fossa BA, Alterio D, Jassem J, Gibelli B, Tradati N, Orecchia R. Radiotherapy-induced thyroid disorders. *Cancer Treat Rev* 2004; 30: 369-384.

Katz P, Hartl DM, Guerre A. Clinical ultrasound of the salivary glands. *Otolaryngol Clin N Am* 2009;42:973-1000.

King AD, Ahuja AT, Yeung DK, Wong JK, Lee YY, Lam WW, et al. Delayed complications of radiotherapy treatment for nasopharyngeal carcinoma: imaging findings. *Clin Radiol* 2007; 62: 195-203.

King AD, Vlantis AC, Tsang RK, Gary TM, Au AK, Chan CY, et al. Magnetic resonance imaging for the detection of nasopharyngeal carcinoma. *Am J Neuroradiol* 2006; 27: 1288-1291.

Kohn WG, Ship JA, Atkinson JC, Patton LL, Fox PC. Salivary gland ^{99m}Tc-scintigraphy: a grading scale and correlation with major salivary gland flow rates. *J Oral Pathol Med* 1992; 21: 70-74.

Kotecha S, Bhatia P, Rout PGJ. Diagnostic ultrasound in the head and neck region. *Dent Update* 2008; 35: 529-534.

Kubicek GJ, Machtay M. New advances in high-technology radiotherapy for head and neck cancer. *Hematol Oncol Clin N Am* 2008;22:1165-80.

Kwong DL, Pow EH, Sham JS, McMillan AS, Leung LH, Leung WK, et al. Intensity-modulated radiotherapy for early-stage nasopharyngeal carcinoma: a prospective study on disease control and preservation of salivary function. *Cancer* 2004a; 101: 1584-93.

Kwong DL, Sham JS, Au GK, Chua DT, Kwong PW, Cheng AC, et al. Concurrent and adjuvant chemotherapy for nasopharyngeal carcinoma: a factorial study. *J Clin Oncol* 2004b; 22: 2643-53.

Larsson SG, Lufkin RB, Hoover LA. Computed tomography of the submandibular salivary glands. *Acta Radiol* 1987; 28: 693-696.

Lee C, Langen KM, Lu W, Haimerl J, Schnarr E, Ruchala KJ, et al. Evaluation of geometric changes of parotid glands during head and neck cancer radiotherapy using daily MVCT and automatic deformable registration. *Radiother Oncol* 2008a; 89: 81-88.

Lee YYP, Wong KT, King AD, Ahuja AT. Imaging of salivary gland tumours. *Eur J Radiol* 2008b; 66: 419-436.

Leek H, Albertsson M. Pilocarpine treatment of xerostomia in head and neck patients. *Micron* 2002; 33: 153-155.

Liem IH, Olmos RA, Balm AJ, Keus RB, van Tinteren H, Takes RP, et al. Evidence for early and persistent impairment of salivary gland excretion after irradiation of head and neck tumours. *Eur J Nucl Med* 1996; 23: 1485-1490.

Liening DA, Duncan NO, Blakeslee DB, Smith DB. Hypothyroidism following radiotherapy for head and neck cancer. *Otolaryngol Head Neck Surg* 1990; 103: 10-13.

Lin Z, Wu VW, Lin J, Feng H, Chen L. A longitudinal study on the radiation-induced thyroid gland changes after external beam radiotherapy of nasopharyngeal carcinoma. *Thyroid* 2011; 21: 19-23.

Liu WS, Su MC, Wu MF, Tseng HC, Kuo HC. Nasopharyngeal carcinoma treatment with precision-oriented radiation therapy techniques including intensity-modulated radiotherapy: preliminary results. *Kaohsiung J Med Sci* 2004; 20: 49-55.

Lo S, Ho WK, Wei WI. Outcome of patients with positive Epstein-Barr virus serologic status in the absence of nasopharyngeal carcinoma in Hong Kong. *Arch Otolaryngol Head Neck Surg* 2004; 130: 770-772.

Loevner LA, Kaplan SL, Cunnane ME, Moonis G. Cross-sectional imaging of the thyroid gland. *Neuroimag Clin N Am* 2008; 18: 445-461.

Lu H, Yao M. The current status of intensity-modulated radiation therapy in the treatment of nasopharyngeal carcinoma. *Cancer Treat Rev* 2008; 34: 27-36.

Malago R, D'Onofrio M, Ferdeghini M, Mantovani W, Colato C, Brazzarola P, et al. Thyroid volumetric quantification: comparative evaluation between conventional and volumetric ultrasonography. *J Ultrasound Med* 2008; 27: 1727-1733.

Marmioli L, Salvi G, Caiazza A, Di Rienzo L, Massaccesi M, Murino P, et al. Dose and volume impact on radiation-induced xerostomia. *Rays* 2005: 145-148.

McGahan JP, Walter JP, Bernstein L. Evaluation of the parotid gland: comparison of sialography, non-contrast computed tomography and CT sialography. *Radiology* 1984; 152: 453-458.

Mehanna HM, Jain A, Morton RP, Watkinson J, Shaha A. Investigating the thyroid nodule. *BMJ* 2009; 338: 705-709.

Mercado G, Adelstein DJ, Saxton JP, Secic M, Larto MA, Lavertu P. Hypothyroidism: a frequent event after radiotherapy and after radiotherapy with chemotherapy for patients with head and neck carcinoma. *Cancer* 2001; 92: 2892-2897.

Mihailescu DV, Collins BJ, Wilbur A, Malkin J, Schneider AB. Ultrasound-detected thyroid nodules in radiation-exposed patients: changes over time. *Thyroid* 2005; 15: 127-133.

Miller-Thomas MM, Kumar AJ, Sellin RV, Azimpoor S, Ang KK. The shrinking thyroid: how dose thyroid size change following radiation therapy for laryngeal cancer? *AJNR Am J Neuroradiol* 2009; 30: 613-616.

Moon WJ, Jung SL, Lee JH, Na DG, Baek JH, Lee YH, et al. Benign and malignant thyroid nodules: US differentiation – multicenter retrospective study. *Radiology* 2008; 247: 762-770.

Muller HW, Schroder S, Schneider C, Siefert G. Sonographic tissue characterisation in thyroid gland diagnosis: a correlation between sonography and histology. *Klin Wochenschr* 1985; 63: 706-710.

Munter MW, Hoffner S, Hof H, Herfarth KK, Haberkorn U, Rudat V, et al. Changes in salivary gland function after radiotherapy of head and neck tumors measured by quantitative pertechnetate scintigraphy: comparison of intensity-modulated radiotherapy and conventional radiation therapy with and without amifostine. *Int J Radiat Oncol Biol Phys* 2007; 67: 651-659.

Nagler RM. The enigmatic mechanism of irradiation-induced damage to the major salivary glands. *Oral Dis* 2002; 8: 141-146.

Niemela RK, Takalo R, Paakko E, Suramo I, Palvansalo M, Salo T, et al. Ultrasonography of salivary glands in primary Sjogren's syndrome. A comparison with magnetic resonance imaging and magnetic resonance sialography of parotid glands. *Rheumatology* 2004; 43: 875-879.

Nishihara E, Fukata S, Kimura N, Hagihara M, Kudo T, Ohye H, et al. A case of hypothyroid Grave's disease following external radiation therapy to the cervical region. *Endocr J* 2006; 53: 357-361.

Nishimura Y, Nakamatsu K, Shibata T, Kanamori S, Koike R, Okumura M, et al. Importance of the initial volume of parotid glands in xerostomia for patients with head and neck cancers treated with IMRT. *Jpn J Clin Oncol* 2005; 35: 375-379.

Nomayr A, Lell M, Sweeney R, Bautz W, Lukas P. MRI appearance of radiation-induced changes of normal cervical tissues. *Eur Radiol* 2001; 11: 1807-1817.

Ota H, Amino N, Morita S, Kobayashi K, Kubota S, Fukata S. Quantitative measurement of thyroid blood flow for differentiation of painless thyroiditis from Grave's disease. *Clin Endocrinol (Oxf)* 2007; 67: 41-45.

Ozawa H, Saitou H, Mizutari K, Takata Y, Ogawa K. Hypothyroidism after radiotherapy for patients with head and neck cancer. *Am J Otolaryngol* 2007; 28: 46-49.

Paulino AC. Hypothyroidism in children with medulloblastoma: a comparison of 3600 and 2350 cGy craniospinal radiotherapy. *Int J Radiat Oncol Biol Phys* 2002; 53: 543-547.

Popowicz B, Klencki M, Lewinski A, Słowinska-Klencka D. The usefulness of sonographic features in selection of thyroid nodules for biopsy in relation to the nodule's size. *Eur J Endocrinol* 2009; 161: 103-111.

Pow EHN, Kwong DLW, McMillan AS, Wong MC, Sham JS, Leung LH, et al. Xerostomia and quality of life after intensity-modulated radiotherapy vs. conventional radiotherapy for early-stage nasopharyngeal carcinoma: initial report on a randomized controlled clinical trial. *Int J Radiation Oncology Biol Phys* 2006; 66: 981-991.

Price RE, Ang KK, Stephens LC, Peters LJ. Effects of continuous hyperfractionated accelerated and conventionally fractionated radiotherapy on the parotid and submandibular salivary glands of rhesus monkeys. *Radiother Oncol* 1995; 34: 39-46.

Radfar L, Sirois DA. Structural and functional injury in minipig salivary glands following fractionated exposure to 70 Gy of ionizing radiation: an animal model for human radiation-induced salivary gland injury. *Oral Surg Oral Med Oral Pathol Oral Radiol Endod* 2003; 96: 267-274.

Ralls PW, Mayekawa DS, Lee KP, Colletti PM, Radin DR, Boswell WD, et al. Color-flow Doppler sonography in Graves disease: "thyroid inferno". *AJR Am J Roentgenol* 1988; 150: 781-784.

Ricardi U, Corrias A, Einaudi S, Genitori L, Sandri A, di Montezemolo LC, et al. Thyroid dysfunction as a late effect in childhood medulloblastoma: a comparison of hyperfractionated versus conventionally fractionated craniospinal radiotherapy. *Int J Radiat Oncol Biol Phys* 2001; 50: 1287-1294.

Rose SR. Cranial irradiation and central hypothyroidism. *Trends Endocrinol Metab* 2001; 12: 97-104.

Rossi A, Tomimori E, Camargo R, Medeiros-Neto G. Determination of thyroid volume by sonography in healthy Brazilian schoolchildren. *J Clin Ultrasound* 2002; 30: 226-231.

Ruggieri M, Fumarola A, Straniero A, Maiuolo A, Coletta I, Veltri A, et al. The estimation of the thyroid volume before surgery – an important prerequisite for minimally invasive thyroidectomy. *Langenbecks Arch Surg* 2008; 393: 721-724.

Saarilahti K, Kouri M, Collan J, Kangasmaki A, Atula T, Joensuu H, et al. Sparing of the submandibular glands by intensity modulated radiotherapy in the treatment of head and neck cancer. *Radiother Oncol* 2006; 78: 270-275.

Saeed S, Haq S, Sohaib M, Khan AN. Skull base involvement by a nasopharyngeal carcinoma shown by Tc-99m MDP SPECT but not by computed tomography. *Clinical Nuclear Medicine* 2001; 26: 930-932.

Schiemann U, Avenhaus W, Konturek JW, Gellner R, Hengst K, Gross M. Relationship of clinical features and laboratory parameters to thyroid echogenicity measured by standardized grey scale ultrasonography in patients with Hashimoto's thyroiditis. *Med Sci Monit* 2003; 9: MT13-17.

Schneider AB, Bekerman C, Leland J, Rosengarten J, Hyun H, Collins B, et al. Thyroid nodules in the follow-up of irradiated individuals: comparison of thyroid ultrasound with scanning and palpation. *J Clin Endocrinol Metab* 1997; 82: 4020-4027.

Scott J. Structure and function in aging human salivary glands. *Gerodontology* 1987; 5: 149-158.

Seifert G. Etiology and differential diagnosis of sialadenitis. *Laryngorhinootologie* 1995; 74: 274-281.

Shabana W, Peeters E, De Maeseneer M. Measuring thyroid gland volume: should we change the correction factor? *AJR Am J Roentgenol* 2006; 186: 234-236.

Shah GV. MR imaging of salivary glands. *Magn Reson Imaging Clin N Am* 2002; 10: 631-662.

Shapiro RS. Techniques in thyroidology: panoramic ultrasound of the thyroid. *Thyroid* 2003; 13: 177-181.

Shiboski CH, Hodgson TA, Ship JA, Schiodt M. Management of salivary hypofunction during and after radiotherapy. *Oral Surg Oral Med Oral Pathol Oral Radiol Endod* 2007 (Suppl 1); S66.e1-S66.e19.

Shimizu M, Okamura K, Yoshiura K, Ohyama Y, Nakamura S, Kinukawa N. Sonographic diagnostic criteria for screening Sjogren's syndrome. *Oral Surg Oral Med Oral Pathol Oral Radiol Endod* 2006; 102: 85-93.

Sinard RJ, Tobin EJ, Mazzaferri EL, Hodgson SE, Young DC, Kunz AL, et al. Hypothyroidism after treatment for non-thyroid head and neck cancer. *Arch Otolaryngol Head Neck Surg* 2000; 126: 652-657.

Soberman N, Leonidas JC, Cherrick I, Schiff R, Karayalcin G. Sonographic abnormalities of the thyroid gland in longterm survivors of Hodgkin disease. *Pediatr Radiol* 1991; 21: 250-253.

Solt I, Gaitini D, Pery M Hochberg Z, Stein M, Arush MW. Comparing thyroid ultrasonography to thyroid function in long-term survivors of childhood lymphoma. *Med Pediatr Oncol* 2000; 35: 35-40.

Stewart RR, David CL, Eftekhari F, Ried HL, Fuller LM, Fornage BD. Thyroid gland: US in patients with Hodgkin disease treated with radiation therapy in childhood. *Radiology* 1989; 172: 159-163.

Surks MI, Ortiz E, Daniels GH, Sawin CT, Col NF, Cobin RH, et al. Subclinical thyroid disease: scientific review and guidelines for diagnosis and management. *JAMA* 2004; 291: 228-238.

Tami TA, Gomez P, Parker GS, Gupta MB, Frassica DA. Thyroid dysfunction after radiation therapy in head and neck cancer patients. *Am J Otolaryngol* 1992; 13: 357-362.

Tartaglino LM, Rao VM, Markiewicz DA. Imaging of radiation changes in the head and neck. *Semin Roentgenol* 1994; 29: 81-91.

Tell R, Sjodin H, Lundell G, Lewin F, Lewensohn R. Hypothyroidism after external radiotherapy for head and neck cancer. *Int J Radiat Oncol Biol Phys* 1997; 39: 303-308.

Tenhunen M, Collan J, Kouri M, Kangasmaki A, Heikkonen J, Kairemo K, et al. Scintigraphy in prediction of the salivary gland function after gland-sparing intensity modulated radiation therapy for head and neck cancer. *Radiother Oncol* 2008; 87: 260-267.

Teymoortash A, Simolka N, Schrader C, Tiemann M, Werner JA. Lymphocyte subsets in irradiation-induced sialadenitis of the submandibular gland. *Histopathology* 2005; 47: 493-500.

Trimboli P, Ruggieri M, Fumarola A, D'Alò M, Straniero A, Maiuolo A, et al. A mathematical formula to estimate in vivo thyroid volume from two-dimensional ultrasonography. *Thyroid* 2008; 18: 879-882.

Tseng YC, Lahiri S, Jackson S, Burman KD, Wartofsky L. Endothelin binding to receptors and endothelin production by human thyroid follicular cells: effects of transforming growth factor-beta and thyrotropin. *J Clin Endocrinol Metab* 1993; 76: 156-161.

Turner SL, Tiver KW, Boyages SC. Thyroid dysfunction following radiotherapy for head and neck cancer. *Int J Radiat Oncol Biol Phys* 1995; 31: 279-283.

Tylenda CA, Ship JA, Fox PC, Baum BJ. Evaluation of submandibular salivary flow rate in different age groups. *J Dent Res* 1988; 67: 1225-1228.

Tzioufas AG, Moutsopoulos HM. Ultrasonography of salivary glands: an evolving approach for the diagnosis of Sjogeren's syndrome. *Nat Clin Pract Rheumatol* 2008;4:454-5.

Ulger S, Ulger Z, Yildiz F, Ozyar E. Incidence of hypothyroidism after radiotherapy for nasopharyngeal carcinoma. *Med Oncol* 2007; 24: 91-94.

Van Acker F, Flamen P, Lambin P, Maes A, Kutcher GJ, Weltens C, et al. The utility of SPECT in determining the relationship between radiation dose and salivary gland dysfunction after radiotherapy. *Nucl Med Commun* 2001; 22: 225-231.

Van De Graaff KM. *Human Anatomy*. 6th ed. New York: McGraw-Hill, 2002.

Vejbjerg P, Knudsen N, Perrild H, Laurberg P, Pedersen IB, Rasmussen LB, et al. The association between hypoechogenicity or irregular echo pattern at thyroid ultrasonography and thyroid function in the general population. *Eur J Endocrinol* 2006; 155: 547-552.

Viglietto G, Manzo G, Romano A, Paoletti I, Mauriello V, Bruni P, et al. TSH and iodine exert opposite effects on thyroid vasculature by modulation of the expression of VEGF and PLGF in rat thyroid gland in vivo and in rat cultured thyrocytes in vitro. *J Endocrinol Invest* 1996; 19 (Suppl 6): 49.

Vissink A, 's-Gravenmade EJ, Ligeon EE, Konings WT. A functional and chemical study of radiation effects on rat parotid and submandibular/sublingual glands. *Radiat Res* 1990; 124: 259-265.

Vokes EE, Liebowitz DN, Weichselbaum RR. Nasopharyngeal carcinoma. *Lancet* 1997; 350: 1087-1091.

Wada A, Uchida N, Yokokawa M, Yoshizako T, Kitagaki H. Radiation-induced xerostomia: objective evaluation of salivary gland injury using MR sialography. *AJNR AM J Neuroradiol* 2009; 30: 53-58.

Yau YY, Samman N, Yeung RWK. Positron emission tomography/computed tomography true fusion imaging in clinical head and neck oncology: early experience. *J Oral Maxillofac Surg* 2005; 63: 479-486.

Ying M, Ahuja A, Brook F, Brown B, Metreweli C. Sonographic appearance and distribution of normal cervical lymph nodes in a Chinese population. *J Ultrasound Med* 1996; 15: 431-436.

Ying M, Brook F, Ahuja A, Metreweli C. The value of thyroid parenchymal echogenicity as an indicator of pathology using sternomastoid muscle for comparison. *Ultrasound Med Biol* 1998; 24: 1097-1105.

Ying M, NG DK, Yung DM, Lee ES. A semi-quantitative approach to compare high-sensitivity power Doppler sonography and conventional power Doppler sonography in the assessment of thyroid vascularity. *Thyroid* 2009; 19: 1265-1269.

Ying M, Sin M, Pang S. Sonographic measurement of thyroid gland volume: a comparison of 2D and 3D ultrasound. *Radiography* 2005; 11: 242-248.

Ying M, Wu VWC, Kwong DLW. Comparison of sonographic appearance of normal and postradiotherapy parotid glands: a preliminary study. *Ultrasound Med Biol* 2007; 33: 1244-1250.

Ying M, Yung DMC, Ho KKL. Two-dimensional ultrasound measurement of thyroid gland volume: a new equation with higher correlation with 3-D ultrasound measurement. *Ultrasound in Med & Biol* 2008; 34: 56-63.

Yu MC, Mo CC, Chong WX, Yeh FS, Henderson BE. Preserved foods and nasopharyngeal carcinoma: a case-control study in Guangxi, China. *Cancer Res* 1988; 48: 1954-1959.

Zimmerman RP, Mark RJ, Tran LM, Juillard GF. Concomitant pilocarpine during head and neck irradiation is associated with decreased posttreatment xerostomia. *Int J Radiat Oncol Biol Phys* 1997; 37: 571-575.

Appendix I

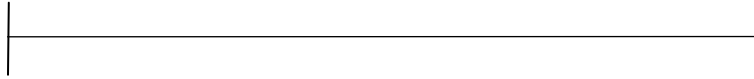
Xerostomia Questionnaire

Below are several questions which will help describe the dryness in your mouth and how that dryness interferes with aspects of your daily life. Please make one vertical mark across the line to show your condition.

1. During the last three days, overall, your mouth or tongue was:

Very dry

Not dry

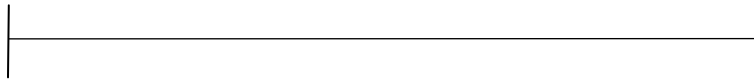


For internal use only

2. In general, during the daytime hours of the last three days, the feeling of your mouth and tongue was:

Extremely uncomfortable

Comfortable

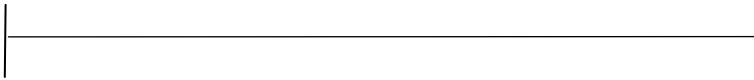


For internal use only

3. During the last three nights, due to the dryness of your mouth and tongue, how difficult was it to sleep? Consider such factors as how difficult it was for you to go to sleep, the duration and quality of your sleep, and how often you woke up to drink or to urinate.

Very difficult

Easy

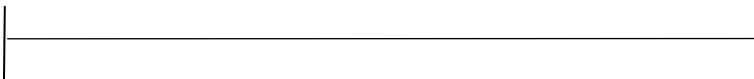


For internal use only

4. During the last three days, overall, due to the dryness of your mouth and tongue, how difficult was it to speak without drinking liquids?

Very difficult

Easy



For internal use only

5. During the last three days, overall, due to the dryness of your mouth and tongue, how difficult was it to chew and swallow food?

Very difficult

Easy

For internal use only

6. If you normally wear dentures, due to the dryness of your mouth and tongue, how difficult was it to wear dentures in the last three days? (If you do not normally wear dentures or could not wear dentures for reasons other than those associated with dry mouth, please circle the X at the right and make no mark on the line.)

Very difficult

Easy

For internal use only

口腔乾涸情況問卷

以下問題是詢問你的口腔乾涸情況及如何影響你的生活。請在每一題下的橫線上劃上一垂直線以表示你的情況。

1. 過去三天，總括來說，你的口腔和舌頭是：

非常乾涸 全不乾涸

|-----|

由研究員填寫

2. 一般來說，過去三天的日間，你的口腔和舌頭的感覺是：

極度不舒服 很舒服

|-----|

由研究員填寫

3. 過去三晚，因著口腔和舌頭的乾涸，你的睡眠情況如何？因素包括睡眠時間，質素，醒來飲水或小便次數等。

非常困難 容易

|-----|

由研究員填寫

4. 過去三天，總括來說，因著口腔和舌頭的乾涸，你沒有飲水時的說話情況如何？

非常困難 容易

|-----|

由研究員填寫

5. 過去三天，總括來說，因著口腔和舌頭的乾涸，你的咀嚼及吞嚥情況如何？

非常困難 容易

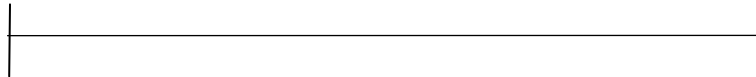
|-----|

由研究員填寫

6. 如果你平日配戴假牙，過去三天，因著口腔和舌頭的乾涸，你配戴假牙的情況如何？
(如果你沒有配戴假牙或因其他原因不能配戴假牙，請在右方 X 上劃上圓圈，而無需在橫線上劃上垂直線。)

非常困難

容易



由研究員填寫

Appendix II

Sonographic evaluation of salivary and thyroid glands in patients treated with radiotherapy for nasopharyngeal carcinoma: repeatability and reproducibility study

High-resolution ultrasonography is useful in examining soft tissue structures including those in head and neck regions like thyroid gland and salivary glands. Grey scale ultrasound allows measurement of thyroid volume, and assessment of thyroid morphology. It helps characterization and detection of diffuse and focal abnormalities of the thyroid gland, and aids distinguishing solid nodules from cysts (Shapiro 2003, Hegedus et al. 2005, Loevner et al. 2008). On the other hand, it is commonly used in the assessing salivary gland diseases like neoplasms, Sjogren's syndrome, sialadenitis and sialolithiasis,

Although ultrasonography has been widely used in head and neck imaging, operator dependency is one of the major limitations, which could lead to inconsistent findings between operators or between trials of the same operator. In order to monitor the recovery progress of the radiation-induced injuries in salivary and thyroid glands of the post-RT NPC patients by ultrasound, repeatable and reproducible measurements are necessary.

It has been reported that ultrasound has high repeatability and reproducibility in thyroid gland size measurement (Ying et al. 2005). However, literatures are devoid of such information in the measurement of salivary gland size. Also, the repeatability and reproducibility of the categorical sonographic appearance such as echogenicity and echogeneity in thyroid and salivary gland has not yet been fully evaluated. Hence, this study was undertaken to investigate the inter- and intra-observer variability of size measurement and sonographic appearance in thyroid and salivary gland ultrasound for post-RT NPC patients.

Materials and Methods:

Part I: Inter- and Intra-observer variability for ultrasound salivary and thyroid glands size measurement

A total of 20 healthy subjects without any known thyroid and salivary gland diseases were recruited for this study. All ultrasound examinations were performed with the Philips HD11 XE or the Philips HD11 ultrasound unit in conjunction with a 12-5 MHz linear transducer (Philips Medical System, Bothell, WA, USA).

Ultrasound examination for parotid, submandibular and thyroid glands was performed on each subject. Ultrasound examination was performed according to the protocols given in Sections 3.2.3, 4.2.3 and 5.2.2 for the measurement of maximum

longitudinal and transverse dimensions of parotid glands, maximum transverse dimension of submandibular glands, and thyroid volume respectively.

Two observers (observer I and observer II) involved in the inter-observer variability (reproducibility) test. Observer II has over 15 years experience in head and neck ultrasound imaging, whilst observer I has only 2 years experience. Each observer scanned each subject once and each observer was blinded to the results of another observer.

Only observer I involved in the intra-observer variability (repeatability) test. In addition to the first ultrasound scan during reproducibility test, each subject was scanned by observer I again with an interval of more than 30 minutes to the first scan. For the second scan, images were stored in the hard-disk of the ultrasound unit, and the images were archived and gland size measurement was performed 2 weeks after the ultrasound scan.

Part II: Inter- and Intra-observer variability for the sonographic appearance of salivary and thyroid glands

The archived ultrasound images of 10 healthy subjects, 10 NPC patients treated with IMRT and 10 NPC patients treated with conventional RT were randomly selected from the subjects in Studies One, Two and Three.

Two observers (observer I and observer II) involved in the inter-observer variability (reproducibility) test. The sonographic appearances of parotid, submandibular and thyroid glands of the subjects/patients were retrospectively reviewed by the observers. The sonographic appearances of the glands were assessed according to the protocol and criteria given in Sections 3.2.3, 4.2.3 and 5.2.2. Each observer was blinded to the results of another observer.

Only observer I involved in the intra-observer variability (repeatability) test. The results of the sonographic appearances assessed in Study One, Two and Three were compared with those assessed during reproducibility test for the evaluation of intra-observer variability.

Statistical analysis

Inter-observer and intra-observer variations for ultrasound measurement of salivary and thyroid glands size were calculated by Intraclass correlation coefficient (ICC) (SPSS for windows 16.0, SPSS Inc., Chicago, Illinois). Inter-observer and intra-observer variations for sonographic appearance of salivary and thyroid glands were calculated by Kappa Test (SPSS for windows 16.0, SPSS Inc., Chicago, Illinois).

Results:

Table A1.1 shows the inter-observer variability (reproducibility) of ultrasound measurement of thyroid and salivary glands size. Results showed high reproducibility in the ultrasound measurement for thyroid volume, longitudinal dimension of parotid gland and transverse dimension of submandibular gland (ICC = 0.79 – 0.96). However, moderate reproducibility of ultrasound measurement for transverse dimension of parotid gland (ICC = 0.52) was noted.

Table A1.1: Inter-observer variability test for ultrasound thyroid and salivary glands size measurement

Ultrasound measurement Parameters	ICC	95% confidence interval	
		Lower bound	Upper bound
Thyroid volume	0.96	0.86	0.98
Parotid gland LS dimension	0.80	0.64	0.88
Parotid gland TS dimension	0.52	0.24	0.72
Submandibular gland TS dimension	0.79	0.63	0.88

ICC = Intraclass correlation coefficient, LS = Longitudinal, TS = Transverse

Table A1.2 shows the intra-observer variability (repeatability) of ultrasound thyroid and salivary glands size measurement. Results shows high repeatability for all ultrasound measurements (ICC = 0.90 – 0.94).

Table A1.2: Intra-observer variability test for ultrasound thyroid and salivary glands size measurement

Ultrasound measurement Parameters	ICC	95% confidence interval	
		Lower bound	Upper bound
Thyroid volume	0.94	0.86	0.98
Parotid gland LS dimension	0.90	0.81	0.94
Parotid gland TS dimension	0.94	0.89	0.97
Submandibular gland TS dimension	0.91	0.83	0.95

ICC = Intraclass correlation coefficient, LS = Longitudinal, TS = Transverse

Table A1.3 shows the inter-observer variability (reproducibility) for the sonographic appearance of thyroid and salivary gland ultrasound. Results demonstrated high reproducibility in examining the incidence of nodules, echogeneity and echogenicity of thyroid gland (Kappa = 0.70 – 1.00); conspicuity of intra-parotid ducts, echogenicity, echogeneity and incidence of hypoechoic areas in parotid gland (Kappa = 0.84 – 0.90); and conspicuity of intra-glandular ducts, echogenicity and echogeneity of submandibular gland (Kappa = 0.77 – 1.00). The reproducibility was moderate in examining the incidence of hypoechoic areas of submandibular gland (Kappa = 0.66). However, low reproducibility was noted in examining the border sharpness of submandibular gland (Kappa = 0.28).

Table A1.3: Inter-observer variability test for the sonographic appearance of thyroid and salivary glands

	Sonographic apperenance	Kappa
Thyroid gland	Incidence of nodules	0.70
	Echogenicity	1.00
	Echogeneity	0.77
Parotid gland	Conspicuity of intra-parotid ducts	0.84
	Echogenicity	0.86
	Echogeneity	0.90
	Incidence of hypoechoic areas	0.90
Submandibular gland	Conspicuity of intra-glandular ducts	0.77
	Echogenicity	1.00
	Echogeneity	0.77
	Incidence of hypoechoic areas	0.66
	Border sharpness	0.28

Table A1.4 shows the intra-observer variability (repeatability) for examining the sonographic appearance of thyroid and salivary gland ultrasound. Most of the sonographic appearances showed high repeatability (Kappa = 0.83 – 1.00) in the examination. However, moderate repeatability was noted in examining the conspicuity of intra-glandular ducts and echogenicity of submandibular glands (Kappa = 0.48 – 0.66).

Table A1.4: Intra-observer variability test for examining the sonographic appearance of thyroid and salivary glands

	Sonographic appearance	Kappa
Thyroid gland	Incidence of nodules	1.00
	Echogenicity	1.00
	Echogeneity	0.88
Parotid gland	Conspicuity of intra-parotid ducts	0.89
	Echogenicity	0.89
	Echogeneity	0.95
	Incidence of hypoechoic areas	0.95
Submandibular gland	Conspicuity of intra-glandular ducts	0.66
	Echogenicity	0.48
	Echogeneity	0.89
	Incidence of hypoechoic areas	0.88
	Border sharpness	0.83

Discussion:

This study was undertaken to investigate the reproducibility and repeatability of ultrasound size measurement and sonographic appearance of thyroid and salivary glands for post-RT NPC patients. For the size measurement, the ICC value of intra-

observer variability for all studied measurement was 0.90-0.94, indicating the repeatability of 90-94%. The repeatability is high and good enough for reliable measurement. Good reproducibility was achieved in most of the salivary gland size measurement. However, only moderate reproducibility (ICC = 0.52, indicating reproducibility of 52%) was noted in the measurement of parotid gland transverse dimension. This was because some patients had long and thin accessory parotid glands which could extend very anteriorly to the head, resulting in increased difficulty for the measurement of transverse dimension. The ICC value of thyroid volume measurement for inter-observer variability is 0.96, indicating reproducibility of 96% which was comparable with and even higher than the previous study (Ying et al. 2005).

For the sonographic appearance, the repeatability of examining most of the sonographic appearances in thyroid and salivary glands was high (ICC = 0.83-1.00, indicating repeatability of 83-100%). However, moderate repeatability was noted in examining the echogenicity (48%) and conspicuity of intra-glandular ducts (66%) of submandibular glands. The lower repeatability of examining these two sonographic appearances could be due to the fact that observer I was relatively inexperienced in head and neck ultrasound, which had the difficulty in giving consistent and repeatable assessment for a given image. On the other hand, the reproducibility of examining most of the sonographic appearances in thyroid and salivary glands was high (ICC = 0.70-1.00, indicating reproducibility of 70-100%). However, moderate reproducibility was noted in examining the incidence of hypoechoic areas (66%) of

submandibular glands and low reproducibility was noted in assessing the border sharpness (28%) of submandibular glands. Such discrepancy between the two observers may be due to the difference in ultrasound experience. Besides, the hypoechoic areas of the irradiated submandibular glands were not as obvious as those found in the irradiated parotid glands, increasing the difficulty in identifying such appearance. On the other hand, the border sharpness of submandibular glands was not easy to be determined, especially most of the irradiated glands were found with neither well-defined nor ill-defined border, but mostly marginally seen. Therefore, low reproducibility of assessing the border sharpness was resulted. In order to achieve a more reliable assessment of the irradiated thyroid and salivary glands, it should be with cautions when interpreting those sonographic appearances with lower reproducibility and repeatability.

To conclude, the reproducibility and repeatability of ultrasound measurement and sonographic appearance for thyroid and salivary glands were good. Ultrasound is reliable to be used for the assessment of post-RT changes of thyroid and salivary glands.